12-2021

Integrating Degradation Forecasting and Abatement Framework Into Advanced Distribution Management System

Huu Phuong Hoang
huuphuh@clemson.edu

12-2021

Integrating Degradation Forecasting and Abatement Framework into Advanced Distribution Management System

Huu Phuong Hoang

Integrating Degradation Forecasting and Abatement Framework into Advanced Distribution Management System

---

A Dissertation
Presented to
the Graduate School of
Clemson University

In Partial Fulfillment
of the Requirements for the Degree
Doctor of Philosophy
Electrical Engineering

---

by
Phuong H. Hoang
December 2021

Accepted by:
Dr. Christopher S. Edrington, Committee Chair
Dr. Johan H. R. Enslin
Dr. Zheyu Zhang
Dr. Benjamin J. Lawler

Abstract

Future distribution grids are expected to face an increasing penetration of heterogeneous distributed energy resources (DERs) and electric vehicles (EVs). This landscape change will pose challenges to the control and management of distribution grids because of the variability of renewable energy resources and EV charging. In addition, multiple DERs dispersed over networks can also challenge the grid operation and maintenance as various DERs at various locations are needed to be monitored and managed. However, customers will not be content with reductions in power quality, reliability, economy, safety, or security. To enhance the effectiveness of grid control and management, future grids will be given more autonomy in the form of advanced distribution management systems (ADMS). Energy management (EM) is one of the main constituents of ADMS to enhance system efficiency. EM typically considers only saving fuel consumption costs. However, grids' components degrade over time, and it adds up to the systems' operation cost. Knowing the degradation behaviors of grids' components to control them properly can reduce their degradation, and consequentially it can reduce the total operation cost. In addition, in order to maintain the highest reliability of the system, degradation models should also be developed along with appropriate decision-making strategies that allow information regarding components' status to be integrated with ADMS. This dissertation proposes a framework to integrate a degradation forecasting (DF) layer into ADMS to abate components' degradation processes, reduce the total operation cost, and enhance system reliability. The DF layer will collaborate with EM to find a solution that compromises fuel consumption costs and degradation costs.

Acknowledgement

First of all, I would like to give a special thank you to my Ph.D. advisor, Dr. Chris S. Edrington. I was fortunate to have Dr. Edrington advising me on my Ph.D. He has spent countless hours guiding me to do research at both Florida State University and Clemson University. He corrected me when my research did not go in the right direction. He fixed a funding issue to allow me to come to the US for this Ph.D. journey without knowing much about me.

I also would like to thank my committee members Dr. Enslin, Dr. Zhang, and Dr. Lawler, for serving on my committee.

I would like to thank Dr. Ozkan for his help: He taught me driving cars and how to do CHIL implementation. He taught me many life lessons helping me understand more about the US's culture when I first came to the US at Florida State University.

Also, I would like to thank Dr. Papari for her guidance at Florida State University and collaboration when she was at the University of North Carolina Charlotte.

Last but not least, I would like to thank other RT-COOLers for their help: Payam, Laxman, Justin, Valerie, and Tanner. Thank you, Payam, for lunchtime with me at Clemson University dinning hall.

Contents

List of Figures

List of Tables

Nomenclature

UQ	Uncertainty quantification
AC	Alternating current
DC	Direct current
EV	Electric vehicle
WT	Wind turbine
MT	Micro turbine
PV	Photovoltaics
BPA	Basic probability assignment
Bel	Belief function
FoD	Frame of discernment
CHIL	Controller-hardware-in-the-loop
DF	Degradation forecasting
DFAF	Degradation forecasting and abatement framework
DLC	Device level control
ADMM	Alternating direction method of multipliers
DoE	Department of Energy
pu	Per unit
DER	Distributed energy resource
DG	Distributed generation
ADMS	Advanced distribution management system
PM	Power management

EM Energy management

FL Forecasting layer

DF Degradation forecasting

ET Evidence theory

Chapter 1

Introduction

Chapter 1's Nomenclature

ADMS	Advanced distribution management system
DER	Distributed energy resource
EV	Electric vehicle
EM	Energy Management
PM	Power management
DLC	Device level control
DF	Degradation forecasting
DFAF	Degradation forecasting and abatement framework
DG	Distributed generation
WT	Wind turbine
MT	Microturbine
PV	Photo-voltaic
ET	Evidence theory
AC	Alternating current
CHIL	Controller-hardware-in-the-loop

1.1 Future Grids: Challenges and Needs

It is expected that there is an upcoming revolution in electrical systems ranging from MW-scale systems such as distribution grids and ship power systems to kW-scale systems like electrified vehicles' powertrain systems. The deployment of control and management strategies to digitally control and manage the systems is a common thing in these revolutionized systems [1, 2, 3]. The subject of this dissertation is alternating current (AC) distribution grids; therefore, their properties, challenges, and needs are studied. The wide deployment of distributed energy resources (DERs), which are also called distributed generation (DG), the growing penetration of electrified transportation, and the increasing adoption of digitalization are key differences between traditional grids and future grids [4, 5]. It is expected that future distribution grids will be populated with DERs to diversify energy sources and exploit renewable energy sources such as solar and wind power. Besides, electrified transportation is widely considered to replace fossil fuel transportation because of environmental and sustainable energy benefits. With these infrastructure changes, it poses new issues to system management, and as a result, it drives changes to deal with the challenges as well as to meet increasing demands from customers.

The uncertain nature of renewable sources can cause problems for distribution systems. First, it increases the complexity of the power supply-demand balance constraints as the generation of these sources is considered non-dispatchable. Consequently, it results in complexities to optimize and control power generation and delivery. Second, it makes the reliability evaluation for grids challenging as the uncertainty poses difficulties to quantify the quantities of interest involving in the evaluation. Multiple DERs dispersed over networks can also challenge grid management as various DERs at various locations are needed to be monitored and managed. In addition to DGs, the electrification of transportation is another problem as it will have significant impacts on future power networks. One of the forms that the electrified trend will proliferate in is electric vehicles (EVs). The demands on short charging time and long-range capabilities result in EV chargers with hundreds of kW of capacity. This amount is hundreds of times higher than those of typical residential loads such as washing and drying machines. Moreover, the EV penetration rate increases every year globally, an increase from 2.6% in 2019 to 3% global car sales in 2020 [6]. The increase in both the number of EVs and their charging capacities pose real difficulties in maintaining required power quality as well as reliability, especially for grids mainly serving residential areas because they are

expected to house EVs and their chargers. Furthermore, because of the variability of DGs and EV loads, stability will also become an issue.

Incorporated with new components, standards, and regulations, the future grids have various requirements and needs: power quality, reliability, safety, security, and economy [5, 4]. Among these mentioned ones, there are ones which are not only demanded in future grids but also in current grids: power quality, energy efficiency, and reliability. However, these key requirements are intensively demanded in future grids. The energy consumption in the U.S. has been projected to be uptrend from 2020 to 2035 [7]. It demands more energy supplied to customers to meet the growing consumption. However, CO_2 emission reduction goals realized by laws and regulations pressure on reducing energy production. Even generation technologies considered to be clean energy generation methods such as solar and wind power are still producing CO_2 in various forms. Energy efficiency improvement will be a key to both reach the environmental goals and satisfy customers. The reliability will also become an issue in future grids with various sources of uncertainty mainly caused by the variations of renewable energy sources and EVs' charging patterns. Traditional methods of reliability assessment for distribution grids are mostly offline and time-based approaches. These methods may not perform well because of uncertainty caused by renewable sources, the dispersion of DERs, and the impact of electrified transportation. Instead, new methods should be integrated into control and management systems to continuously and automatically monitor the reliability of the system.

With these above challenges, it is imperative to consider changes in regulating and managing distribution grids. Along with adopting new public policies, technological innovations should be developed and adopted to cope with the infrastructure changes as well as to meet increasing customer demands. Fortunately, the power system industry has been benefited from the progress of other industries. The advancements in the semiconductor industry accelerate the digitalization and the deployment of power electronics components in many industries, including power systems. It is expected that future grids will be populated with various computational devices and power electronics converters. In addition, advancements in the communication industry are adopted to power grids. This progress is an enabler to the integration of new control and management strategies into grids.

1.2 Advanced Distribution Management System

The future grids will be given more autonomy in the form of advanced distribution management systems (ADMS). The U.S. Department of Energy (DoE) is adopting the definition of ADMS from Gartner IT Glossary [8] as "An ADMS is the software platform that supports the full suite of distribution management and optimization. An ADMS includes functions that automate outage restoration and optimize the performance of the distribution grid. ADMS functions being developed for electric utilities include fault location, isolation, and restoration; volt/voltampere reactive optimization; conservation through voltage reduction; peak demand management; and support for microgrids and electric vehicles". Adopting this concept, ADMS with a hierarchical structure are used to deploy control and management strategies for power systems in [9, 1]. The underlying idea of the multi-layer architecture is taking advantage of different time steps of the layers as upper layers have the duties of providing commands to lower layers. This architecture has been used in both AC and DC grids; however, depending on the type of grid, quantities of interest are controlled and optimized. In the literature, a three-layer concept which consists of primary control layer, secondary control layer, and tertiary control layer, is introduced in [1]. For AC networks, the primary layer is the internal control of DG units. The secondary layer regulates the frequency and voltages by controlling their amplitude deviations. The tertiary layer manages the power flow in the network. With the same concept, the primary layer, secondary layer, and tertiary layer are also named device-level control (DLC), power management (PM), and energy management (EM) [9], respectively.

The two main objectives of the existing hierarchical system are stability and energy efficiency for the grids. To realize the goals, the knowledge of control and optimization is utilized. The DLC and PM layers mainly have control activities aiming at stabilizing qualities of interest to satisfy the power quality requirement. With the power electronics interface, the DLC are mainly converters' internal control. At the PM layer, the droop control methodology is typically used because of its simplicity and effectiveness. The EM layer primarily aims at reducing the grid's operational cost at the system level in a well-defined sense. The EM is to reach the energy efficiency goal by making use of optimization methods. It is noted that there have been various optimization paradigms solving the EM's optimization problems.

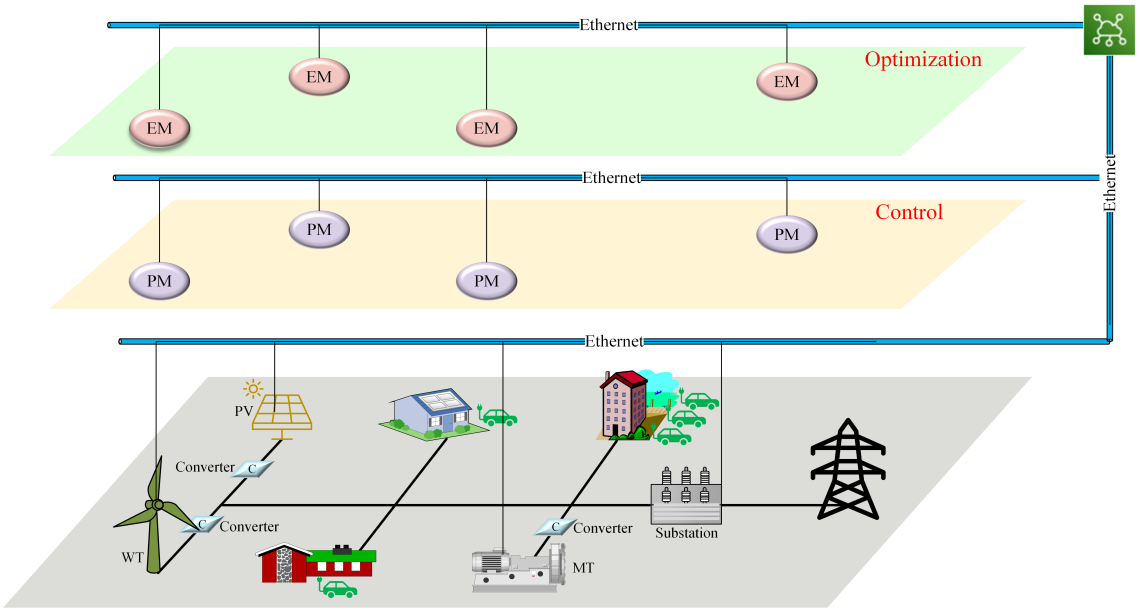

Figure 1.1: Existing ADMS for distribution grids.

1.3 Dissertation Problems and Approaches

Solving the challenges of future grids before the changing electrical landscape happens is critical. Broadly, the objective of this dissertation is to solve some challenges of future grids to achieve power quality, energy efficiency, and reliability requirements at the system level. To this end, the ADMS concept is used as a means to convey proposed approaches. Specifically, this dissertation aims to integrate a degradation forecasting (DF) layer into the ADMS to enhance system reliability, save system operation coss, and aid grid operation and planning. The following discusses problems and briefly presents approaches.

1.3.1 Energy Management

EM is one of the constituents of distribution networks' ADMS [10]. The primary function of EM is to allocate power generation to sources of energy to optimize an objective function in a well-defined sense while honoring constraints [11, 12, 13, 14, 15, 16]. Distributed EM is considered superior to the centralized counterpart in terms of resiliency and scalability. However, distributed EM's optimization problem is still a matter of discussion as global optimality becomes an issue.

There is work considering the economic dispatch problem as EM's optimization problem to have a convex optimization problem [17]. However, voltage constraints and power limits on

transmission lines are not taken into account. Alternating direction method of multipliers (ADMM) [18] is among the most widely used methods in existing distributed algorithms to solve EM's problems with these constraints are considered [19, 20, 21], to name just a few. The popularity of ADMM is attributed to its efficiency and straightforwardness to apply to applications with three clear updating steps. It is worth noticing that ADMM is confined to convex problems. However, EM's optimization problems for AC networks are well known to be non-convex; therefore, it fails to deliver theoretical guarantees on convergence.

This dissertation's approach to the problem is designing a dual optimization algorithm. In particular, the EM strategy is composed of two steps. In the first step, some conditions of EM's optimization task are relaxed to apply an algorithm converging to the global optimality, which is an issue in existing work because of the non-convex nature of the original optimization problem. The results of the first step are used to reconfigure constraints of the full optimization problem in step 2.

1.3.2 Integrating Degradation Forecasting and Abatement Framework into ADMS

Forecasting has received tremendous interest in the last two decades due to its importance. It results in numerous forecasting paradigms and algorithms, neural networks and support vector machine, to name just a few. Load, solar power generation, wind power generation forecasting are the most active research topics in the literature. Recently, degradation forecasting of components of electrical systems has attracted significant interest. Having precise predictions of future events can help systems have well-prepared plans, and in many scenarios, it can preclude severe events, even deadly events such as the 2021 Texas power outage. A grid satisfying a certain level of well-defined reliability is considered a requirement in the future. To this end, grids' elements such as DGs should be continuously monitored and maintained before a failure event happens. With a population of DGs dispersed geographically, monitoring and maintaining these DGs will become an issue. The traditional methods of scheduled maintenance may not perform well. While the chance of missing critical maintenance increases when the maintenance frequency decreases, increasing the frequency increases the operational costs, which opposes the cost-saving goal. In order to maintain the highest reliability of the system, degradation models should be developed along with appropriate decision-making strategies that allow information regarding components' status to be integrated with control.

It has been pointed out in [4] that future grids will need the integration of planning and operations. Planning activities such as maintenance and unit commitment should be involved in real-time control and management activities in an automatic and collaborative manner.

As mentioned earlier, EM is to solve a well-defined optimization problem to find optimal energy allocation for different energy sources. EM's outputs are then passed down as references to a lower control layer called power management (PM). Therefore, EM decides operating conditions for each energy conversion unit. It has been reported in the literature that the degradation rate of an energy conversion unit depends on operating conditions [22, 23, 24]; thus, degradation models should take into account components' operating conditions. Given the analysis, the mutual effects of components' degradation processes are mainly decided by EM. Therefore, EM can be considered as a means to abate system components' degradation processes.

With these considerations, integrating an upper layer with DF functionalities into the hierarchical ADMS can reduce system operating costs and enhance system reliability. In this dissertation, degradation models alongside appropriate decision-making strategies are developed to integrate the component status information into the control. A DF layer is developed considering a certain time horizon to 1) give timely advisory actions to avoid unpleasant events, 2) enhance system reliability, 3) compromise degradation cost and fuel consumption cost, consequentially save the total operation cost.

1.3.3 Evidence Theory's Combination Rule

Quantifying uncertainty in DF is a challenging task. Degradation data are scarce because generating them is challenging, costly, and time-consuming, and those data are typically confidential. In addition, degradation processes are impacted by various internal and external variables of a component. Methodologies demanding a large amount of data, such as deep learning may not fit well with the DF problems. Instead, methodologies that combine multiple sources of information to arrive at a more informative piece with higher confidence to deal with the epistemic uncertainty are better.

Evidence theory (ET) is a powerful tool to fuse multiple sources of information [25]. However, existing combination rules cannot deal with the conflict of information sources, and it is an unsolved problem for decades. Reasons for the conflict could be there exists a non-reliable source among the sources, or considered frame of discernments (FoDs) is not exhaustive.

1.4 Dissertation Organization

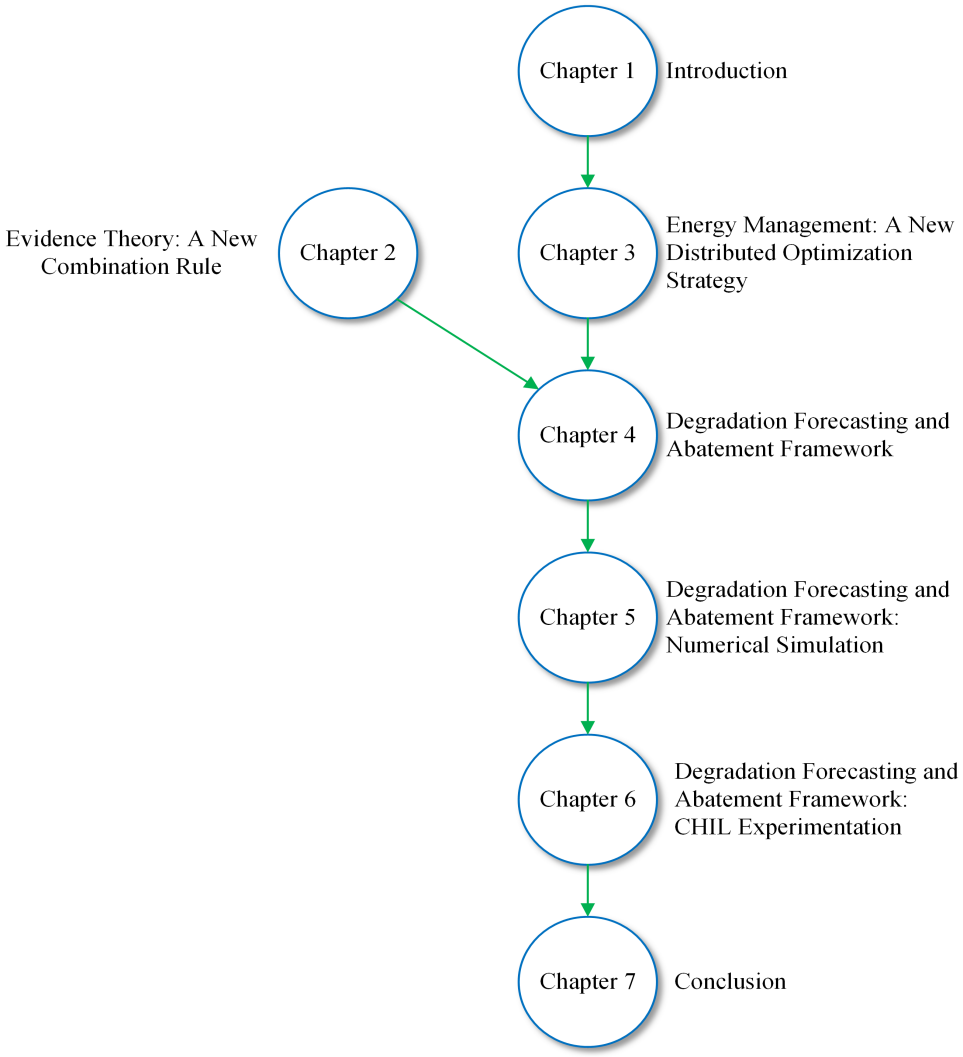

Figure 1.2: Dissertation reading flow.

This dissertation has 7 chapters. Figure 1.2 shows the dissertation reading flow. The following lists and briefly summarizes these chapters.

Chapter 1: Introduction

The chapter discusses challenges and needs in future grids. Furthermore, existing problems are briefly discussed as motivation for this dissertation. These problems are summarized as follows.

- The degradation of distribution grids' components with the penetration of EVs and non-dispatchable DERs will become an issue. This dissertation aims to develop and integrate

a DF layer into the hierarchical ADMS of distribution grids to enhance system reliability and reduce the total operation cost.

- Distributed EM is still a matter of discussion because global optimality becomes an issue in existing work. This dissertation proposes a distributed EM strategy to obtain a global optimum for EM.

- ET is used to quantify uncertainty as it is a powerful tool to fuse multiple sources of information. Degradation data is typically scarce, and thus multiple sources of information are used to quantify uncertainty. However, there is a fundamental problem in ET's combination rules. In particular, existing combination rules are not able to solve the conflict problem of information sources.

Chapter 2: Evidence Theory: A New Combination Rule

ET is used to quantify uncertainty as it is a powerful tool to fuse multiple sources of information. With the limitation mentioned previously, a new combination rule is proposed as a theoretical contribution. Although there have been extensive efforts to solve the conflict problem of combination rule for decades, the problem still remains unsolved for decades.

Chapter 3: Energy Management: A New Distributed Optimization Strategy

EM is one of the layers in the hierarchical control and management system. Distributed algorithms for EM are more challenging in comparison to centralized ones. A new distributed algorithm is proposed to overcome the global optimality issue of existing ones.

Chapter 4: Degradation Forecasting and Abatement Framework

EM only considers a limited number of aspects because of real-time constraints, and components' degradation is typically not of its concern. In this dissertation, a degradation forecasting and abatement framework (DFAF) considering to enhance system reliability and save the total operation cost is proposed. A DF layer is integrated to forecast components' degradation to adjust EM's objective function to consider components' degradation aspects.

Chapter 5: Degradation Forecasting and Abatement Framework: Numerical Simulation

In the chapter, numerical simulations are demonstrated to show the effectiveness of the algorithm proposed in Chapter 4.

Chapter 6: Degradation Forecasting and Abatement Framework: CHIL Exper-

imentation

In the chapter, the proposed framework proposed in Chapter 4 is realized by a controller-hardware-in-the-loop (CHIL) experimentation.

Chapter 7: Conclusion

The chapter concludes this dissertation.

Chapter 2

Evidence Theory: A New Combination Rule

Chapter 2's Nomenclature

ET	Evidence theory
FoD	Frame of discernment
Θ	Frame of discernment's notation
2^{Θ}	Power set
BPA	Basic probability Assignment
m	Mass function or basic probability assignment
m_A	Mass function of source of information A
Bel	Belief function
Bel_A	Belief function of source of information A
Pl	Plausibility function
Pl_A	Plausibility function of source of information A
Q	Commonality function
Q_A	Commonality function of source of information A
$\oplus$	Combination rule's notation
$m^A_{i \oplus j}$	Combined mass function from information sources i and j using combination rule A
$\emptyset$	Empty set

κ_{ij}	Conflict between sources of information i and j
$MBetP_{\Theta}$	Modified pignistic probability function with frame of discernment Θ
PPT	Pignistic probability transformation
N	Number of sources of information

2.1 The theory of belief functions

Evidence theory (ET) is a general framework for representing, aggregating and reasoning from partial information. Its two more popular names are Dempster-Shafer theory or the theory of belief functions. The theory was initiated by Dempster in a framework for statistical inference in 1967 [26], and then developed into a formal framework for modeling epistemic uncertainty by Shafer in 1976 [25] and became more popular after that. There is also a large number of researchers extensively involved in the development of ET such as Zadeh [27, 28], Pearl [29], Yager [30], Smets [31, 32], Nguyen [33], Dubois and Prade [34, 35], Denoeux [36, 37], Florea [38], Deng [39], and Dezert [40]. Of course, this list of names is by no means exhaustive when mentioning authors who have contributed to ET. Applications of ET are in many fields with huge numbers of works: expert systems [41, 42], information fusion [43, 44, 45], pattern recognition and machine learning [46, 47, 48, 49, 50, 51], to name just a few.

The theory of belief functions introduced in Shafer's book [25] is mathematically presented now. Let Θ be a finite nonempty set:

$$\Theta = \{\theta_1, \theta_2, ..., \theta_n\} \tag{2.1}$$

Θ is called a frame of discernment (FoD) if it satisfies $\theta_i \cup \theta_j = \emptyset, \forall i, j = \{1, ..., n\}$. Let 2^{Θ} be the set of all subsets of Θ, which is called the power set. The set can be mathematically stated as

$$2^{\Theta} = \{A | A \subseteq \Theta\} \tag{2.2}$$

Developing from the upper and lower probability theory of Dempster [26], Shafer introduced the belief function and the basic probability assignment (BPA):

Definition 2.1.1 (Belief function definition [25]) *Let Θ be an FoD, then $Bel : 2^{\Theta} \longrightarrow [0, 1]$ is*

a belief function if it satisfies the three conditions:

$$1) Bel(\emptyset) = 0 \tag{2.3a}$$

$$2) Bel(\Theta) = 1 \tag{2.3b}$$

3)*For every positive integer n and every collection* A_1,...,A_n *of subsets of* Θ,

$$Bel(A_1 \cup ... \cup A_n) \geq \sum_{I \subseteq \{1,...,n\}, I \neq \emptyset} (-1)^{|I|+1} Bel(\cap_{i \in I} A_i) \tag{2.3c}$$

Definition 2.1.2 (BPA definition [25]) *Let m be a mapping from* 2^Θ *to [0,1]. m is called a BPA if the following two conditions are imposed on it:*

$$1) m(\emptyset) = 0 \tag{2.4a}$$

$$2) \sum_{A \in 2^\Theta} m(A) = 1 \tag{2.4b}$$

Note that $A \in 2^\Theta$ is equivalent to $A \subseteq \Theta$. $A \in 2^\Theta \setminus \emptyset$ is called a focal element if $m(A) > 0$. In addition, m is also called a mass function and the quantity $m(A)$ is A's basic probability number. By developing the above belief function, Shafer pointed out that the Bayesian theory or the traditional probability theory in fact is a special case of the theory of belief functions. As an example of the generalization, with $\Theta = \{\theta_1, \theta_2\}$, while the expression $m(\theta_1, \theta_2)$ is allowed, the expression $P(\{\theta_1, \theta_2\})$ is not allowed in the traditional probability, where $Pr(.)$ is the probability function.

Given a BPA, one can compute the belief function's value for $A \in 2^\Theta$ as

$$Bel(A) = \sum_{B \subseteq A} m(B) \tag{2.5}$$

The relation of the belief function and the mass function is a one-to-one mapping. Therefore, one can trace back to obtain $m(A)$, where $A \subseteq \Theta$, given the values of the belief function as

$$m(A) = \sum_{B \subseteq A} (-1)^{|A-B|} Bel(B) \tag{2.6}$$

The upper probability function which is also known as the plausibility function $Pl : 2^\Theta \longrightarrow$

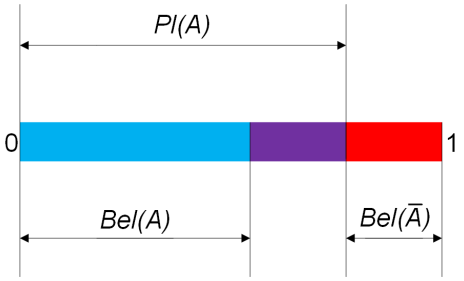

Figure 2.1: The relation between Bel and Pl.

$[0, 1]$ computed as

$$Pl(A) = 1 - Bel(\bar{A}) = \sum_{B \cap A \neq \emptyset} m(B) \tag{2.7}$$

where $\bar{A} = \Theta - A$. The functions Bel and Pl express the lower and upper bounds for the support of subset A, respectively, as

$$Bel(A) \leq P(A) \leq Pl(A) \tag{2.8}$$

where $P(A)$ is the probability of event A in the point of view of the probability theory. In the Bayesian theory $Bel(A) + Bel(\bar{A}) = 1$ and $Bel(A) = Pl(A)$ are guaranteed, while in ET these equations are not necessarily true that is a major difference between the two theories. Figure 2.1 illustrates the relation between Bel and Pl. Another function which is called the commonality function was introduced in Shafer's work as

$$Q(A) = \sum_{B \subseteq \Theta, A \subseteq B} m(B). \tag{2.9}$$

Equipped with the above theory, let us take an example to illustrate it.

Example 2.1.1 (Oral exam example) *A student at a university is defending his oral exam to a committee composed of three professors, namely X, Y, and Z. After the defense, the three professors have to independently make decisions whether the student is passed or failed. Let P and F stand for passed and failed, respectively. Professor X gives a BPA that the student is passed with $m_X(\{P\}) = 0.8$, the student is failed with $m_X(\{F\}) = 0.1$, and he is not certain $m_X(\{P, F\}) = 0.1$. Professor Y is an expert in the student's research field, and he believes that the student is passed; that is, $m_Y(\{P\}) = 1$. Professor Z did not completely understand the student's work and presentation, so he gives $m_Z(\{P\}) = 0.5$ and $m_Z(\{P, F\}) = 0.5$. Table 2.1 shows the beliefs of the three professors*

on the student's exam.

Table 2.1: Information in *Example 2.1.1*

Professor i	$m_i(\{P\})$	$m_i(\{F\})$	$m_i(\{P,F\})$
X	0.8	0.1	0.1
Y	1.0	0.0	0.0
Z	0.5	0.0	0.5

With this example, the FoD is $\Theta = \{P, F\}$ and the power set is $2^{\Theta} = \{\emptyset, P, F, \{P, F\}\}$. Note that $\sum_{A \in 2^{\Theta}} m(A) = 1.0$. Given the information, one can compute the belief, plausibility and commonality values as

- Professor X on the student's exam:

$$Bel_X(\{P\}) = m_X(\{P\}) = 0.8 \tag{2.10a}$$

$$Bel_X(\{F\}) = m_X(\{F\}) = 0.1 \tag{2.10b}$$

$$Bel_X(\{P,F\}) = m_X(\{P\}) + m_X(\{F\}) + m_X(\{P,F\}) = 1.0 \tag{2.10c}$$

$$Pl_X(\{P\}) = m_X(\{P\}) + m_X(\{P,F\}) = 0.9 \tag{2.10d}$$

$$Pl_X(\{F\}) = m_X(\{F\}) + m_X(\{P,F\}) = 0.2 \tag{2.10e}$$

$$Pl_X(\{P,F\}) = m_X(\{P\}) + m_X(\{F\}) + m_X(\{P,F\}) = 1.0 \tag{2.10f}$$

$$Q_X(\{P\}) = m_X(\{P\}) + m_X(\{P,F\}) = 0.9 \tag{2.10g}$$

$$Q_X(\{F\}) = m_X(\{F\}) + m_X(\{P,F\}) = 0.2 \tag{2.10h}$$

$$Q_X(\{P,F\}) = m_X(\{P,F\}) = 0.1 \tag{2.10i}$$

- Professor Y on the student's exam:

$$Bel_Y(\{P\}) = m_Y(\{P\}) = 1.0 \tag{2.11a}$$

$$Bel_Y(\{F\}) = m_Y(\{F\}) = 0.0 \tag{2.11b}$$

$$Bel_Y(\{P,F\}) = m_Y(\{P\}) + m_Y(\{F\}) + m_Y(\{P,F\}) = 1.0 \tag{2.11c}$$

$$Pl_Y(\{P\}) = m_Y(\{P\}) + m_Y(\{P,F\}) = 1.0 \tag{2.11d}$$

$$Pl_Y(\{F\}) = m_Y(\{F\}) + m_Y(\{P,F\}) = 0 \tag{2.11e}$$

$$Pl_Y(\{P,F\}) = m_Y(\{P\}) + m_Y(\{F\}) + m_Y(\{P,F\}) = 1.0 \tag{2.11f}$$

$$Q_Y(\{P\}) = m_Y(\{P\}) + m_Y(\{P,F\}) = 1.0 \tag{2.11g}$$

$$Q_Y(\{F\}) = m_Y(\{F\}) + m_Y(\{P,F\}) = 0 \tag{2.11h}$$

$$Q_Y(\{P,F\}) = m_Y(\{P,F\}) = 0 \tag{2.11i}$$

- Professor Z on the student's exam:

$$Bel_Z(\{P\}) = m_Z(\{P\}) = 0.5 \tag{2.12a}$$

$$Bel_Z(\{F\}) = m_Z(\{F\}) = 0 \tag{2.12b}$$

$$Bel_Z(\{P,F\}) = m_Z(\{P\}) + m_Z(\{F\}) + m_Z(\{P,F\}) = 1.0 \tag{2.12c}$$

$$Pl_Z(\{P\}) = m_Z(\{P\}) + m_Z(\{P,F\}) = 1.0 \tag{2.12d}$$

$$Pl_Z(\{F\}) = m_Z(\{F\}) + m_Z(\{P,F\}) = 0.5 \tag{2.12e}$$

$$Pl_Z(\{P,F\}) = m_Z(\{P\}) + m_Z(\{F\}) + m_Z(\{P,F\}) = 1.0 \tag{2.12f}$$

$$Q_Z(\{P\}) = m_Z(\{P\}) + m_Z(\{P,F\}) = 1.0 \tag{2.12g}$$

$$Q_Z(\{F\}) = m_Z(\{F\}) + m_Z(\{P,F\}) = 0.5 \tag{2.12h}$$

$$Q_Z(\{P,F\}) = m_Z(\{P,F\}) = 0.5 \tag{2.12i}$$

2.2 Evidence theory vs other theories

Uncertainty is categorized into two types: aleatoric uncertainty and epistemic uncertainty [52]. On the one hand, the aleatoric uncertainty is an inherent variation associated with the physical systems or the environment under consideration, for example, different outputs when running the

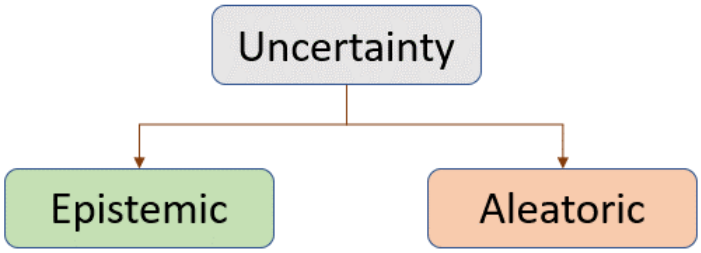

Figure 2.2: Uncertainty classification.

same experiment. On the other hand, epistemic uncertainty is due to lack of knowledge/information or some level of ignorance about systems or considered environment, for instance, inaccurate modeling. Figure 2.2 illustrates the classification. The following observations can be seen when comparing ET to other theories:

- The probability theory represents epistemic uncertainties with a uniform probability distribution function or represents the mixture of aleatory and epistemic uncertainties with the second-order probability theory.
- The fuzzy set theory can be used to represent the epistemic uncertainties; however, it is impossible to combine the fuzzy sets with the probabilistic information.
- The possibility theory is capable of representing epistemic uncertainties; however, there are no clear methods for combining the belief degrees and probabilistic information.
- The interval analysis is a subset of the possibility theory.

2.3 Rules of Combination

A rule of combination is considered as one of the main constituents of ET. It is a law to fuse different pieces of information on the same reference set to arrive at a combined measure of belief. Included as a component in the whole of Dempster's work [26], Dempster's rule is the first one being introduced [25, 53]. The rule has associative and communicative properties. With high compatible sources of information, the rule indeed provides compelling results. However, by a simple but conceivable example, Zadeh has drawn much attention to the rule [28]. Specifically, given two highly paradoxical sources, the rule provides a result that backs the belief that the two sources

strongly disagree. Note that Zadeh is not the only one questioning the validity and the consistency of Dempster's rule as there are also works skeptical about the rule, such as [29, 40]. Perhaps the most straightforward guideline is using the rule properly [54]. Although it should be agreed that a blind aggregation should be avoided, it is believed that ET is a powerful tool as it has been proved through an enormous quantity of applications as well as rigorous mathematical analysis. Thus, seeking out a solution or at least understanding such a behavior of a combination rule for examples like Zadeh's one could be worthy. As another direction to solve the issue, pieces of information are being modified rather than touching on the rule itself. For instance, redistributing a sufficiently small amount to zero elements of a BPA before a combination was proposed in [35]. The third direction to seek out the answers, and perhaps also to explain the counterintuitive behavior, is modifying the rule. In this direction, a plethora of rules has been introduced. These works are categorized into two main approaches. On the one hand, the first one allows the possibility of non-exhaustivity of an FoD [39, 55]. On the other hand, the second one is to try to seek laws to reallocate the degree of belief over the elements other than the empty set in a considered FoD [30, 35, 38, 56]. In between, there are also works conceding the existence of a non-zero quantity belief of the empty set, but the authors did not state it explicitly in their rules [38]. In essence, to the best of the author's knowledge, no rule has been able to explain the behavior completely.

Suppose two sources of information 1 and 2 create the same FoD Θ. Let m_1 and m_2 be two independent BPAs over the same FoD Θ. Bel_1 and Bel_2 correspondingly denote the belief functions of m_1 and m_2. Let us review some combination rules to fuse the two sources of information. To avoid verbose presentation, it is noted that the term rule is used to refer to combination rule in this paper. Moreover, the term sources indicates sources of information or BPAs. Existing rules to fuse sources 1 and 2 are reviewed next.

2.3.1 Existing rules

Dempster's rule is also known as the orthogonal sum. The rule is used to combine two independent BPAs m_1 and m_2. It is an operation with the following formula:

$$m_{1\oplus 2}^{DS}(A) = \begin{cases} \frac{1}{1-\kappa_{12}} \sum\limits_{A=B\cap C} m_1(B)m_2(C), & A \neq \emptyset \\ 0, & \text{otherwise} \end{cases} \tag{2.13}$$

where

$$\kappa_{12} = \sum_{B \cap C = \emptyset} m_1(B) m_2(C) \tag{2.14}$$

It is noted that Dempster's rule is unusable to combine the two sources if $\kappa_{12} = 1$. In [25], the quantity $\log K_{12} = \log \frac{1}{1-\kappa_{12}} = -\log(1-\kappa_{12})$ is called the weight of conflict between Bel_1 and Bel_2 and $K_{12} = \frac{1}{1-\kappa_{12}}$ is called the renormalizing constant. In works other than [25], κ_{12} is called the amount of conflict between two sources [35], the weight of conflict or the global conflict [38], the degree of conflict [30, 40]. In this report, κ_{12} is simply called the conflict between source 1 and 2. In [27] and [28], Zadeh challenged the validity of ET. He showed a counterintuitive example. Here is the example.

Example 2.3.1 (Zadeh's example) *A patient P is examined by two doctors, namely D_1 and D_2. Let M, B and C represent meningitis, brain tumor and concussion, respectively. D_1's diagnosis for P is $m_{D_1}(\{M\}) = 0.99$, $m_{D_1}(\{B\}) = 0.01$, and $m_{D_1}(\{C\}) = 0.0$, while D_2 gives $m_{D_2}(\{M\}) = 0.0$, $m_{D_2}(\{B\}) = 0.01$, and $m_{D_2}(\{C\}) = 0.99$.*

Without much difficulty, we can obtain the conflict's value $\kappa_{D_1 D_2} = 0.9999$. Then, Dempster's rule gives us a very counterintuitive result for the above example as $m^{DS}_{D_1 \oplus D_2}(\ \{M\}) = 0$, $m^{DS}_{D_1 \oplus D_2}(\{B\}) = 1.0$, and $m^{DS}_{D_1 \oplus D_2}(\{C\}) = 0$. Zadeh stated that the counterintuition might be the effect of the normalization factor $\frac{1}{1-\kappa_{D_1 D_2}}$. In [35], the strong conflict, i.e., the value of $\kappa_{D_1 D_2}$ is close to 1, is explained by three reasons listed as:

1) The two sources of information are unreliable or one of the two sources is not reliable.

2) The considered FoD is not exhaustive. There could be some possible elements outside of it.

3) The two sources are inconsistent; they point to different objects.

In response to Zadeh's criticisms, various researchers have put extensive efforts to revise Dempster's rule resulting in many alternative rules. We categorize modified rules into two approaches: the first one attempts to redistribute the mass function but still assume the close world prerequisite and the second one supports the open world hypothesis by relaxing $m(\emptyset)$ as $1 \geq m(\emptyset) \geq 0$. The idea of open world is interpreted by the reason 2) for strong conflicts stated above that there may be some other unknown elements lying in $\emptyset$ should be added to considered FoDs. In contrast, proponents of the close world firmly assume $m(\emptyset) = 0$. Obviously, $m(\emptyset) = 0$ means that there is no chance for unknown elements outside FoD Θ.

In what follows, some other rules other than Dempster's rule are presented. In [30], Yager proposed the following rule:

$$m^{Y}_{1\oplus 2}(A) = \sum_{A=B\cap C} m_1(B)m_2(C),\ A \in 2^{\Theta} \setminus \{\Theta, \emptyset\} \tag{2.15a}$$

$$m^{Y}_{1\oplus 2}(\Theta) = m_1(\Theta)m_2(\Theta) + \sum_{B\cap C=\emptyset} m_1(B)m_2(C) \tag{2.15b}$$

$$m^{Y}_{1\oplus 2}(\emptyset) = 0 \tag{2.15c}$$

It can be seen that the conflict κ_{12} is assigned to Θ in Yager's rule. In another attempt to redistribute the conflict, Inagaki introduced a rule which was named as the unified combination rule [56]:

$$m^{I}_{1\oplus 2}(A) = \sum_{A=B\cap C} m_1(B)m_2(C) + \kappa_{12} f^{I}(A), A \in 2^{\Theta} \setminus \emptyset \tag{2.16a}$$

$$m^{I}_{1\oplus 2}(\emptyset) = 0 \tag{2.16b}$$

where $\sum_{A\in 2^{\Theta}\setminus\emptyset} f^{I}(A) = 1$. In [35], Dubois and Prade pointed out that Dempster's rule turns out to be a conjunctive consensus with the normalization factor $\frac{1}{1-\kappa_{12}}$. Additionally, there is also another operation called disjunctive consensus. Particularly, the conjunctive consensus is defined as

$$m^{CC}_{1\oplus 2}(A) = \sum_{A=B\cap C} m_1(B)m_2(C), A \in 2^{\Theta} \setminus \emptyset \tag{2.17a}$$

$$m^{CC}_{1\oplus 2}(\emptyset) = 0 \tag{2.17b}$$

and the disjunctive consensus is defined as

$$m^{DC}_{1\oplus 2}(A) = \sum_{A=B\cup C, B\cap C=\emptyset} m_1(B)m_2(C), A \in 2^{\Theta} \setminus \emptyset \tag{2.18a}$$

$$m^{DC}_{1\oplus 2}(\emptyset) = 0 \tag{2.18b}$$

The authors then proposed a hybrid rule which is a trade-off between the conjunctive and disjunctive

consensus called Dubois and Prade's rule as

$$m_{1\oplus 2}^{DP}(A) = \sum_{A=B\cap C} m_1(B)m_2(C) + \sum_{A=B\cup C, B\cap C=\emptyset} m_1(B)m_2(C), A \in 2^{\Theta} \setminus \emptyset \tag{2.19a}$$

$$m_{1\oplus 2}^{DP}(\emptyset) = 0 \tag{2.19b}$$

It can be seen that the conflict k_{12} is redistributed over $2^{\Theta} \setminus \emptyset$ by the second term of the right-hand side of equation (2.19a). The following rule was of Florea *et al.* [38]:

$$m_{1\oplus 2}^{F}(A) = g(\kappa_{12}) \sum_{A=B\cap C} m_1(B)m_2(C) + h(\kappa_{12}) \sum_{A=B\cup C} m_1(B)m_2(C), A \neq \emptyset \tag{2.20a}$$

$$m_{1\oplus 2}^{F}(\emptyset) = 0 \tag{2.20b}$$

where $g(\kappa_{12}) : [0,1] \longrightarrow [0,\infty)$ and $h(\kappa_{12}) : [0,1] \longrightarrow [0,\infty)$ are functions of κ_{12} satisfying:

$$(1-\kappa_{12})g(\kappa_{12}) + h(\kappa_{12}) = 1 \tag{2.21}$$

Florea *et al.*'s rule is similar to Dubois and Prade's one in the sense that $g(\kappa_{12})$ and $h(\kappa_{12})$ were introduced to redistribute the conflict in the trade-off between the conjunctive consensus and disjunctive consensus.

Next, papers supporting the open world idea are reviewed, i.e., $m(\emptyset) \neq 0$ is possible. However, allowing non-zero values for $m(\emptyset) \neq 0$ requires redefining BPA as

Definition 2.3.1 (Modified BPA definition) *Let m be a mapping from 2^{Θ} to [0,1]. m is called a modified BPA if $\sum_{A\in 2^{\Theta}} m(A) = 1$ is satisfied.*

The following two papers discuss rules for two modified BPAs. In [39], Deng exploited the open world idea by generalizing Dempster's rule. The proposed rule, which is called the generalized combination rule by the author, has the following operation:

$$m_{1\oplus 2}^{D}(A) = \frac{1-m^{D}(\emptyset)}{1-\kappa} \sum_{A=B\cap C} m_1(B)m_2(C), A \neq \emptyset \tag{2.22a}$$

$$m_{1\oplus 2}^{D}(\emptyset) = m_1(\emptyset)m_2(\emptyset) \tag{2.22b}$$

where

$$\kappa_{12} = \sum_{B \cap C = \emptyset} m_1(B) m_2(C) \tag{2.23}$$

In addition, Deng addresses the undefined problem of Dempster's rule when $\kappa_{12} = 1$ by letting $m(\emptyset) = 1$ if $\kappa_{12} = 1$. Recently, Jiang and Zhan, [55], modified Deng's rule by implementing the normalizing step for the mass quantity of the empty set and recalculating the conflict κ_{12}:

$$m^{JZ}_{1\oplus 2}(A) = \frac{1}{1-\kappa_{12}} \sum_{A = B \cap C} m_1(B) m_2(C),\ A \neq \emptyset \tag{2.24a}$$

$$m^{JZ}_{1\oplus 2}(\emptyset) = \frac{m_1(\emptyset) m_2(\emptyset)}{1-\kappa_{12}} \tag{2.24b}$$

where

$$\kappa_{12} = \sum_{B \cap C = \emptyset, B \cup C \neq \emptyset} m_1(B) m_2(C) \tag{2.25}$$

(2.24) is called Jiang and Zhan's rule. In case of $\kappa_{12} = 1$, the authors force $m^{JZ}_{1\oplus 2}(\emptyset) = 1$ to avoid the undefined issue. Figure 2.3 illustrates the open-world concept in which $A \in 2^\Theta \setminus \emptyset$ is in the blue circle, while dashed red circle contains $\emptyset$ and all the non-empty subsets of Θ. The blue circle refers to the close world, and the red one indicates the open world. $\emptyset$ refers to the unknown. But neither [39] nor [55] concerns about the unreliability of information sources. Let us see the following example.

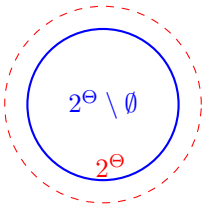

Figure 2.3: The open world concept.

Example 2.3.2 *Let* $\Theta = \{\theta_1, \theta_2, \theta_3\}$. *Assume we have 4 BPAs as in Table 2.2.*

Applying Dempster's rule (2.13) for *Example 2.3.2*, one can obtain $m^{DS}_{1\oplus 2\oplus 3}(\{\theta_2\}) = 1$. The same result can be seen when calling Deng's rule (2.22) and Jiang and Zhan's rule (2.24). A hypothesis here is that source 3 is not reliable. This hypothesis seems acceptable since the majority highly disagree with source 3. But the three aforementioned rules are not able to address this problem.

Table 2.2: Sources in *Example 2.3.2*

Source i	$m_i(\{\theta_1\})$	$m_i(\{\theta_2\})$	$m_i(\{\theta_3\})$
1	0.8	0.1	0.1
2	0.8	0.1	0.1
3	0.0	1.0	0.0
4	0.9	0.1	0.0

2.4 Pignistic probability transformation

In the framework of ET, a single decision is ambiguous as there is typically no clear probability expression on a single event. Pignistic probabilities are typically used to make decisions in ET. They can be obtained after implementing the pignistic probability transformation given a BPA [31, 32].

Definition 2.4.1 (Pignistic transformation [32]) *Let m be a modified BPA on a FoD Θ. Its associated pignistic probability function $BetP_\Theta$: $\Theta \longrightarrow [0,1]$ is defined as*

$$BetP_\Theta(\omega) = \sum_{A \subseteq \Theta, \omega \in A} \frac{1}{|A|} \frac{m(A)}{1 - m(\emptyset)}, m(\emptyset) \neq 1 \tag{2.26}$$

The transformation between m and $BetP_\Theta$ is called the pignistic transformation.

It is worth mentioning that the the pignistic transformation allows modified BPAs as inputs but ignores $\emptyset$ in the output phase.

2.5 New generalized rule considering open world and unreliability of sources

2.5.1 Generalized combination rule

As mentioned earlier, Dubois and Prade stated that the occurrence of strong conflict might be explained by the three situations [35]. We rule out the third one because we assume that the two sources concern the same objects. It is then reduced to two possibilities; the FoD is not exhaustive, and the sources are not liable. As an instance for a non-exhaustive FoD, in Zadeh's example, the

patient could be affected by another disease that is unknown to the two doctors other than by the three diagnosed ones. Dubois and Prade also discussed treatments for the strong conflict, but each situation is treated separately. Particularly, relaxing the condition $m(\emptyset) = 0$ was proposed in [34, 57]. For the case of information unreliability, Dubois and Prade's rule was suggested.

We instead attempt to address both situations simultaneously. To this end, we first permit assigning a non-zero number to $\emptyset$'s basic probability number, e.g., $m_1(\emptyset) \neq 0$ and $m_2(\emptyset) \neq 0$ are permitted. In addition, the operations $\emptyset \cap \emptyset = \emptyset$ and $\emptyset \cup \emptyset = \emptyset$ are allowed. Note that we do not distinguish $\emptyset_1$ and $\emptyset_2$ as the authors in [39] and [55] did because $\emptyset$ refers to the unknown. Allowing such operations leads us to redefine the conflict of source 1 and source 2 as

$$\begin{aligned} \kappa_{12} &= \sum_{B \cap C = \emptyset, B \cup C \neq \emptyset} m_1(B) m_2(C) \\ &= \sum_{B \cap C = \emptyset} m_1(B) m_2(C) - m_1(\emptyset) m_2(\emptyset) \end{aligned} \tag{2.27}$$

The reason for the modification can be seen in the following example.

Example 2.5.1 *Let $\Theta = \{\theta_1, \theta_2\}$. Assume we have 2 modified BPAs as in Table 2.3.*

Table 2.3: Sources in *Example 2.5.1*

Source i	$m_i(\{\theta_1\})$	$m_i(\{\theta_2\})$	$m_i(\emptyset)$
1	0.1	0.2	0.7
2	0.1	0.2	0.7

Applying Deng's rule:

$$\begin{aligned} \kappa_{12} =& m_1(\{\theta_1\}) m_2(\{\theta_2\}) + m_1(\{\theta_1\}) m_2(\emptyset) \\ &+ m_1(\{\theta_2\}) m_2(\{\theta_1\}) + m_1(\{\theta_2\}) m_2(\emptyset) \\ &+ m_1(\emptyset) m_2(\{\theta_1\}) + m_1(\emptyset) m_2(\{\theta_2\}) \\ &+ m_1(\emptyset) m_2(\emptyset) = 0.95 \end{aligned} \tag{2.28}$$

Intuitively, the result of Deng's rule seems unreasonable because the two sources have a high degree of agreement on the existence of the unknown. If applying the redefined conflict, it gives us $\kappa_{12} = 0.46$ that is more rational in which the term $m_1(\emptyset) m_2(\emptyset)$ is not added to κ_{12}. Jiang and Zhan's rule also

exploits this weakness of Deng's rule. Next, let us study the function $f(\kappa_{12}) : [0,1] \longrightarrow [0,1]$ which is a monotonically increasing function. Due to its monotonicity, one can have:

$$\text{If } \kappa_{12} = 0, \text{ then } f(\kappa_{12}) = 0 \tag{2.29a}$$

$$\text{If } \kappa_{12} = 1, \text{ then } f(\kappa_{12}) = 1 \tag{2.29b}$$

Such a function tells us that when the conflict decreases and approaches 0, so the value of $f(\kappa_{12})$. Conversely, a strong conflict yields a large $f(\kappa_{12})$ close to 1. Suppose, after implementing a rule for two sources which have BPAs m_1 and m_2, a mass function $m_{1\oplus 2}^{(.)}$ is obtained, where $(.)$ indicates the combination rule used to fuse source 1 and 2. Let α be an unknown scalar satisfying $0 \leq \alpha \leq 1$. To address the second situation, we distribute additionally an amount of $\alpha f(\kappa_{12})$ to the basic probability number of $\emptyset$. It is noted that $m(\emptyset)$ is not necessarily equal to $\alpha f(\kappa_{12})$ as we additionally assign this amount to the empty set because of the conflict. α can be interpreted as the probability that the FoD is not exhaustive due to the conflict. Thus, it seems reasonable to postulate the assignment, given that α is unknown in the range from 0 to 1. We progress by adopting Dubois and Prade's approach and Florea *et al.*'s approach in utilizing the disjunctive consensus to manage the unreliability of sources. Consequently, based on what we have been reasoning and the rules mentioned previously, we introduce the following new rule called OR which consider the open world idea and to cope with the reliability of sources. That is, the new rule inherits effectual properties from existing rules with improvements.

Definition 2.5.1 (Combination rule OR to combine two sources) *Let m_1 and m_2 be two modified BPAs defined on the same FoD Θ. Then, the new combination rule to fuse m_1 and m_2 is defined as*

$$\begin{aligned} m_{1\oplus 2}^{OR}(A) =& \Big(1 - \alpha f(\kappa_{12})\Big)\Big(g(\kappa_{12}) \sum_{A=B\cap C} m_1(B)m_2(C) \\ &+ h(\kappa_{12}) \sum_{A=B\cup C} m_1(B)m_2(C)\Big),\ A \neq \emptyset \end{aligned} \tag{2.30a}$$

$$\begin{aligned} m_{1\oplus 2}^{OR}(\emptyset) =& \alpha f(\kappa_{12}) + \Big(1 - \alpha f(\kappa_{12})\Big)\Big(g(\kappa_{12})m_1(\emptyset)m_2(\emptyset) \\ &+ h(\kappa_{12})m_1(\emptyset)m_2(\emptyset)\Big) \end{aligned} \tag{2.30b}$$

where

$$\begin{aligned}\kappa_{12} &= \sum_{B\cap C=\emptyset, B\cup C\neq\emptyset} m_1(B)m_2(C) \\ &= \sum_{B\cap C=\emptyset} m_1(B)m_2(C) - m_1(\emptyset)m_2(\emptyset)\end{aligned} \tag{2.31}$$

and $g(\kappa_{12}) : [0,1] \longrightarrow [0,1]$ *and* $h(\kappa_{12}) : [0,1] \longrightarrow [0,1]$ *which are imposed the following condition:*

$$(1-\kappa_{12})g(\kappa_{12}) + h(\kappa_{12}) = 1 \tag{2.32}$$

In general, the term $\alpha f(\kappa_{12})$ is hard to determine, and thus it is more wise to determine it case by case. But without this term, the new rule is not complete in the sense that if $m_1(\emptyset) = 0$ and $m_2(\emptyset) = 0$, then $m^{OR}_{1\oplus 2}(\emptyset)$ is always 0. Recalling Zadeh's example, if $\alpha = 0$, then $m^{OR}_{1\oplus 2}(\emptyset) = 0$ is always true. Let $\alpha = 0.5$, $f(\kappa_{12}) = \frac{e^{\kappa_{12}}-1}{e-1}$, $g(\kappa_{12}) = \frac{1}{1-\kappa_{12}}$, and $h(\kappa_{12}) = 0$. Applying the new rule (2.30), $m^{OR}_{1\oplus 2}(\{B\}) \approx 0.5$ and $m^{OR}_{1\oplus 2}(\emptyset) \approx 0.5$. If there are some hints indicating the existence of an unknown disease, we increase α to 0.6 and we obtain $m^{OR}_{1\oplus 2}(\{B\}) \approx 0.4$ and $m^{OR}_{1\oplus 2}(\emptyset) \approx 0.6$.

To simplify the presentation later, the following expressions for $A \neq \emptyset$ are adopted from [38]:

$$m^{\cap}(A) = \sum_{A=B\cap C} m_1(B)m_2(C) \tag{2.33a}$$

$$m^{\cup}(A) = \sum_{A=B\cup C} m_1(B)m_2(C) \tag{2.33b}$$

The following theorem is to guarantee $\sum_{A\in 2^\Theta} m^{OR}_{1\oplus 2}(A) = 1$, which is a must for a rule.

Theorem 2.5.1 *Suppose combining two modified BPAs* m_1 *and* m_2 *by the new rule defined in Definition 2.5.1 results in* $m^{OR}_{1\oplus 2}$*. Then,* $m^{OR}_{1\oplus 2}$ *is a modified BPA defined in Definition 2.3.1.*

Proof: With some manipulation and notice the equation (2.32), the two following equations can be obtained:

$$\sum_{A\in 2^\Theta\setminus\{\emptyset\}} m^{\cap}(A) + m_1(\emptyset)m_2(\emptyset) = 1 - \kappa_{12} \tag{2.34a}$$

$$\sum_{A\in 2^\Theta} m^{\cup}(A) = 1 \tag{2.34b}$$

Applying the equations (2.34a) and (2.34b) into (2.30a), one can have

$$\begin{aligned}\sum_{A\in 2^{\Theta}} m^{OR}_{1\oplus 2}(A) =&\alpha f(\kappa_{12}) + \Big(1-\alpha f(\kappa_{12})\Big) \\ &\times \Big(g(\kappa_{12})\Big(\sum_{A\in 2^{\Theta}\setminus\{\emptyset\}} m^{\cap}(A) + m_1(\emptyset)m_2(\emptyset)\Big) \\ &+ h(\kappa_{12})\sum_{A\in 2^{\Theta}} m^{\cup}(A)\Big) \\ =&\alpha f(\kappa_{12}) + \Big(1-\alpha f(\kappa_{12})\Big)\Big(g(\kappa_{12})(1-\kappa_{12}) + h(\kappa_{12})\Big) = 1\end{aligned} \tag{2.35}$$

QED. ■

In relation to other rules, the observations below can be easily proved:

1) In *Definition 2.5.1*, if $\alpha = 0$, $h(\kappa_{12}) = 0$, $m_1(\emptyset) = m_2(\emptyset) = 0$, and $g(\kappa_{12}) = \frac{1}{1-\kappa_{12}}$ when $0 \leq \kappa_{12} < 1$ and $g(\kappa_{12})$ is undefined when $\kappa_{12} = 1$, then the new rule and Dempster's rule (2.13) are identical.

2) In *Definition 2.5.1*, suppose $\alpha = 0$, $g(\kappa_{12}) = \frac{1}{1-\kappa_{12}}$, and $h(\kappa_{12}) = 0$. In addition, $\emptyset_1 = \emptyset_2 = \emptyset$. Furthermore, if $\kappa_{12} = 1$, then $m^{OR}_{1\oplus 2}(\emptyset) = 1$. Then, Jiang and Zhan's rule (2.24) and the new rule are are identical.

3) In *Definition 2.5.1*, if $\alpha = 0$ and $m_1(\emptyset) = m_2(\emptyset) = 0$, then Florea *et al.*'s rule (2.20) and the new rule are are identical.

In addition, Florea *et al.* [38] proved that their rule can be written under Inagaki's form (2.16). Thus, because of 3) above, the relation between the new rule and Inagaki's rule can be investigated, but it is not in the scope of this work.

The new rule has commutativity which is important for a rule. The following theorem states the property.

Theorem 2.5.2 *The new combination rule defined in Definition 2.5.1 is commutative.*

Proof: Swapping m_1 and m_2 in (2.30a) and (2.30b) does not change the results. QED. ■

2.5.2 The form of functions $h(\kappa_{12})$ and $g(\kappa_{12})$

Finding out the true functions or values for $f(\kappa_{12})$, $h(\kappa_{12})$, $g(\kappa_{12})$ and α in *Definition 2.5.1* is not trivial. Each problem has its own characteristics, and there have been various forms for the

functions. Hence, attempting to approximate functions or tuning parameters with respect to each problem is more rational. Now some suggestions are provided on the selection of functions' forms and parameters. First, we study the function $f(\kappa_{12})$ and assume that $f(\kappa_{12})$ can be expressed in a polynomial form, i.e., $f(\kappa_{12}) = a_0 + a_1\kappa_{12} + ... + a_n\kappa_{12}^n$. Since (2.29a), $a_0 = 0$. In addition, (2.29b) yields $a_1 + ... + a_n = 1$. We also have the differentiation of $f(\kappa_{12})$ with respect to κ_{12} satisfies $f'(\kappa_{12}) = a_1 + 2a_2\kappa_{12} + ... + na_n\kappa_{12}^{n-1} > 0$ due to the monotonicity of $f(\kappa_{12})$. One of the possible functions for $f(\kappa_{12})$ is

$$f(\kappa_{12}) = \frac{e^{\gamma\kappa_{12}} - 1}{e^{\gamma} - 1} \tag{2.36}$$

where $\gamma > 0$. The reason for choosing $f(\kappa_{12})$ in (2.36) can be explained by applying the Taylor series theorem as

$$\begin{aligned} \frac{e^{\gamma\kappa_{12}} - 1}{e^{\gamma} - 1} =& 0 + \frac{1}{(e^{\gamma} - 1)1!}\gamma\kappa_{12} + \frac{1}{(e^{\gamma} - 1)2!}\gamma^2\kappa_{12}^2 + ... \\ &+ \frac{1}{(e^{\gamma} - 1)n!}\gamma^n\kappa_{12}^n + ... \end{aligned} \tag{2.37}$$

Next, the forms of $g(\kappa_{12})$ and $h(\kappa_{12})$ are discussed. Florea *et al.* [38] suggested the following forms for the two functions.

$$g(\kappa_{12}) = \frac{1 - \kappa_{12}}{1 - \kappa_{12} + \kappa_{12}^2} \text{ and } h(\kappa_{12}) = \frac{\kappa_{12}}{1 - \kappa_{12} + \kappa_{12}^2} \tag{2.38}$$

Such forms can avoid the undefined situation when $\kappa_{12} = 1$, and their behaviors respecting to the conflict κ_{12} seem persuasive. But through many examples, Dempster's rule (2.13) demonstrates it to be a powerful tool. Additionally, the extreme case $\kappa_{12} = 1$ is rare and does not provide much information for making decisions. Let us see an extreme example.

Example 2.5.2 *Let $\Theta = \{\theta_1, \theta_2, \theta_3\}$. Assume we have 3 BPAs as in Table 2.4.*

Table 2.4: Sources in *Example 2.5.2*

Source i	$m_i(\{\theta_1\})$	$m_i(\{\theta_2\})$	$m_i(\{\theta_3\})$
1	1.0	0.0	0.0
2	0.0	1.0	0.0
3	0.0	0.0	1.0

In *Example 2.5.2*, the three sources do not have any agreement. In such a case, it seems proper to assign either $m^{(.)}_{1\oplus 2\oplus 3}(\{\theta_1, \theta_2, \theta_3\}) = 1$ or $m^{(.)}_{1\oplus 2\oplus 3}(\emptyset) = 1$ after carrying out a rule. Dempster's rule with modifications can also be adopted as an alternative solution for the selection of $g(\kappa_{12})$ and $h(\kappa_{12})$:

$$g(\kappa_{12}) = \frac{1 - \beta\kappa_{12}}{1 - \kappa_{12}} \text{ and } h(\kappa_{12}) = \beta\kappa_{12} \tag{2.39}$$

where $0 \leq \beta \leq 1$. For the extreme case $\kappa_{12} = 1$, it is reasonable to force $g(\kappa_{12}) = 0$ and $h(\kappa_{12}) = 1$. Finally, the parameters α, γ, and β should be tuned based on each problem is recommended.

2.5.3 Modified pignistic transformation

By accepting the open world concept, it is necessary to redefine the pignistic probability transformation because it is possible that $\emptyset$ is an output of a decision making, i.e., $m^{(.)}_{1\oplus 2\oplus \ldots \oplus N}(\emptyset)) \neq 0$ is possible.

Definition 2.5.2 (Modified pignistic transformation) *Let m be a modified BPA on a FoD Θ. Its associated modified pignistic probability function $MBetP_\Theta$: $\{\theta_1, ..., \theta_n, \emptyset\} \longrightarrow [0, 1]$ is defined as*

$$MBetP_\Theta(\omega) = \sum_{A \subseteq \Theta, \omega \in A} \frac{m(A)}{|A|}, \omega \neq \emptyset \tag{2.40}$$

and

$$MBetP_\Theta(\emptyset) = m(\emptyset) \tag{2.41}$$

The transformation between m and $MBetP_\Theta$ is called the modified pignistic transformation.

2.5.4 Combine N sources

Similar to Florea *et al.*'s rule (2.20), the new rule in *Definition 2.5.1* is not associative in general. Thus, it is necessary to study how multiple sources are combined. A simple solution is adopting Florea *et al.*'s approach [38] to combine N sources, where N is a positive integer greater than 1. In particular, let $\{m_1, ..., m_N\}$ be a set of N modified BPAs over the FoD Θ. If Florea *et*

al.'s approach is adopted, one can have the following combination rule

$$\begin{aligned} m^{(.)}_{1\oplus 2\oplus ...\oplus N}(A) =&\Big(1-\alpha f(\kappa_{1...N})\Big)\Big(g(\kappa_{1...N}) \sum_{A=A_1\cap ...\cap A_n} m_1(A_1)...m_n(A_N) \\ &+ h(\kappa_{1...N}) \sum_{A=A_1\cup ...\cup A_n} m_1(A_1)...m_n(A_N)\Big),\ A\neq \emptyset \end{aligned} \tag{2.42}$$

and

$$\begin{aligned} m^{(.)}_{1\oplus 2\oplus ...\oplus N}(\emptyset) =&\alpha f(\kappa_{1...N}) + \Big(1-\alpha f(\kappa_{1...N})\Big)\Big(g(\kappa_{1...N}) m_1(\emptyset)...m_N(\emptyset) \\ &+ h(\kappa_{1...N}) m_1(\emptyset)...m_N(\emptyset)\Big) \end{aligned} \tag{2.43}$$

where the conflict

$$\kappa_{1...N} = \sum_{A_1\cap ...\cap A_n=\emptyset, A_1\cup ....\cup A_N\neq\emptyset} m_1(A_1)...m_N(A_N) \tag{2.44}$$

However, adopting the above approach does not take advantage of sources which are reliable and other sources which are unreliable. Hence, we seek another solution. Let κ_{ij} be the conflict between m_i and m_j, $i,j \in \{1,...,N\}$. Let $\kappa_i = \sum_{j\in\{1,...,N\}, j\neq i} \kappa_{ij}$, for all $i \in \{1,...,N\}$. The degree of reliability of the sources are then ranked based on κ_i; the higher κ_i is, the less the source i is reliable. We call κ_i the sum of conflict to source i to differ from the conflict. Let us see *Example 2.5.3*.

Example 2.5.3 *Let $\Theta = \{\theta_1, \theta_2\}$. Assume we have 3 BPAs as in Table 2.5.*

Table 2.5: Sources in *Example 2.5.3*

Source i	$m_i(\{\theta_1\})$	$m_i(\{\theta_2\})$
1	0.75	0.25
2	0.7	0.3
3	0.1	0.9

Intuitively, if we follow the majority rule and observe that

$$\sum_{i=\{1,2,3\}} m_i(\{\theta_1\}) = 1.55 > \sum_{i=\{1,2,3\}} m_i(\{\theta_2\}) = 1.45 \tag{2.45}$$

we then lean towards θ_1. However, Dempster's rule does not provide a result matching with our intuition; $m^{DS}_{1\oplus 2\oplus 3}(\{\theta_1\}) = 0.4375$ and $m^{DS}_{1\oplus 2\oplus 3}(\{\theta_2\}) = 0.5625$. As known, Dempster's rule is

associative; the result is the same when combining sources in any order. But this democracy may not be proper for cases like *Example 2.5.3*. Florea *et al.*'s rule (2.20) is also not fit here. Let $g(\kappa_{123}) = \frac{1-\kappa_{123}}{1-\kappa_{123}+\kappa_{123}^2}$ and $h(\kappa_{123}) = \frac{1-\kappa_{123}}{1-\kappa_{123}+\kappa_{123}^2}$, where κ_{123} is defined in (2.44) for three sources 1, 2, and 3. Then, $m^F_{1\oplus 2\oplus 3}(\{\theta_1\}) \approx 0.0587$ and $m^F_{1\oplus 2\oplus 3}(\{\theta_2\}) \approx 0.0755$, and $m^F_{1\oplus 2\oplus 3}(\{\theta_1, \theta_2\}) \approx 0.8658$. Let us try to combine the sources in a different order using the new rule in *Definition 2.5.1*. From *Example 2.5.3*, we can have $\kappa_1 = 1.1$, $\kappa_2 = 1.06$, and $\kappa_3 = 1.36$. The reliability of sources are ranked in an increasing order as: source 3, source 1, source 2. $g(\kappa_{ij})$ and $h(\kappa_{ij})$ are the two functions in (2.39), and let $\alpha = 0$. We combine source 3 with source 1. Then, this result is used to combine with source 2. The discrimination seems proper as the final results of the combincation are obtained as $m^{OR}_{(3\oplus 1)\oplus 2}(\{\theta_1\}) \approx 0.4875$, $m^{OR}_{(3\oplus 1)\oplus 2}(\{\theta_2\}) \approx 0.2780$, and $m^{OR}_{(3\oplus 1)\oplus 2}(\{\theta_1, \theta_2\}) \approx 0.2345$.

These above observations motivate us to propose a sequence of a combination of N sources in *Algorithm 2.1* in which our underlying idea is that if a source is more reliable, then it is asked late in the sequence of combination. As a result, the most reliable source is asked at the end to make final decisions. It is noted that *argsort* in *Algorithm 2.1* is a sort algorithm in ascending order, and it returns a set of indices.

Algorithm 2.1 The new rule to combine N sources

1. Initialize: $\{m_1, ..., m_N\}$
2. **for** $i := 1$ *to* N **do**
   - **for** $j := 1$ *to* N **do**
     - $\kappa_{ij} = \sum_{B\cap C=\emptyset, B\cup C\neq\emptyset} m_i(B)m_j(C)$
   - $\kappa_i = \sum_{j\in\mathcal{N}, j\neq i} \kappa_{ij}$
3. $\{I_1, ..., I_n\}$=argsort($[\kappa_1, ..., \kappa_N]$); Ascending sort and return indices
4. Define α, $f(\kappa_{ij})$, $g(\kappa_{ij})$ and $h(\kappa_{ij})$
5. $m^{OR}_{\oplus}$= Combining m_{I_n} and $m_{I_{N-1}}$ using (2.30a) and (2.30b)
6. **for** $i := 2$ *to* $N-1$ **do**
   - $m^{OR}_{\oplus}$= Combining m^{OR} and $m_{I_{N-i}}$ using (2.30a) and (2.30b)

return $m^{OR}_{\oplus}$

Let us justify *Algorithm 2.1* more. First, recall *Example 2.3.2* and apply Florea *et al.*'s rule with $g(\kappa_{ij})$ and $h(\kappa_{ij})$ defined in (2.38). It gives us $m^F_{1\oplus 2\oplus 3}(\theta_2) \approx 0.001$, $m^F_{1\oplus 2\oplus 3}(\{\theta_1, \theta_2\}) \approx 0.809$, $m^F_{1\oplus 2\oplus 3}(\{\theta_2, \theta_3\}) \approx 0.003$, $m^F_{1\oplus 2\oplus 3}(\{\theta_1, \theta_2, \theta_3\}) \approx 0.187$. If one uses the PPT, then $BetP_\Theta(\theta_1) \approx 0.4668$, $BetP_\Theta(\theta_2) \approx 0.4693$, and $BetP_\Theta(\theta_3) \approx 0.0638$. Since $BetP_\Theta(\theta_3) < BetP_\Theta(\theta_1) < BetP_\Theta(\theta_2)$, θ_2 is selected as the final decision because $BetP_\Theta(\theta_2)$ is the largest. This decision is the same if applying Dempster's, Deng's, and Jiang and Zhan's rules as we realized previously. As discussed,

Yager's rule is just to redistribute the conflict to Θ, the rule has no improvement on the situation either. *Example 2.3.2* can be generalized as

Example 2.5.4 *(Generalized Example 2.3.2) Let* $\Theta = \{\theta_1, \theta_2, \theta_3\}$. *Assume we have N BPAs as in Table 2.6.*

Table 2.6: Sources in *Example 2.5.4*

Source i	$m_i(\{\theta_1\})$	$m_i(\{\theta_2\})$	$m_i(\{\theta_3\})$
1	a_{11}	a_{12}	a_{13}
2	a_{21}	a_{22}	a_{23}
3	0.0	1.0	0.0
4	a_{41}	a_{42}	a_{43}
...	...	...	...
N	a_{S1}	a_{N2}	a_{N3}

It is easy to prove that if applying Dempster's rule, Yager's rule, Florea *et al.*'s rule, Deng's rule, Jiang and Zhan's rule, and Dubois and Prade's rule, and also the PPT is used, then θ_2 is always being selected. Let us study *Algorithm 2.1* for *Example 2.3.2*. Let $g(\kappa_{ij})$ and $h(\kappa_{ij})$ be defined in (2.38), and $\alpha = 0$. Then, we can have $\kappa_1 = 1.51$, $\kappa_2 = 1.51$, $\kappa_3 = 2.7$ and $\kappa_4 = 1.44$ as source 3 has the highest sum of conflict is reasonable. Finally, applying *Algorithm 2.1* gives us a result shown in Table 2.7. This result is more rational when considering source 3 as an unreliable source.

Table 2.7: Result of applying *Algorithm 2.1* for *Example 2.3.2*

$m_{\oplus}^{OR}(\{\theta_1\})$	$m_{\oplus}^{OR}(\{\theta_2\})$	$m_{\oplus}^{OR}(\{\theta_1, \theta_2\})$
≈ 0.871	≈ 0.0415	≈ 0.0745
$m_{\oplus}^{OR}(\{\theta_1, \theta_3\})$	$m_{\oplus}^{OR}(\{\theta_2, \theta_3\})$	$m_{\oplus}^{OR}(\{\theta_1, \theta_2, \theta_3\})$
≈ 0.0015	≈ 0.0004	≈ 0.0111

One may cast some doubt on the new rule. First, in *Example 2.3.2* and *Example 2.5.4*, it is possible that sources 1, 2 and 4 lack reliability. Recalling *Example 2.5.3*, there is also a hypothesis that source 3 is reliable and the other sources are not reliable. In the literature, there are works that weight sources with coefficients such as [45]. That is, each source is multiplied by a coefficient during a combination. It may be, however, not trivial to obtain coefficients' values. Second, it is critical to

Table 2.8: Result of applying *Algorithm 2.1* for *Example 2.3.2*

$m^{OR}(\{\theta_1\})$	$m^{OR}(\{\theta_2\})$	$m^{OR}(\{\theta_1,\theta_2\})$
≈ 0.871	≈ 0.0415	≈ 0.0745
$m^{OR}(\{\theta_1,\theta_3\})$	$m^{OR}(\{\theta_2,\theta_3\})$	$m^{OR}(\{\theta_1,\theta_2,\theta_3\})$
≈ 0.0015	≈ 0.0004	≈ 0.0111

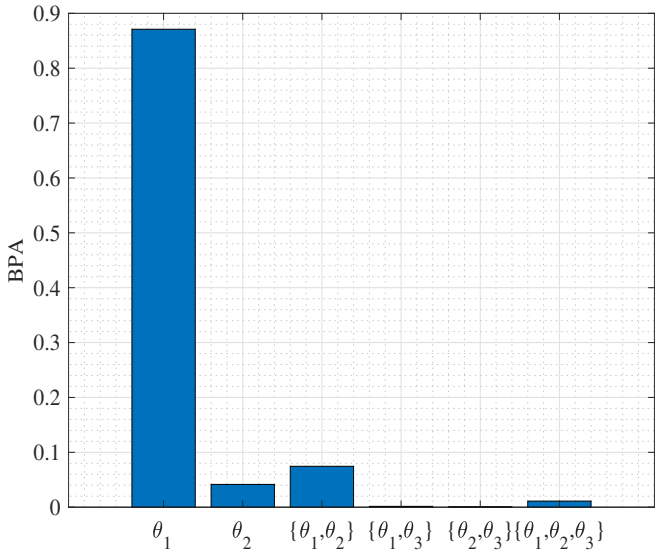

Figure 2.4: Results of appplying *Algorithm 2.1* to *Example 2.3.2*.

know the behavior of the new rule in case of all sources having a high degree of agreement as the existing rules well address. As the first answer to defend our approach, we count on the majority voting rule principle in a reverse order that each κ_{ij} is considered as a vote. As can be seen, we allow interactions among sources before making combinations. A complementary answer lies in the problem of function and parameter selection in step 4 of *Algorithm 2.1*. To see, let us exploit the function forms in (2.39) to *Example 2.5.3*. Let β range from 0 to 1. Figure 2.5 shows $BetP_\Theta(\{\theta_1\})$ and $BetP_\Theta(\{\theta_2\})$ with two orders of combination: 1) 2→1→3 and 2) 3→1→2. Obviously, the latter gives a reasonable result. As seen, the chance of either θ_1 or θ_2 being selected depends on the parameter selection in the case of the second sequence, while there is no chance for θ_1 if applying the first sequence. For the second doubt, our approach can be judged by the following example, which is a modification of *Example 2.5.3*.

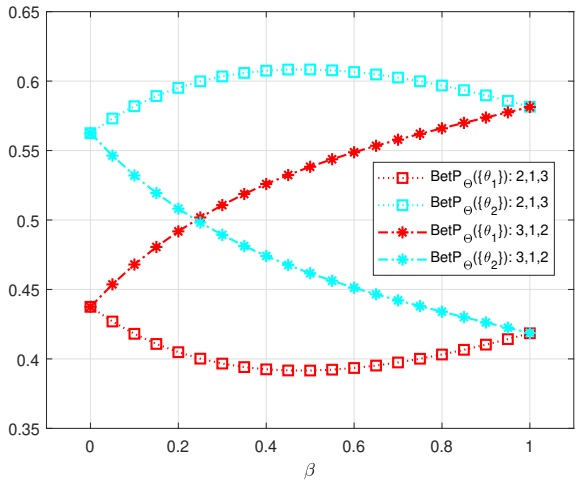

Figure 2.5: Pignistic probabilities of *Example 2.5.3*.

Example 2.5.5 *Let* $\Theta = \{\theta_1, \theta_2\}$. *Assume we have 3 BPAs as in Table 2.9.*

Table 2.9: Sources in *Example 2.5.5*

Source i	$m_i(\{\theta_1\})$	$m_i(\{\theta_2\})$
1	0.75	0.25
2	0.7	0.3
3	0.7	0.3

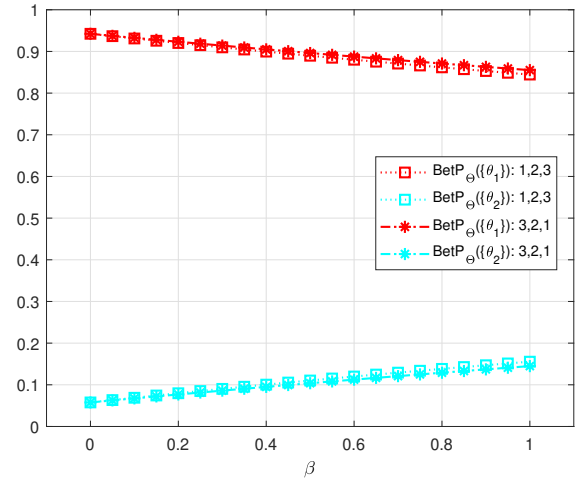

Figure 2.6: Pignistic probabilities of *Example 2.5.5*.

For this example, one can have $\kappa_1 = 0.8$, $\kappa_2 = 0.82$, and $\kappa_3 = 0.82$. Similarly, one can obtain Figure 2.6 which demonstrates an appropriate decision making.

Chapter 3

Energy Management: A New Distributed Optimization Strategy

Chapter 3's Nomenclature

DG	Distributed generation
DER	Distributed energy resources
EM	Energy Management
EV	Electric Vehicle
ADMM	Alternating Direction Method of Multipliers
CHIL	Controller-Hardware-In-the-Loop
MG	Main grid
MT	Microturbines
WT	Wind turbines
PV	Photovoltaic
N	Number of buses
r, s	Region index
n, m	Bus index
PF	Power factor
$P_n^A(Q_n^A)$	Active (reactive) power generated by DER type A at bus n
$P_n(Q_n)$	Active (reactive) power injected at bus n

$V_n = V_n^{re} + jV_n^{im}$	Complex bus voltage
θ_n	Bus voltage angle
$\mathcal{N}$	Set of all buses
$\mathbf{Y}$	Admittance matrix
$\mathcal{MT}$	Set of buses where an MT is installed
$\mathcal{WT}$	Set of buses where a WT is installed
$\mathcal{PV}$	Set of buses where a PV system is installed
$\overline{A}$	Maximum of variable A
$\underline{A}$	Mimimum of variable A

3.1 Literature Review in EM

EVs are widely considered as a replacement for internal combustion engine vehicles as they are environmentally friendly and beneficial to sustainable energy goals. However, the increases of EV penetration and EV charging capacities negatively impact distribution grids as it is shown in [58] that a distribution grid fails to maintain required voltages when the EV penetration level reaches 30%. Besides, it is expected that distribution grids will be populated with heterogeneous DERs [4]. Therefore, an EM coordinating energy sources to gain economic objectives while maintaining power quality under the impact of EV penetration is valuable.

EM is one of the constituents of future distribution grids' control and management system [10]. The primary function of EM is to optimally allocate power generation and delivery to sources of energy in a well-defined sense while adhering to system constraints [11], [12], [13], [14], [15], [16]. Distributed EM is considered superior to the centralized counterpart in terms of resiliency and scalability. Yet, the global optimality of the distributed EM's optimization problem is still an issue.

The alternating direction method of multipliers (ADMM) [18] is a popular method to solve the EM's optimization problem [19], [20], [21]. The popularity of the ADMM is attributed to its efficiency and straightforwardness as it is applied to various applications with three clear updating steps. It is worth noticing that the theoretical guarantee of convergence of the ADMM is confined to convex optimization problems. However, the EM's optimization problem for AC networks are well known to be non-convex. There are papers that do not consider the bus voltage constraints and power limits on transmission lines in the EM's optimization problem [17]. However, it is likely to violate these constraints with the adoptions of DERs and EVs.

Realistic representation of EV charging demand is a major need for examining the effectiveness of innovative EM approaches accurately. The studies in the literature are mainly based on either direct use of charging profile data collected from field demonstrations [59] or deterministic charging scenarios built on general assumptions [60]. However, these conventional methodologies have some drawbacks. Charging data from a field pilot usually has limited representation (due to a low number of participants, short testing period, and cars from a few brands) and constrained availability to other researchers. On the other hand, widespread assumptions about using the same charging demand and energy storage capabilities, considering starting and ending times from a limited time period of the day, straightforward determination of the number of charging sessions, initial and final State of Charge (SoC) values, distinguished consideration of slow and fast charging profiles are considerably far from observations in the field [61].

For a better representation of the EV charging demand of a large group of customers, a novel and easily replicable methodology is developed and used. It is based on the combined use of characteristics of a wide range of cars available on a country level, charging starting and ending time probabilities, SoC value probabilities, and driving statistics. A unique feature of the methodology is consecutive relations built between slow and fast charging sessions.

3.1.1 Statement of Contributions

In this paper, a two-step distributed EM scheme is proposed. The first step is to search for the global optimality by relaxing some constraints in the EM's optimization problem to reduce it to a convex one. In doing so, a secured global optimality algorithm can be applied. Its optimized results are used to reconfigure dispatchable active and reactive constraints in the second step considering the full problem. Reconfiguring the active power constraints makes an ADMM-based algorithm in the second step seeks solutions in a narrowed region around the global optimality. Besides, the reconfiguration of the reactive constraints ensures power factor (PF) requirements are satisfied. EV charging load profiles, generated through a novel approach for a highly realistic representation of daily cases in EV integrated distribution grids, are used to test the proposed strategy. Slow and fast charging sessions of a large number and a wide range of cars available in the US market are considered together in the explored scenarios. Based on a thorough literature review, there is no existing work implementing distributed EM via a CHIL setup. This work is one step further as CHIL experimental evidence is shown.

3.1.2 Chapter Organization

The remainder of this Chapter is organized as follows. In Section 3.2, the EM problem is derived and formulated. For ease of understanding, common notations are presented in the section. Section 3.3 is dedicated to present the two-step distributed EM strategy. The CHIL demonstration of the proposed scheme is discussed in Section 3.4.

3.2 Problem Formulation

Consider a grid-connected distribution network consisting of heterogeneous DERs dispersed over the network: microturbines (MT), wind turbines (WT), and photovoltaic (PV) systems. It is desired that the grid 1) operates at economically optimal points, 2) maintains voltage satisfaction for all the buses, and 3) adheres to power generation and delivery capacity limits while meeting the power balance constraint.

3.2.1 Notations

Let an undirected graph $(\mathcal{N}, \mathcal{E})$ represent the grid, where $\mathcal{N} = \{1, ..., N\}$ is the set of nodes and $\mathcal{E} = \{(n, m)\} \subseteq \mathcal{N} \times \mathcal{N}$ is the set of lines. The terms *bus* and *node* are used interchangeably in this paper. The bus connecting directly with the substation is indexed 1. Let $\mathcal{MT} \subset \mathcal{N}$ be the set of nodes that have MTs installed. Additionally, $\mathcal{PV} \subset \mathcal{N}$ and $\mathcal{WT} \subset \mathcal{N}$ are the sets of buses where PVs and WTs are installed, respectively. The system is divided into R regions; each has a dispatchable source of energy, either a substation or an MT. Assume that each bus in a region does not have more than one connection with buses outside the region. Let $\mathcal{R} = \{1, ..., R\}$ and $\mathcal{R}_r$ be the set of nodes in region r. Denote $\mathcal{N}_n$ ($\mathcal{N}_r$) is the neighboring nodes (regions) of node n (region r).

Let $Tr(.)$, $(.)^*$, $(.)^T$, and $(.)^H$ be the trace operator, complex conjugate, transposition, and complex conjugate transposition operators, respectively. Let $[a_{ij}]_{l\times k}$ be a $l \times k$ matrix. Throughout this paper, there are some common notations. P and Q accordingly indicate active and reactive power. Subscripts m and n are the bus index and subscripts r and s are the region index. Moreover, superscripts re, im, MG, MT, EV, PV, and L accordingly indicate the real part, the imaginary part, the main grid, MT, EV, PV, and non-EV load. For example, with these notations, P_n^{MT} and Q_n^{MT} are active and reactive power generated from an MT at bus n, respectively. Overline and underline indicate lower and upper limits of a quantity, respectively. Let $V_n = V_n^{re} + jV_n^{im}$ be the

bus voltage at bus n. The signs of active power P_n (reactive power Q_n) at node n is defined as follows: if $P_n > 0$ ($Q_n > 0$), then node n injects active (reactive) power to the network, otherwise it absorbs active (reactive) power.

3.2.2 Cost Functions

The active power of the dispatchable sources can be adjusted to gain economic objectives formed in the following function:

$$f_1(P_1^{MG}) + \sum_{n \in \mathcal{M}} f_n(P_n^{MT}) \tag{3.1}$$

The first term in (3.1) is the cost of buying power from the main grid which is a multiplication of the market price c^{MG} ($\$/kWh$) and the amount of active power supplied from the main grid. The second term is the cost of power generated by the MTs which has the following form

$$f_n(P_n^{MT}) = c^F \Big(\alpha_n (P_n^{MT})^2 + \beta_n P_n^{MT} + \gamma_n \Big), \alpha_n > 0 \tag{3.2}$$

where c^F ($\$$/gallon) is the cost of fuel.

3.2.3 EV Charging

A probabilistic charging profile generation methodology that combines characteristics and statistics from a range of data resources is employed. The profile generator builds relations between slow and fast charging sessions to represent the EV charging profile of a large number of cars, including residential and public charging cases. In the first stage, characteristics of the 23 cars that are available in the US market over the last decade are considered based on the information available in [62] and [63]. Slow and fast charging demand and times, energy storage capability, and energy consumption per kilometer are imported into the charging profile generation methodology as the main car characteristics. The slow charging demand of the considered cars ranges between 3.6 to 16.5 kW with 3 to 14 hours full charging time. The fast charging demand of the considered EVs ranges between 22 to 110 kW with 20 to 80 minutes charging time up to around 90% SoC level. Depending on the number of customers defined in a scenario, a random EV from the determined pool of cars is assigned to each customer.

In the next stage, probabilities for slow charging sessions are defined based on [61]. The detailed probabilities are available in the cited publication. These consist of the overall share of customers who charge their car at least once a day, probabilities of charge starting time (in 15-minute ranges), initial and final SoC values (in 8.33% ranges -due to SoC recording resolution used in the considered field pilot-, depending on the period of starting time, called as morning peak between 06:00-09:00 AM, evening peak from 03:00 to 09:00 PM and the rest of the day). After a range is selected for a customer's charging session, a random number inside that range is chosen as the exact starting time. A similar approach is followed to assign initial and final SoC values for the considered sessions. Using the assigned initial and final SoC values and charging times from car characteristics, the charging duration for each car is calculated. Taking into account the assigned charge starting times and the calculated charging durations, charge ending times are derived. Additional idle waiting times/parking times are assigned based on the statistics provided in [64]. A charging model that is based on the constant current charging up to around 90% SoC, and then the linear limitation of power for most of the vehicles provided in [65] is used as part of the profile generation tool. The details of this model can be found in the reference.

A transitional period follows the slow charging session, considering only the cars that are charged more than once a day. During this period, cars are driven, spend the energy stored in their batteries, and park based on the comprehensive statistics provided in [66] on distance traveled and time spent between charging sessions.

The fourth stage is fast charging in public charging stations. Considering the departure times from the previous charging session and adding on the time spent during the transitional period, fast charge starting times are calculated. In a similar manner, considering the final SoC values from the previous charging sessions and the energy spent/SoC reduced (calculated according to the distance traveled and energy consumed per kilometer) between two charging sessions, the initial SoC values for the fast charging session are derived. Since full fast charging times (ranging from 20 to 80 minutes, with around 40 minutes on average) are below typical charging durations, all the cars are assumed to be fully charged up to 90% SoC in fast charging sessions. Considering the derived fast charge starting times, initial SoC values, and minimum charging up to 90% SoC, fast charge ending times are calculated. As in stage 2, an additional time for parking or idle waiting is assigned, and departure times are calculated.

If a charging session ends on the next day, all the hours with charging demand in the next

day are also considered. This is required to make clear comparisons between the cases without and with distributed EM. Random assignment of cars to each customer and random selection of the exact charge starting times and exact initial SoC values for the first slow charging session allow generation of different individual and aggregated daily charging profiles at each run.

3.2.4 Constraints

An MT unit has lower and upper generation capacity limits on both active and reactive power as

$$\underline{P_n^{MT}} \leq P_n^{MT} = (P_n - P_n^L - P_n^{EV}) \leq \overline{P_n^{MT}} \tag{3.3a}$$

$$\underline{Q_n^{MT}} \leq Q_n^{MT} = (Q_n - Q_n^L - Q_n^{EV}) \leq \overline{Q_n^{MT}} \tag{3.3b}$$

Similarly, the main grid is imposed these constraints as

$$\underline{P_1^{MG}} \leq P_1^{MG} = (P_1 - P_1^L - P_1^{EV}) \leq \overline{P_1^{MG}} \tag{3.4a}$$

$$\underline{Q_1^{MG}} \leq Q_1^{MG} = (Q_1 - Q_1^L - Q_1^{EV}) \leq \overline{Q_1^{MG}} \tag{3.4b}$$

For a PV node, i.e., $n \in \mathcal{PV}$, all injections and withdrawals at the bus equals 0; that is,

$$P_n - (P_n^{PV} + P_n^L + P_n^{EV}) = 0 \tag{3.5}$$

It is assumed that PV systems actively participate in regulating bus voltages by adjusting reactive power, which is confined in following range:

$$\underline{Q_n^{PV}} \leq Q_n^{PV} = (Q_n - Q_n^L - Q_n^{EV}) \leq \overline{Q_n^{PV}} \tag{3.6}$$

WTs are similar to PVs as

$$P_n - (P_n^{WT} + P_n^L + P_n^{EV}) = 0 \tag{3.7a}$$

$$\underline{Q_n^{WT}} \leq Q_n^{WT} = (Q_n - Q_n^L - Q_n^{EV}) \leq \overline{Q_n^{WT}}. \tag{3.7b}$$

Let bus 1 be the slack bus. The voltage magnitude at bus $n \in \mathcal{N} \setminus \{1\}$ are desired to be

confined in a bounded region defined as

$$\underline{|V_n|} \leq |V_n| \leq \overline{|V_n|} \tag{3.8}$$

Typically, $\underline{|V_n|} = 0.95$ per units (pu) and $\overline{|V_n|} = 1.05$ pu are used. If phase angles of voltages at the buses are confined, power transmitted on lines are bounded. Therefore, a constraint is set on the voltage phase angle at bus $n \in \mathcal{N} \setminus \{1\}$ as

$$-\overline{\theta_n} \leq \theta_n = \arctan(\frac{V_n^{im}}{V_n^{re}}) \leq \overline{\theta_n} \tag{3.9}$$

3.2.5 EM's Optimization Task

Given the costs and constraints presented in the previous subsections, the optimization task is stated as

$$\min \Big(f_1(P_1^{MG}) + \sum_{n \in \mathcal{M}} f_n(P_n^{MT}) \Big) \tag{3.10a}$$

$$s.t. \quad (3.3), (3.4), (3.5), (3.6), (3.7), (3.8), (3.9). \tag{3.10b}$$

The problem (3.10) can be transformed into an equivalent one which has voltages as the only variables [67], [68]. Denote the bus voltage vector by $\mathbf{V} = [V_1, ..., V_N]^T$ and the bus admittance matrix by $\mathbf{Y} = [Y_{lk}]_{N \times N}$. Let $\{\mathbf{e}_n\}_{n \in \mathcal{N}}$ form standard basis vectors in $\mathbb{R}^n$, in which $\mathbf{e}_n \coloneqq [0, ..., 1, ..., 0]^T$ is defined as the $n-$element of $\mathbf{e}_n$ is 1 and the others are 0. The following transformation can be obtained [67], [68]:

$$\mathbf{Y}_n \coloneqq \mathbf{e}_n \mathbf{e}_n^T \mathbf{Y} \tag{3.11a}$$

$$|V_n|^2 = \mathrm{Tr}(\mathbf{V}\mathbf{V}^H) \tag{3.11b}$$

$$\mathscr{P}_n \coloneqq \frac{1}{2}\Big(\mathbf{Y}_n + (\mathbf{Y}_n)^H\Big) \tag{3.11c}$$

$$P_n = \mathrm{Tr}(\mathscr{P}_n \mathbf{V}\mathbf{V}^H) \tag{3.11d}$$

$$\mathscr{Q}_n \coloneqq \frac{j}{2}\Big(\mathbf{Y}_n - (\mathbf{Y}_n)^H\Big) \tag{3.11e}$$

$$Q_n = \mathrm{Tr}(\mathscr{Q}_n \mathbf{V}\mathbf{V}^H) \tag{3.11f}$$

P_n and Q_n can be expressed as functions of $\mathbf{V}$, so do the cost function and the constraints in (3.10).

3.3 Distributed EM Strategy

In this section, a distributed strategy, which consists of two steps, is discussed. In the first step, the optimization task is relaxed by neglecting the voltage and reactive power constraints; i.e., (3.10) is relaxed to

$$\min f(\mathbf{P}^D) = \Big(f_1(P_1^{MG}) + \sum_{n\in\mathcal{M}} f_n(P_n^{MT})\Big) \tag{3.12a}$$

$$s.t. \quad (3.3a), (3.4a), (3.5), (3.7a). \tag{3.12b}$$

where $\mathbf{P}^D = [..., P_r^D, ...]^T$, $r \in \mathcal{R}$, is a vector consisting of the dispatchable active power of all the regions, and P_r^D is P_1^{MG} if region r has the substation and P_n^{MT} if region r has an MT at bus n.

The goal of the first step is to find the optimal allocation of active power for the dispatchable sources. Its optimized outcomes are then fed into the second step in which constraints (3.3) and (3.4) are reconfigured based on the inputs. The active power inequality constraints are reconfigured such that the box constraints are narrowed to the region around the solutions of (3.12), which are denoted as $P^{MG,*}$ and $P_n^{MT,*}$, as

$$\max(P_n^{MT,*} - \Delta P_n^{MT}, \underline{P_n^{MT}}) \le P_n^{MT} \le \min(P_n^{MT,*} + \Delta P_n^{MT}, \overline{P_n^{MT}}) \tag{3.13a}$$

$$\max(P^{MG,*} - \Delta P^{MG}, \underline{P^{MG}}) \le P^{MG} \le \min(P^{MG,*} + \Delta P^{MG}, \overline{P^{MG}}) \tag{3.13b}$$

where $\Delta P_n^{MT} = \sigma|P_n^{MT,*}|$ and $\Delta P^{MG} = \sigma|P^{MG,*}|$, where $0 < \sigma < 1$. For the reactive power inequality constraints at buses where MTs are installed, a minimum PF of 0.95 with active power referred to solutions of (3.12) are allowed. In the second step, the optimization task (3.10) is considered. In [17], only step 1 is considered. However, with the adoptions of EVs and DERs, the voltage constraints and power transmission limits on transmission lines are likely violated. There are work that consider only step 2 and utilize the ADMM to solve the EM's optimization problem [19], [20], [21]. But (3.10) is a non-convex optimization problem, and the convergence and global

optimality are not ensured.

3.3.1 Step 1

Denote the sum of non-dispatchable active power and loads at bus n by $P_n^S = P_n^{PV} + P_n^{WT} + P_n^L + P_n^{EV}$, $\forall n \in \mathcal{N}$. The augmented Lagrangian of (3.12) is

$$\begin{aligned} L_1 = & f(\mathbf{P}^D) + \mu\Big(\sum_{r\in\mathcal{R}} P_r^D + \sum_{n\in\mathcal{N}} P_n^S\Big) \\ & + \sum_{r\in\mathcal{R}} \lambda_r^{max}(P_r^D - \overline{P_r^D}) + \sum_{r\in\mathcal{R}} \lambda_r^{min}(-P_r^D + \underline{P_r^D}) \\ & + \frac{\rho_1}{2} \parallel \sum_{r\in\mathcal{R}} P_r^D + \sum_{n\in\mathcal{N}} P_n^S \parallel^2 \end{aligned} \tag{3.14}$$

where μ, λ_r^{max}, and λ_r^{min} are Lagrange multipliers, and $\rho_1 > 0$. In [69] and [70], a distributed algorithm based on the singular perturbation method is proposed aiming to solve a general optimization problem. The underlying idea of the algorithm is constructing a two-time-scale dynamical system which has an equilibrium point satisfying the Karush–Kuhn–Tucker conditions: the first set of equations is called the fast dynamic layer and the second set is called the slow dynamic layer. The fast dynamic layer can be derived as

$$\begin{aligned} \dot{\xi}_r^h = & -\xi_r^h - \sum_{s\in\mathcal{N}_r}(\xi_r^h - \xi_s^h) - \sum_{s\in\mathcal{N}_r}(\zeta_r^h - \zeta_s^h) \\ & + \Big(P_r^D + \sum_{n\in\mathcal{R}_r} P_n^S\Big) \end{aligned} \tag{3.15a}$$

$$\dot{\zeta}_r^h = \sum_{s\in\mathcal{N}_r}(\xi_r^h - \xi_s^h) \tag{3.15b}$$

$$\dot{\xi}_r^\mu = -\xi_r^\mu - \sum_{s\in\mathcal{N}_r}(\xi_r^\mu - \xi_s^\mu) - \sum_{s\in\mathcal{N}_r}(\zeta_r^\mu - \zeta_s^\mu) + \mu_r, \tag{3.15c}$$

$$\dot{\zeta}_r^\mu = \sum_{s\in\mathcal{N}_r}(\xi_r^\mu - \xi_s^\mu), \tag{3.15d}$$

It is noted that (3.15a) is to estimate the average of $(\sum_{r\in\mathcal{R}} P_r^D + \sum_{n\in\mathcal{N}} P_n^S)$, i.e., $\xi_r^h \longrightarrow \frac{1}{R}(\sum_{r\in\mathcal{R}} P_r^D + \sum_{n\in\mathcal{N}} P_n^S)$. The following is the slow dynamic layer

$$\dot{x}_r = -\epsilon k_r^x \Big(\frac{\partial f_r}{\partial x_r}(x_r) + \xi_r^\mu + \lambda_r^{max} - \lambda_r^{min} + \rho_1 \xi_r^h \Big) \tag{3.16a}$$

$$\dot{\mu}_r = \epsilon k_r^\mu \Big(\xi_r^h - \sum_{s\in\mathcal{N}_r} (\mu_r - \mu_s) \Big) \tag{3.16b}$$

$$\dot{\lambda}_r^{max} = \epsilon k_r^{\lambda^{max}} (x_r - \overline{P_r^D}) \tag{3.16c}$$

$$\dot{\lambda}_r^{min} = \epsilon k_r^{\lambda^{min}} (-x_r + \underline{P_r^D}) \tag{3.16d}$$

While $\epsilon \ll 1$ is a real positive number which aims to have (3.16) having a slower dynamics than that of (3.15), k_r^x, k_r^μ, $k_r^{\lambda^{max}}$, and $k_r^{\lambda^{min}} \in \mathbb{R}_{>0}$ are to cope with differences in the dynamics of x_r, μ_r, λ_r^{max}, and λ_r^{min}.

3.3.2 Step 2

The ADMM algorithm [18] is briefly presented before deriving its application to the considered optimization problem. Consider the following optimization problem:

$$\min \Big(f(\mathbf{x}) + g(\mathbf{z}) \Big) \tag{3.17a}$$

$$s.t. \qquad \mathbf{A}\mathbf{x} + \mathbf{B}\mathbf{z} = \mathbf{c} \text{ and } \mathbf{x} \in \mathcal{C}_x, \mathbf{z} \in \mathcal{C}_z \tag{3.17b}$$

where $\mathbf{x}$ and $\mathbf{z}$ are vectors of variables, $\mathbf{c}$ is a constant vector, $\mathcal{C}_x$ and $\mathcal{C}_z$ are their constraint sets, and $\mathbf{A}$ and $\mathbf{C}$ are matrices. Suppose the vectors and matrices have appropriate dimensions. The associated augmented Lagrangian is

$$\begin{aligned} L_2(\mathbf{x}, \mathbf{z}, \mathbf{y}) =& f(\mathbf{x}) + g(\mathbf{z}) + \mathbf{y}^T(\mathbf{A}\mathbf{x} + \mathbf{B}\mathbf{z} - \mathbf{c}) \\ &+ \frac{\rho_2}{2} \parallel \mathbf{A}\mathbf{x} + \mathbf{B}\mathbf{z} - \mathbf{c} \parallel_2^2 \end{aligned} \tag{3.18}$$

where $\rho_2 > 0$. The ADMM has three repetitively updating steps as

$$\mathbf{x}^{k+1} = \arg\min_{\mathbf{x}\in\mathcal{C}_x} L_2(\mathbf{x}, \mathbf{z}^k, \mathbf{y}^k) \tag{3.19a}$$

$$\mathbf{z}^{k+1} = \arg\min_{\mathbf{z}\in\mathcal{C}_z} L_2(\mathbf{x}^{k+1}, \mathbf{z}, \mathbf{y}^k) \tag{3.19b}$$

$$\mathbf{y}^{k+1} = \mathbf{y}^k + \rho_2(\mathbf{A}\mathbf{x}^{k+1} + \mathbf{B}\mathbf{z}^{k+1} - \mathbf{c}) \tag{3.19c}$$

The ADMM's configuration is now specified to fit the optimization problem. Applying the ADMM for consensus optimization problem [18], let $g(\mathbf{z}) = 0$ and $\mathbf{c} = 0$. Define a voltage vector $\mathbf{V}_r = [..., V^{re}_{r,n}, ..., V^{re}_{r,m}, ..., V^{im}_{r,n}, ..., V^{im}_{r,m}, ...]^T$, where bus n is in region r and bus m is not region r but it has a neighbor in region r. Let $\mathbf{x} = [\mathbf{V}_1^T, ..., \mathbf{V}_R^T]^T$ and decompose $f(\mathbf{x})$ as

$$f(\mathbf{x}) \equiv \sum_{n\in\mathcal{MT}\cup\{1\}, n\in\mathcal{R}_r} f_n(\mathbf{V}_r) \tag{3.20}$$

Define the matrix $\mathbf{A} = [a_{ij}]_{4l\times k}$ such that it is full row rank and l is the number of edges connecting two nodes of two different regions and k is the dimension of $\mathbf{x}$. Additionally, $a_{ij} = |\kappa|$ if $j-$th element of $\mathbf{x}$, which is either $V^{re}_{r,n}$ or $V^{im}_{r,n}$ with bus n has a neighbor not in region r. Otherwise, $a_{ij} = 0$. The matrix $\mathbf{B}$ is defined as $\mathbf{B} = -\mathbf{I}_{4l\times 4l}$, where $\mathbf{I}_{4l\times 4l}$ is the $4l \times 4l$ identity matrix. In the second updating step, z^{k+1} is the solution of the following equation

$$\frac{\partial L_2(\mathbf{x}^{k+1}, \mathbf{z}, \mathbf{y}^k)}{\partial \mathbf{z}}|_{\mathbf{z}\in\mathcal{C}_z} = 0 \tag{3.21}$$

which can be expressed as

$$\mathbf{z}^{k+1}|_{\mathbf{z}\in\mathcal{C}_z} = \mathbb{P}(\frac{1}{\rho_2}\mathbf{y}^k + \mathbf{A}\mathbf{x}^{k+1}) \tag{3.22}$$

If $\mathbf{y}$ has a zero initialization and $\mathbf{z}^0 = \mathbb{P}(\mathbf{A}\mathbf{x}^0)$, then $\mathbf{z}^{k+1} = \mathbb{P}(\mathbf{A}\mathbf{x}^{k+1})$, where $\mathbb{P}$ is the orthogonal projection operator on $\mathcal{C}_z$. The orthogonal projection matrix $\mathbb{P} = [p_{ij}]_{4l\times 4l}$ is selected such that $p_{ii} = \frac{1}{2}$, $p_{ij} = -\frac{1}{2}$ if both the $i-$th and $j-$th elements of $\mathbf{A}\mathbf{x}^{k+1}$ are either the real part or the imaginary part of a bus's voltage optimized in two regions, otherwise $p_{ij} = 0$. With the specified configuration, voltages of a bus (both the real part and imaginary) optimized in two different controllers reach a consensus as $(\mathbf{A}\mathbf{x}^k - \mathbf{z}^k) \longrightarrow 0$ when $k \longrightarrow \infty$.

3.4 CHIL Experimentation

This section first describes the CHIL implementation of the proposed distributed EM that system modeling, experimental equipment, and data preparation are presented. Then, the CHIL system is run to collect experimental results, which are later shown and discussed.

3.4.1 CHIL Implementation

3.4.1.1 CHIL Setup

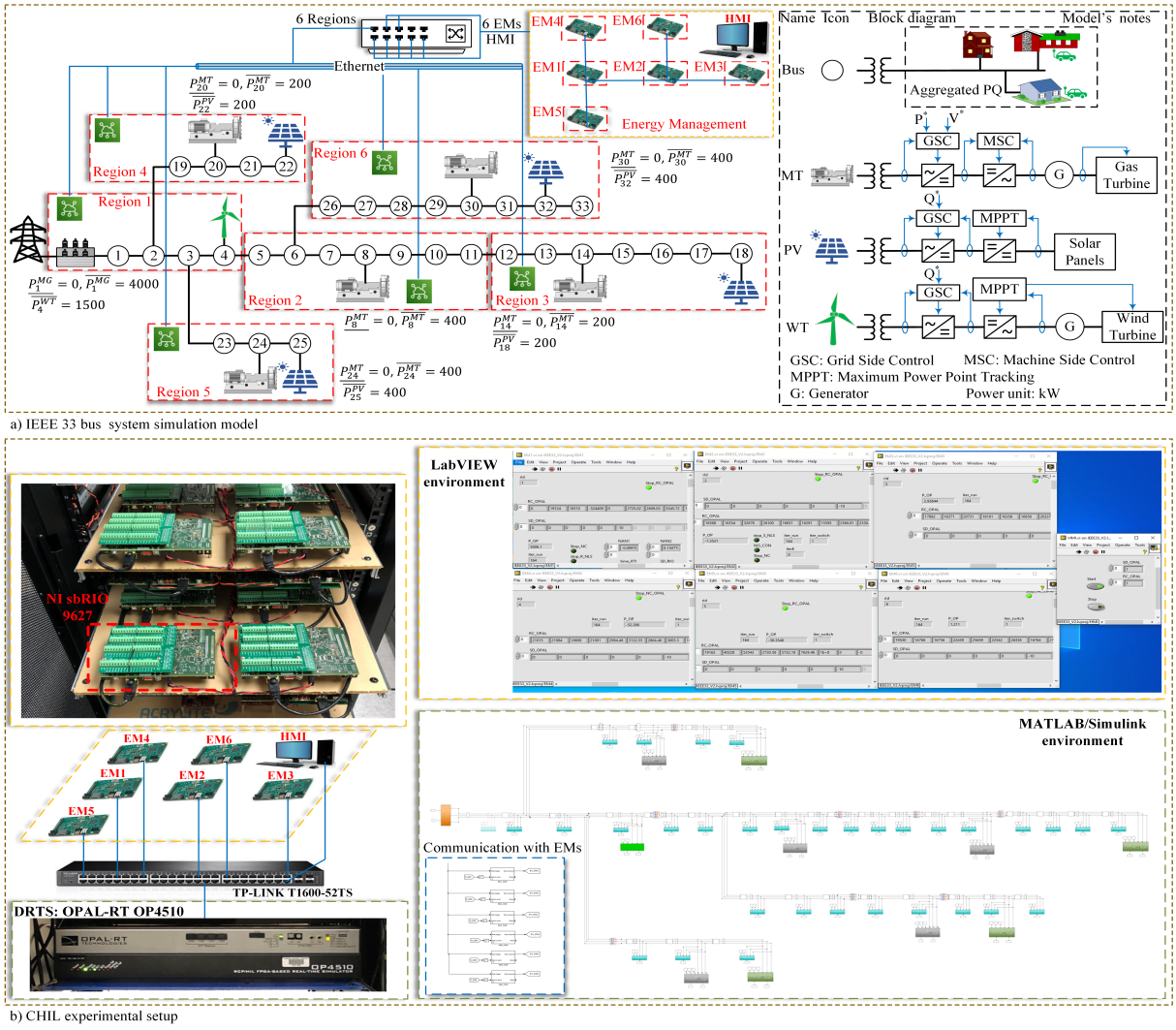

Figure 3.1: CHIL experimentation: a) IEEE bus system simulation model b) CHIL experimental setup.

The IEEE 33 bus system in [71] with additions of DERs is used to validate the proposed scheme. The system is geographically divided into 6 regions, and each has an EM to manage the region. These DERs' locations, parameters, and block diagrams are shown in Figure 3.1a. Rowen's model is used to simulate MTs' engines [72], and the control structure in [73] is applied to integrate the MTs with the grid through power electronics converters. Furthermore, the type 4 wind turbine model in [74] is used, and the control model of the PVs is taken from [75]. Additionally, PV panels are modeled by the double-diode model with parameters extracted from the Siemens SM50 solar panel's specifications. Because the main focus of this paper is EM and the real-time simulator has a computational limitation, average models for power electronics converters of the MTs, and PVs, and WT are sufficient to demonstrate the EM strategy. The system is simulated by MATLAB/Simulink and deployed to a real-time simulator OPAL-RT OP4510. The EM strategy is realized by LabVIEW and deployed into NI sbRIO 9627 controllers. EM's results are passed to the model running in the simulator as setpoints. The MTs have a duty of controlling active and reactive power injected into the network and bus voltages at which the MTs are installed, while the WT and the PVs are controlled to reach the commanded reactive power from EMs. A 1-Gbps ethernet network is established by a TP-LINK T1600G-52TS switch. The real-time simulator communicates with the controllers by the User Datagram Protocol (UDP), while the communication protocol among the controllers is the RTI Data Distribution Service (DDS). Figure 3.1b illustrate the CHIL experimental setup.

Figure 3.2a illustrates the EM program. There are two main blocks running in parallel: Optimization Block and Communication Block. The former is to implement the two-step optimization process while the latter exchanges data among the controllers and the simulator with the controllers. NI sbRIO 9627 boards are powered by a dual core ARM Cortex-A9 microprocessor which allows the parallel running of the two blocks. Every 15 minutes, information of non-EV load, EV load, and weather data are fed into EMs, each EM can only receive these information of buses which it manages. Although these values can be generated from forecasting engines online, they are stored in the simulator and are sent to sbRIOs by the UDP protocol as this work primarily studies EM. Each controller uses this information and local system data of the region to form a struct called $sysInfo$. Local system data are admittance matrix, and WT and PVs's system parameters to estimate their power generation outputs given weather data. Information of cost functions and constraints can be extracted from the struct.

Distributed algorithms are typically designed with the synchronous updating assumption.

Therefore, we design a synchronous updating mechanism to meet this assumption. In the exchanging data frame, the iteration index is added at the end. A circular buffer reads the data coming from neighboring nodes, and the buffer is updated by the first in first out rule if it discerns a difference in the iteration index, otherwise it ignores the receiving data. Every iteration, the controller reads the circular buffer and matches the iteration index in order to have a synchronous update. This applies to both step 1 and step 2 as both steps use only one RTI DDS communication module and one circular buffer. After step 1, active and reactive power constraints are reconfigured by modifying corresponding fields in $sysInfo$, and then fed into step 2. To solve (3.19a), the LabVIEW's Constrained Nonlinear Optimization module, which utilizes the sequential quadratic programming algorithm, is used. To obtain the information of the optimization problem, this module accesses $sysInfo$ via a Formula Node with C++ syntax structure code deployed inside. Although each iteration of step 1 has computational time less than 60 milliseconds (ms) by implementing on the NI sbRIO 9627 controllers, time for each iteration of step 1 is set to 60 ms which is higher than 40 ms of the RTI DDS module to ensure data is received for the next iteration. Step 2 is more computationally expensive than step 1 because the duration is 3 seconds for each iteration. Maximum number of iterations is the stopping condition for both step 1 and step 2.

As an illustration of exchanging data between two EMs, Figure 3.2b) shows the exchange of data between EM1 and EM5. Buses which are managed in region 1 are 1, 2, 3, and 4, and buses are managed in region 5 are 23, 24, and 25. These nodes are illustrated by circles. There is a connection between nodes 3 and 23. Although region 1 does not contain bus 23, EM1 has $V^{re}_{1,23}$ and $V^{im}_{1,23}$ as variables in the optimization process. Note that the first subscript indicates the region index and the second indicates the bus index. Bus 23 in region 1 is illustrated by a pentagon. Region 5 contains bus 23 and its bus voltage can be represented by $[V^{re}_{5,23}, V^{im}_{5,23}]$. The optimization process aims to reach a consensus between $[V^{re}_{1,23}, V^{im}_{1,23}]$ and $[V^{re}_{5,23}, V^{im}_{5,23}]$. This applies to the other buses which have connections between regions.

3.4.1.2 Load Profiles

The original load is replaced by the sum of EV load profiles generated from the method presented in subsection 3.2.3 and non-EV load generated from the CREST model [76]. 100 load profiles are generated from the model and average these load profiles, and observe that the peak value of the 15-min averaged load per individual profile is around 1 kW. Originally, the IEEE 33 bus

system has a fixed 3.715 MW of load in total. Considering this as the peak load, then we assume the residential area has 3715 households and generate this number of load profiles. The load profiles are randomly distributed to the buses such that the number of load profiles are proportional to the original load values at the buses. The CREST model does not generate reactive power, so we assume PF follows uniform distribution in the range [0.95,0.99] which is close to that of [77]. For EV reactive load, a PF of 0.99 is assumed which is specified in Texas Instrument's design recommendation [78]. With the assumption of 3715 households, three levels of EV penetration are considered: 500 EVs, 1000 EVs, and 1500 EVs. The number of EVs assigned to each bus is also proportional to the amount of original load values. Fast charging profile generation feature of the EV profile generation tool for the public charging stations outside the analysis area is taken in to account to better represent the car arrival times and starting SoC levels of the second charging sessions for the residential chargers in the considered network. While the CREST model can be used to generate weather data for PVs, wind speed is generated by the Weibull distribution. Figure 3.3 shows data generated by using the methodology described above for the day of January 15. Furthermore, the market price of electricity is taken from [79] and the fuel price is $C^F = 5.807$ ($/gallon) which is taken from [80] on August 24, 2020.

3.4.2 CHIL Experimental Results and Discussion

3.4.2.1 Scenario 1

The system without distributed EM is setup. MTs are simulated in the grid following mode that they generate active power to serve the load locally in their regions until they reach limits. Reactive power of the three types of DERs are set to 0. With this setup, the impact of EV charging under the three levels of EV penetration at the peak load which is at 19:30 is studied. Figure 3.4 shows bus voltages of the three testing cases. While voltages for the cases of 500 and 1000 EVs are in the range [0.95,1.05] pu, buses 16, 17, and 18 have voltages less than 0.95 pu when the system populates 1500 EVs.

In this scenario, 1500 EVs is populated. Three cases are tested: at 00:00 when the load is the lowest, at 12:45 when the renewable generation is max, and at 19:30 when the total load is at peak. The simulation results are shown in Figure 3.5. Figure 3.5a) shows the amount of power delivered at the 6 active power suppliers. For the case of 19:30, the MTs generate at full capacity.

This is because the grid price is high and EMs allocates generation to the 5 MTs to meet the power load balance. The total cost of generation is shown in Figure 3.5b) in which we also computed the case generation is allocated to the 6 sources proportional to their maximum capacities. It can be seen that deploying EM is economically beneficial in the 12 AM and 12:45 PM cases. In Figure 3.5c) voltages are in the range of [0.95, 1.05] pu. Compared to the case of without EM, bus voltages are maintained under the impact of 1500 EVs. Define the following quantity

$$\epsilon = \max_{n \in \Omega} |V_{r,n} - V_{s,n}| \tag{3.23}$$

where Ω is the set of buses which have voltage optimized in both region r and region s. ϵ is shown in Figure 3.5d) and it can be seen that voltages converge after 60 iterations for all three cases.

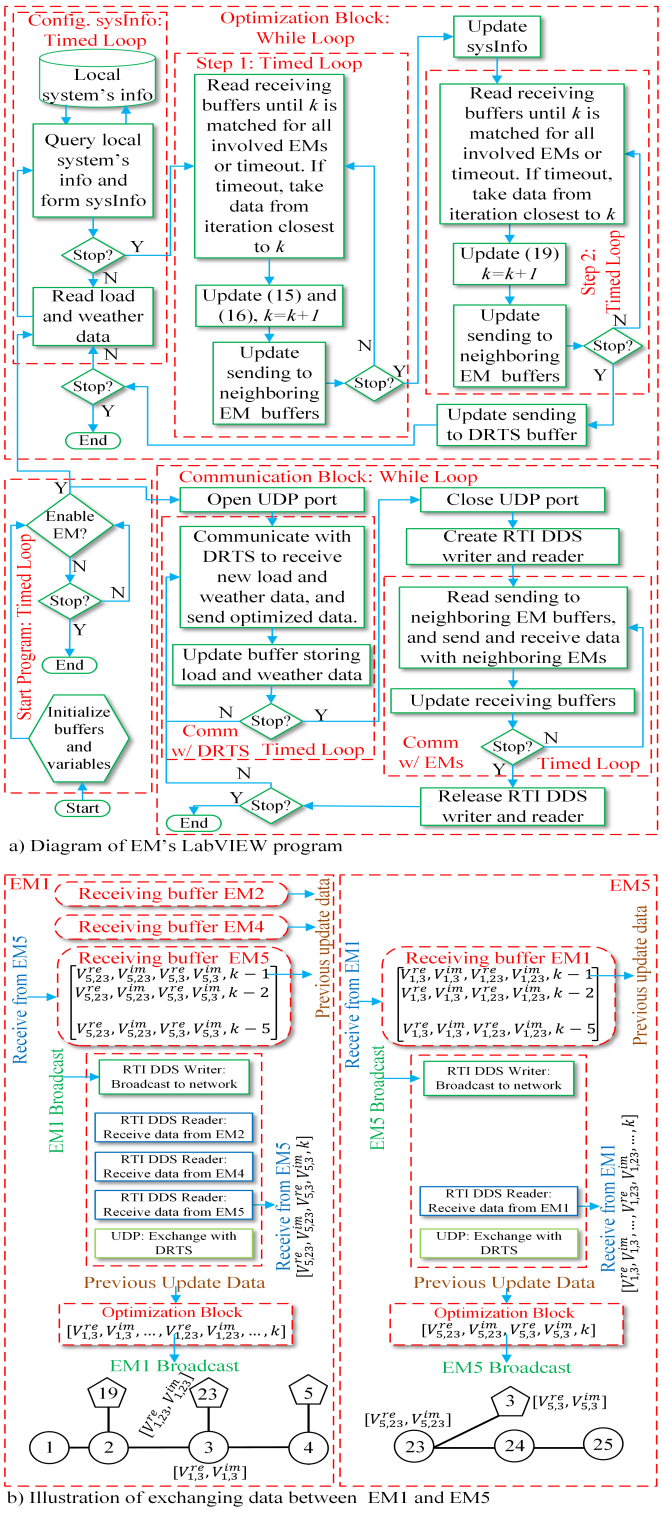

Figure 3.2: Distributed EM: a) Diagram of EM's LabVIEW program b) Illustration of exchanging data between two EMs.

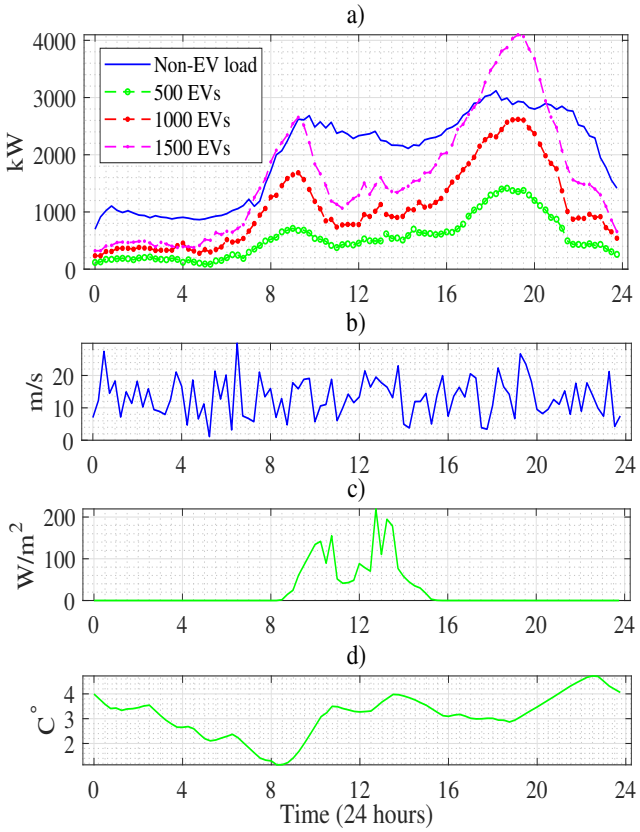

Figure 3.3: Simulated data used in experiment: a) load profile and renewable generation, b) wind speed, c) solar irradiance, and d) temperature.

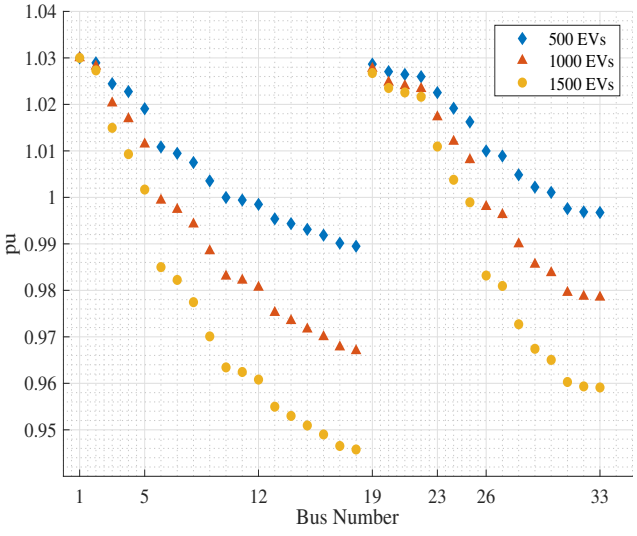

Figure 3.4: Bus voltage of scenario 1.

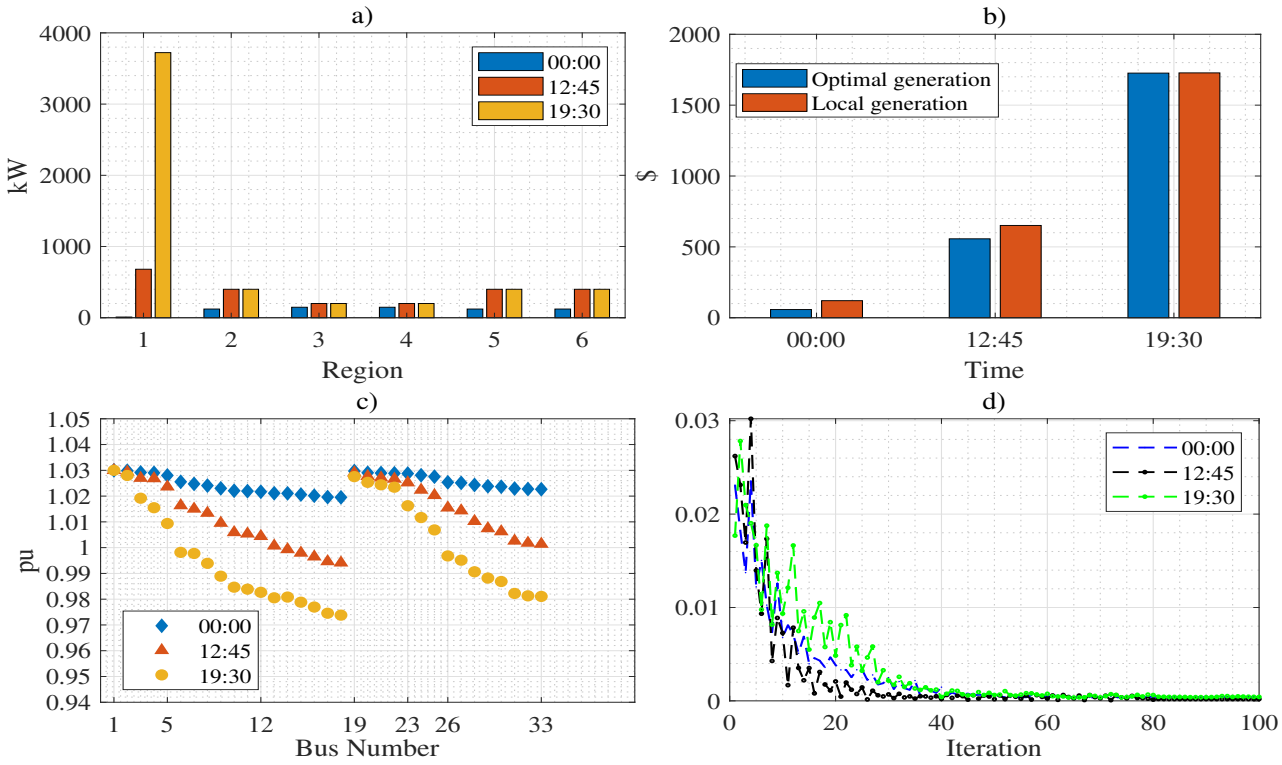

Figure 3.5: Experimental results of scenario 2: a) power generation allocation b) cost of generation c) bus voltages d) ϵ.

Chapter 4

Degradation Forecasting and Abatement Framework

Chapter 4's Nomenclature

DER	Distributed energy resource
DG	Distributed generation
EM	Energy management
PM	Power management
DF	Degradation forecasting
DFAF	Degradation forecasting and abatement framework
ET	Evidence theory
N	Number of buses
K	Number of discrete time horizon for degradation prediction
n, m	Bus index
k	time index
t_k	time instant
i, j	State index
d_n^e	Estimated degradation signal of DG unit at bus n
d_i^a	Actual degradation signal of DG unit at bus n
σ_i	Error of degradation estimation

λ_{ij}	Degradation intensity from state i to state j
$\underline{\lambda_{ij}}$	Minimum degradation intensity from state i to state j
$\overline{\lambda_{ij}}$	Maximum degradation intensity from state i to state j
π_{ij}	Transition probability from state i to state j
$\mathbf{\Pi}$	Markov transition matrix
$x_{n,i}$	Probability that energy conversion unit at bus n at state i
P_n^{ND} (Q_n^{ND})	Active (reactive) power generated by a non-dispatchable energy source at bus n
$\mathbf{P}^{ND}$ ($\mathbf{Q}^{ND}$)	Vector of active (reactive) power of all non-dispatchable sources
P_n^D (Q_n^D)	Active (reactive) power generated by a dispatchable energy source at bus n
$\mathbf{P}^D$ ($\mathbf{Q}^D$)	Vector of active (reactive) power of all dispatchable sources
V_n	Bus voltage
$\mathbf{V}$	Vector of all bus voltages
$\mathcal{C}^a$	Constraint set for variable(s) a
$\overline{A}$	Maximum of variable A
$\underline{A}$	Mimimum of variable A
$\mathbb{P}_n^D$	Maximum capacity expectation of dispatchable energy conversion unit at bus n
Δ_n^D	Maximum capacity degradation expectation of dispatchable energy conversion unit at bus n

4.1 Introduction

Distributed energy resources (DERs) are expected to be deployed widely in future distribution grids [81]. The integration of DERs will bring challenges for system control, management, and monitoring. To cope with the challenges, the future distribution grids will be given more autonomy in the form of digital control and management systems [81] to ease their control and management, and the advanced distribution management system (ADMS) concept is one of those [82]. With the dispersion of DERs, it is important to develop and integrate a degradation forecasting (DF) layer to ADMS to predict grid components' degradation behaviors to aid maintenance planning and real-time operation. Recently, DF for engineering systems has received growing interest because of the benefits of proper predictions of unpleasant events to take preventive actions [83, 84, 85]. However, DF is typically implemented for specific components, and there is a lack of frameworks to integrate DF into real-time control and management.

An ADMS is a software platform and contains a set of functions [8]. In the literature, a three-layer ADMS architecture consisting of device-level control (DLC), power management (PM),

and energy management (EM) is proposed [9]. DLC, PM, and EM are also called primary control layer, secondary control layer, and tertiary control layer, respectively [1]. The underlying idea of the multi-layer architecture is taking advantage of different time steps of the layers as upper layers have the duties of providing commands to lower layers. This architecture has been used in both alternating current (AC) and direct current (DC) grids; however, depending on the type of grid, quantities of interest are controlled and optimized.

EM has been extensively studied for electrical systems ranging from MW-scale systems like terrestrial power systems and ship power systems to kW-scale systems like electrified vehicles' powertrain systems. It is expected that EM will be one of the main constituents of future distribution grids' ADMS to enhance system performance. The cost-saving goal is one of the main objectives of EM. To obtain the goal, EM is to solve a well-defined optimization problem to find optimal energy allocation for different energy sources. EM's outputs are then passed down as references to lower control layers for control activities. Therefore, EM decides operating conditions for each energy conversion unit.

It has been reported in the literature that the degradation rate of energy conversion units depends on their operating conditions [22, 23, 24, 86]; thus, degradation models should take into account components' operating conditions. Given the analysis of EM above, the mutual effects of components' degradation processes are mainly decided by EM. Therefore, EM can be considered as a means to abate the degradation of components.

Quantifying uncertainty in DF is a challenging task. Degradation data are scarce because generating degradation data is challenging, costly, time-consuming. Additionally, degradation data is generally confidential by many involved parties such as utilities and manufacturers. There are works that take the historical data of degradation signals to predict its future values by data-driven methods, for example, linear regression [87], Gaussian process regression [88]. However, the degradation process of a component is complex as it depends on its current state and future operating conditions. Furthermore, degradation data is scarce, that it is challenging to have sufficient information to construct a statistical model to predict the future degradation behavior in order to have optimal and accurate real-time operation and maintenance planning. Instead, methodologies combine multiple sources of information to arrive at a more informative piece with higher confidence. There are works that integrate expert knowledge in the degradation prediction to enhance forecasting performance. In fact, sensed data, expert knowledge, knowledge of engineering models are used in

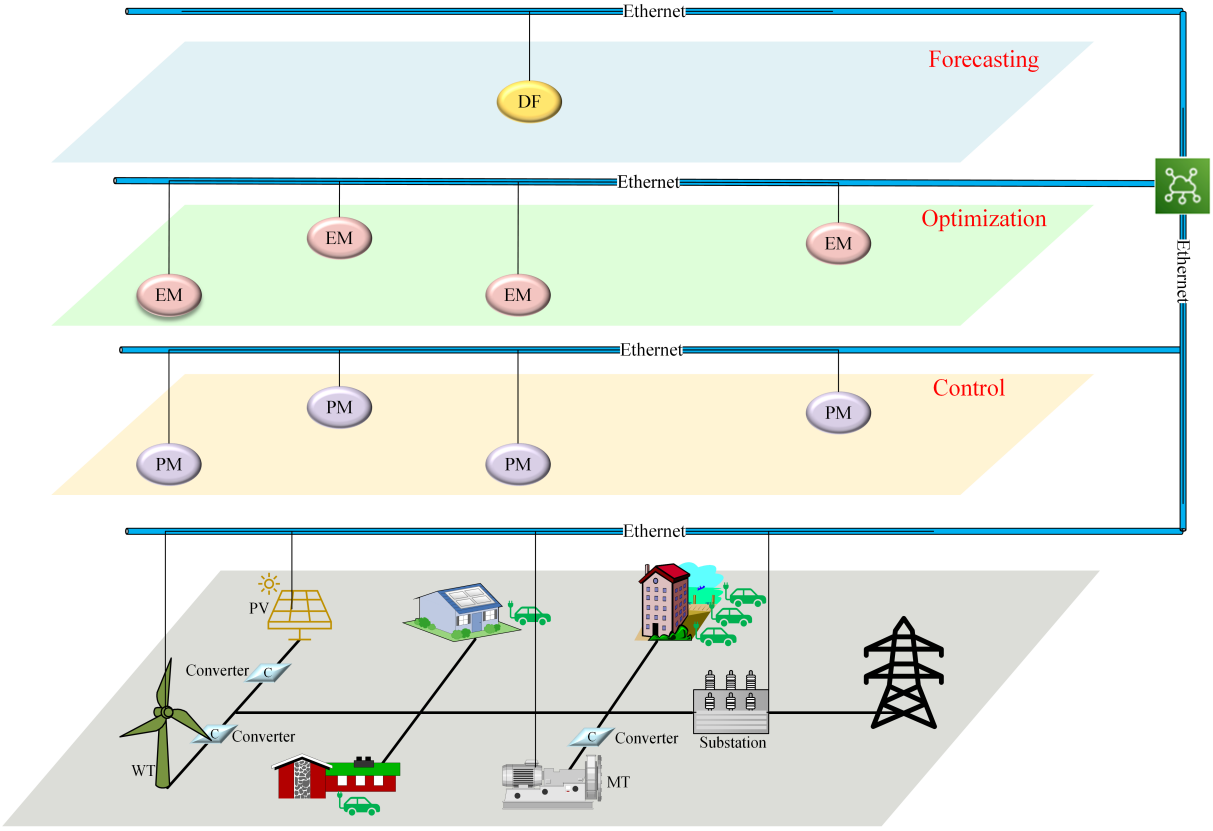

Figure 4.1: Integration of degradation forecasting into ADMS.

the Watchdog Agent intelligent maintenance system [89].

The main contributions of this paper can be summarized as follows. First, a Markov chain-based DF model is introduced to predict degradation paths of a grid's components in which components' states are modeled by a multi-state model. The model is a load-dependent model reasoning from observations of degradation behaviors of interested energy conversion units. Because degradation data is typically scarce, multiple sources of information are used to enhance the reliability of the prediction, and Evidence Theory's (ET) combination rule [86] is used to fuse multiple sources of data. The predicted results can aid maintenance planning and real-time operation. Second, this work focuses on the real-time aspect that a degradation abatement strategy for grid components is proposed that the DF layer is integrated into the existing hierarchical ADMS as an upper layer to EM. The DF's predicted results are used to adjust EM's optimization problem to abate the degradation of higher degradation cost components. Numerical simulations and controller-hardware-in-the-loop (CHIL) experimentation are carried to show the cost-saving benefits of the proposed strategy.

4.2 Problem Formulation

4.2.1 System Model and Notations

Consider a grid-connected radial distribution network consisting of multiple heterogeneous DERs dispersed over the network. As the granularity, a DER or a substation is considered as a component of the distribution grid. Let an undirected graph $(\mathcal{N}, \mathcal{E})$ represent the grid, where $\mathcal{N} = \{1, ..., N\}$ is the set of nodes and $\mathcal{E} = \{(n, m)\} \subseteq \mathcal{N} \times \mathcal{N}$ is the set of lines. The terms *bus* and *node* are used interchangeably. The bus connecting directly with the substation is indexed 1. DERs can be categorized into dispatchable DERs and non-dispatchable DERs. An example of dispatchable DERs is microturbines (MTs), and examples of non-dispatchable DERs are wind turbines (WTs) and photovoltaic systems (PVs). Let P_n^D and Q_n^D be generated by a dispatchable DER connected to bus n. Furthermore, active and reactive power generated by a non-dispatchable DER at bus n are P_n^{ND} and Q_n^{ND}, respectively. Let $\mathbf{P}^D$ and $\mathbf{Q}^D$ be the vectors of active power and reactive power of all dispatchable energy sources, including the substation, respectively. In addition, let $\mathbf{P}^{ND}$ and $\mathbf{Q}^{ND}$ be the vectors of active power and reactive power of all non-dispatchable DERs, respectively. Let V_n be the complex bus voltage at bus n. Denote $\mathbf{V} = [V_1, ..., V_N]^T$.

4.2.2 Energy Management

EM has been extensively studied for electrical systems ranging from MW-scale systems like terrestrial power systems and ship power systems to kW-scale systems like electrified vehicles' powertrain systems. It is expected that EM will be one of the main constituents of future distribution grids' ADMS to enhance system performance. The primary function of EM is to optimally allocate power generation and delivery to sources of energy in a well-defined sense while adhering to system constraints [11, 12, 13, 14, 15, 16]. For distribution grids with DERs, EM takes forecasted load and non-dispatchable active power generation information as inputs for its optimization process. Non-dispatchable active power generation information of DERs like WTs and PVs can be estimated from weather information and their systems' models. Mathematically, EM's optimization problem

can be stated as

$$\min f(\mathbf{P}^D) \tag{4.1a}$$

$$s.t.\ \mathbf{P}^D \in \mathcal{C}^{\mathbf{P}^D}, \mathbf{Q}^D \in \mathcal{C}^{\mathbf{Q}^D}, \tag{4.1b}$$

$$\mathbf{P}^{ND} \in \mathcal{C}^{\mathbf{P}^{ND}}, \mathbf{Q}^{ND} \in \mathcal{C}^{\mathbf{Q}^{ND}} \tag{4.1c}$$

$$\mathbf{P} \in \mathcal{C}^{\mathbf{P}}, \mathbf{Q} \in \mathcal{C}^{\mathbf{Q}}, \mathbf{V} \in \mathcal{C}^{\mathbf{V}} \tag{4.1d}$$

where $\mathcal{C}^{\mathbf{P}^D}$, $\mathcal{C}^{\mathbf{Q}^D}$, $\mathcal{C}^{\mathbf{P}^{ND}}$, $\mathcal{C}^{\mathbf{Q}^{ND}}$, $\mathcal{C}^{\mathbf{Q}^{ND}}$, $\mathcal{C}^{\mathbf{P}}$, $\mathcal{C}^{\mathbf{Q}}$, $\mathcal{C}^{\mathbf{V}}$ are the constraint sets of $\mathbf{P}^D$, $\mathbf{Q}^D$, $\mathbf{P}^{ND}$, $\mathbf{Q}^{ND}$, $\mathbf{P}$, $\mathbf{Q}$, and $\mathbf{V}$, respectively.

EM outputs references for PM to control the grid's components to follow the references. Specifically, it outputs active power and voltage references for PM to control dispatchable DERs. In this work, non-dispatchable DERs are set up to involve in voltage regulation by injecting reactive power; therefore, EM outputs reactive references for PM to control non-dispatchable DERs. Furthermore, the bus connected to the substation is set up as a slack bus. Hence, EM provides voltage references to control the substation. As can be seen, EM decides operating conditions for DG units and the substation. Hence, EM has impacts to the degradation processes of grid's components. Figure 4.2 shows the operating process of EM.

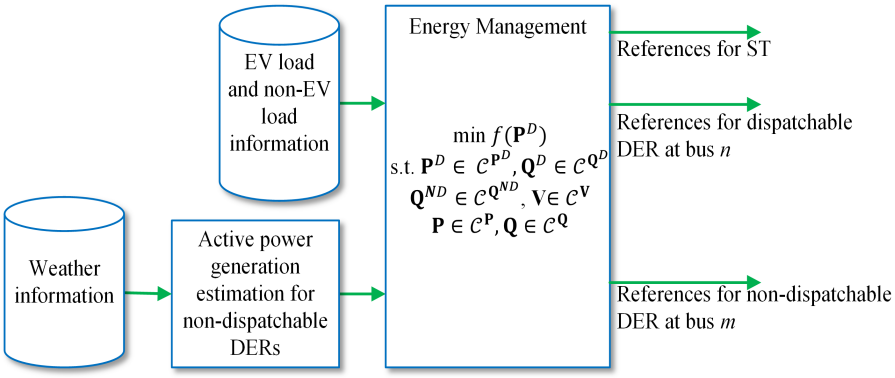

Figure 4.2: Illustration of EM of distribution grids with DERs and EVs.

4.3 Degradation Forecasting and Abatement Framework

The proposed DFAF is discussed in this section. First, components' degradation models are constructed and discussed. A Markov-based degradation prediction model is presented. Then,

a degradation abatement strategy is proposed to reduce the degradation of components with higher capital expenditure (CAPEX) costs, and consequentially it reduces the overall operation costs.

4.3.1 Components' Degradation Model

4.3.1.1 Multi-state Degradation Representation

Conventionally, the binary model is used to model the state of a system because of its simplicity, and computational efficiency [90, 91]. By using the model, a system can only be represented by either the working or failed state. In doing so, the aging aspects are not taken into consideration, and consequently, the precision of reliability assessment is not reliable to allow decision makings in operation and maintenance planning. The multi-state model is utilized to increase the granularity of the binary model [92, 93, 94, 95]. However, increasing the number of states increases the model complexity and computational burden. A model of 4 states is typically used to compromise the precision and the complexity [94, 95, 96, 97]. For instance, the authors in [94] describe a component by 4 states: perfect, useful, pseudo-fault, and fault. Moreover, the authors in [95] represent a coal-fired generating unit by 4 states, which are named by numbers as $\{1, 2, 3, 4\}$, based on its available generation capacity ranging from zero to its original maximum capacity. Furthermore, in [96], the state of drivetrain components of wind turbines are represented by normal working, degraded, critical, and functional failure states. In addition, in [97], transformers are described by 4 states: good, fair, poor, and very poor.

Enabling by the advancements in sensor technologies, industrial networks, and the semiconductor industry, online health monitoring for engineering systems have been widely proposed to aid operation and maintenance planning, consequently, enhance the system performance, for example, transformers [97], gas turbines [98], PV systems [83], and wind turbines [99]. It is noted that different technologies have different real-time health monitoring methodologies and configurations. But there is a common process that data sensed by sensors are processed, and then they are input to degradation estimation engines to output degradation signals which are numerically represented and typically normalized [97, 83, 100, 84, 101]. For generating units, the degradation signals typically are the performance ratio, for example, performance ratio for gas turbines [100], for wind turbines [84], for PVs [101, 102]. Let $d_n^e(t_k)$ be the degradation signal of the component at bus n which is estimated at time t_k. The estimation of degradation signals is generally not a deterministic process.

Therefore, it is assumed that the estimation has uncertainty that $d_n^e(t_k)$ is a sum of the actual degradation $d_n^a(t_k)$ and the error of the estimation $\sigma_n(t_k)$ as:

$$d_n^e(t_k) = d_n^a(t_k) + \sigma_n(t_k) \tag{4.2}$$

As mentioned, degradation signals are typically normalized. Additionally, it is reasonable to assume that the state of a component has no improvement between two consecutive maintenance or repair times. These assumptions are formally stated as

Assumption 4.3.1

a) The maximum of the actual degradation $d_n^a(t)$ is 1.

b) The actual degradation $d_n^a(t)$ is monotonically decreasing between two consecutive maintenance or repair times.

There are works that take the historical data of $d_n^e(t)$ to predict its future values by data-driven methods, for example, linear regression [87], Gaussian process regression [88]. However, the degradation processes of a component is complex that it depends not only on its current state but also on future operating conditions. Furthermore, degradation data is scarce that it is challenging to have sufficient information to construct a statistical model to predict the future degradation behavior in order to have optimal and accurate operation and maintenance plans. In stead, various . There are works which integrate expert knowledge in the degradation prediction to enhance forecasting performance. For example, in [89], an intelligent maintenance program called Watchdog Agent is discussed. The involvement of human expertise demands representing a component's aging degree in a way that eases the human perception. In [97], the authors convert degradation signals into 4 states by assigning each state in an interval. This work uses 4 states named by numbers from 1 to 4 and each state has a maximum capacity representation as the authors in [95] do. Also, the conversion from degradation signals to states as follows

- State 1: In this state, the hard constraint for this state is $d_n^a \geq \rho_1$. The maximum capacity representation for this state is $\overline{P_{n,1}^D}$ and $\overline{P_{n,1}^{ND}}$ for dispatchable and non-dispatchable sources, respectively.

- State 2: In this state, the hard constraint for this state are $\rho_1 > d_n^a \geq \rho_2$. The maximum

capacity representation for this state is $\overline{P_{n,2}^{D}}$ and $\overline{P_{n,2}^{ND}}$ for dispatchable and non-dispatchable sources, respectively.

- State 3: In this state, the hard constraint for this state are $\rho_2 > d_n^a \geq \rho_3$. The maximum capacity representation for this state is $\overline{P_{n,3}^{D}}$ and $\overline{P_{n,3}^{ND}}$ for dispatchable and non-dispatchable sources, respectively.

- State 4: In this state, the hard constraint for this state are $\rho_3 > d_n^a$. The maximum capacity representation for this state is $\overline{P_{n,4}^{D}}$ and $\overline{P_{n,4}^{ND}}$ for dispatchable and non-dispatchable sources, respectively. When a component enters this state, it is either considered not functional or required maintenance or replacement.

4.3.1.2 Markov Based Degradation Prediction Model

A Markov chain based model of the four states mentioned in the previous section is used to forecast the degradation process of a component. Let $x_{n,i}$ be the probability that the component at bus n is at State i, $i \in \{1, 2, 3, 4\}$. Let $\mathbf{x}_n$ be the vector of all $x_{n,i}$, i.e., $\mathbf{x}_n = [x_{n,1}, x_{n,2}, x_{n,3}, x_{n,4}]$. The Markov model transitioning $\mathbf{x}_n$ at time t_k to $\mathbf{x}_n$ at time t_{k+1}, which is illustrated in Figure 4.3 b), has the following formula:

$$\mathbf{x}_n(t_{k+1}) = \mathbf{x}_n(t_k)\mathbf{\Pi} \tag{4.3}$$

where $\mathbf{\Pi}$ is the transition matrix with the following form

$$\mathbf{\Pi} = \begin{bmatrix} \pi_{11} & \pi_{12} & \pi_{13} & \pi_{14} \\ \pi_{21} & \pi_{22} & \pi_{23} & \pi_{24} \\ \pi_{31} & \pi_{32} & \pi_{33} & \pi_{34} \\ \pi_{41} & \pi_{42} & \pi_{43} & \pi_{44} \end{bmatrix} \tag{4.4}$$

Next, the transition matrix is derived. Maintenance and repair are not considered in the model because the model is to aid decision makings on operation and maintenance strategies. The exponential distribution is typically assumed for the sojourn time in a state [90, 94]. Let λ_{ij} be the degradation rate from state i to state j, $i \neq j$. It is noted that if the binary model is used the

degradation rate is the failure rate. Figure 4.3 a) is the state space diagram of the degradation rate. Looking at the inflow and outflow of State i in the figure, the following equation can be derived:

$$\frac{dx_{n,i}(t)}{dt} = -x_{n,i}(t) \sum_{j=i+1}^{4} \lambda_{ij} + \sum_{j=1}^{i-1} x_{n,j}(t)\lambda_{ji} \tag{4.5}$$

In (4.5), it can be undstood that the term $x_{n,i}(t)\sum_{j=i+1}^{4}\lambda_{ij}$ is the intensity of transitioning from state i to the other states and the term $\sum_{j=1}^{i-1} x_{n,j}(t)\lambda_{ji}$ is the intensity of transitioning to State i from the other states. Solve (4.5) and discretize the solutions with sampling time Δt, we can obtain

$$\pi_{11} = e^{-(\lambda_{14}+\lambda_{13}+\lambda_{12})\Delta t} \tag{4.6a}$$

$$\pi_{12} = \frac{\lambda_{12}}{\lambda_{14}+\lambda_{13}+\lambda_{12}}(1 - e^{-(\lambda_{14}+\lambda_{13}+\lambda_{12})\Delta t}) \tag{4.6b}$$

$$\pi_{13} = \frac{\lambda_{13}}{\lambda_{14}+\lambda_{13}+\lambda_{12}}(1 - e^{-(\lambda_{14}+\lambda_{13}+\lambda_{1,2})\Delta t}) \tag{4.6c}$$

$$\pi_{14} = \frac{\lambda_{1,4}}{\lambda_{1,4}+\lambda_{13}+\lambda_{12}}(1 - e^{-(\lambda_{14}+\lambda_{13}+\lambda_{12})\Delta t}) \tag{4.6d}$$

$$\pi_{21} = 0 \tag{4.6e}$$

$$\pi_{22} = e^{-(\lambda_{23}+\lambda_{24})\Delta t} \tag{4.6f}$$

$$\pi_{23} = \frac{\lambda_{23}}{\lambda_{23}+\lambda_{24}}(1 - e^{-(\lambda_{23}+\lambda_{24})\Delta t}) \tag{4.6g}$$

$$\pi_{24} = \frac{\lambda_{24}}{\lambda_{23}+\lambda_{24}}(1 - e^{-(\lambda_{23}+\lambda_{24})\Delta t}) \tag{4.6h}$$

$$\pi_{31} = 0 \tag{4.6i}$$

$$\pi_{32} = 0 \tag{4.6j}$$

$$\pi_{33} = e^{-\lambda_{34}\Delta t} \tag{4.6k}$$

$$\pi_{34} = 1 - e^{-\lambda_{34}\Delta t} \tag{4.6l}$$

$$\pi_{41} = 0 \tag{4.6m}$$

$$\pi_{42} = 0 \tag{4.6n}$$

$$\pi_{43} = 0 \tag{4.6o}$$

$$\pi_{44} = 1 \tag{4.6p}$$

It is reasonable to assume that an energy conversion system has a degradation rate depending

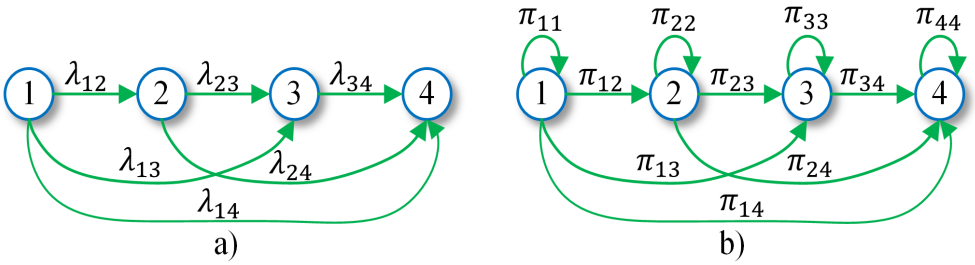

Figure 4.3: Markov chain model: a) State space diagram of degradation rates b) Markov model transition diagram.

on its operating conditions. One of the main reasons for this assumption is the thermal aspects: Increasing power generation or transfer is likely to increase its operating temperature, and therefore it increases the degradation rate because of thermal effects, which is described by the exponential relation [22, 23]. In this work, the relation between the degradation rate and power that a component generates and transfers P is expressed in (4.7). In particular, a component has a constant degradation rate when its load is less than or equal to P^{norm}, but it exponentially increases when its load exceeds P^{norm} because it is assumed that the operating temperature started increases exponentially at this point. It is noted that with the deployment of EM, P is regulated to be less than its maximum capacity $\overline{P}$. Three are works that confirm the load dependence of degradation rates, for example, gas turbines [103] and batteries [104].

Let $\underline{\lambda_{ij}}$ be the degradation rate when the component works in the region $P < P^{norm}$ and $\overline{\lambda_{ij}}$ when the component works at $\overline{P}$. The degradation rate's model is expressed as

$$\lambda_{ij} = \eta e^{\zeta P} \tag{4.7}$$

where

$$\zeta = \frac{\ln(\underline{\lambda_{ij}}/\overline{\lambda_{ij}})}{P^{norm} - \overline{P}} \tag{4.8a}$$

$$\eta = \frac{\underline{\lambda_{ij}}}{e^{\zeta P^{norm}}}. \tag{4.8b}$$

4.3.2 Combine Multiple Sources of Information

The degradation rate model is expressed in (4.7). The degradation rate is used in the Markov chain model (4.3). In (4.7), $\overline{\lambda_{ij}}$ is understood as the maximum degradation rate and $\underline{\lambda_{ij}}$

is the minimum degradation rate. They are needed to be estimated. Three are many sources used to estimate them, for example, 1) field data, 2) accelerated testing data, 3) data provided by manufacturers, and 4) expert opinion. Expert opinion can be a time-based judgment of an expert. For example, an expert believes that a component will transition from state 1 to state 2 in around from 1 month to 3 months. Based on this judgment, the degradation rates can be estimated.

As can be seen, the model (4.7) is sensitive the parameters $\overline{\lambda_{ij}}$ and $\underline{\lambda_{ij}}$. If a single source of information is used and the source is not reliable, the model does not provide accurate results to support decision makings. Therefore, multiple sources of information are used. In particular, each source of information such as field data, manufacturers' data is used independently to estimate $\overline{\lambda_{ij}}$, and $\underline{\lambda_{ij}}$ to run the Markov model. The results of running the Markov model are used to fuse using ET. Figure 4.4 illustrates the combination.

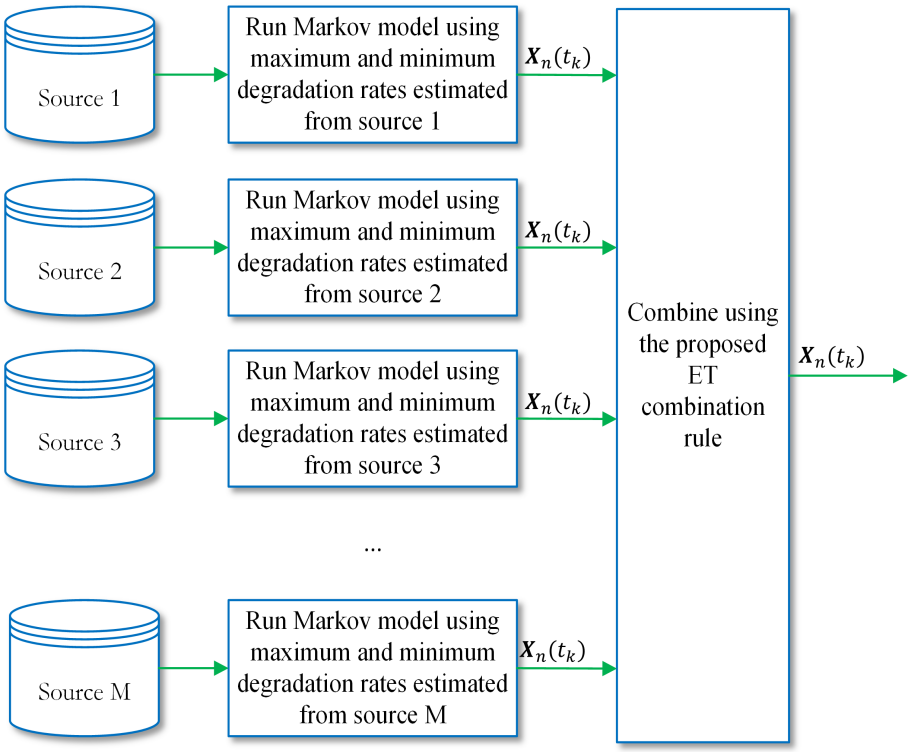

Figure 4.4: Combining multiple sources of information using ET.

4.3.3 Maximum Capacity Expectation Degradation

This work introduces a quantity to measure the degradation of a component's generation capacity. Let $\mathbb{P}_n^D(t_k)$ be the maximum capacity expectation at time t_k of a dispatchable-source component. The maximum capacity expectation of a dispatchable source at bus n at time t_k is the maximum capacity that it is expected to be able to generate, and it has the following formula

$$\mathbb{P}_n^D(t_k) = \mathbb{E}(\overline{P_n^D}) = \sum_{i=1}^{4} x_{n,i}(t_k)\overline{P_{n,i}^D} \tag{4.9}$$

where $\mathbb{E}$ is the expectation operator. For non-dispatchable DERs, the maximum capacity expectation is similar as

$$\mathbb{P}_n^{ND}(t_k) = \mathbb{E}(\overline{P_n^{ND}}) = \sum_{i=1}^{4} x_{n,i}(t_k)\overline{P_{n,i}^{ND}} \tag{4.10}$$

It is desired to know how $\mathbb{P}_n^D(t_k)$ degrades over time. Let $\mathbb{P}_n^D(t_0)$ be the reference to measure the degradation. The following metric called capacity degradation from time t_0 to t_k is introduced:

$$\delta_n^D(t_k) = \mathbb{P}_n^D(t_0) - \mathbb{P}_n^D(t_k) \tag{4.11}$$

Similarly, the capacity degradation for non-dispatchable sources are computed by

$$\delta_n^{ND}(t_k) = \mathbb{P}_n^{ND}(t_0) - \mathbb{P}_n^{ND}(t_k) \tag{4.12}$$

Dispatchable and non-dispatchable components are discriminated because the degradation of non-dispatchable DERs is considered uncontrollable by EM while dispatchable components are considered controllable.

4.3.4 Component Degradation Abatement

EM is briefly discussed in section 4.2.2 and mathematically presented in a general manner in (4.1). As discussed earlier, EM allocates power generation and transfer to the grid's components to gain economic benefits; it decides operating conditions for these units, and thus it impacts the components' degradation processes as described in (4.7). By adjusting the configuration of EM's optimization problem, the components' operating condition can be adjusted; thus, it impacts the components' degradation processes. This section will analyze the EM's optimization problem in a

detailed manner in order to propose a degradation abatement strategy for the grid's components. There are two strategies to adjust the operating conditions of components through EM. The first one is adjusting the EM's objective function, and the second one is adjusting the components' generating or transferring maximum capacities.

First, the EM's objective function is analyzed. In the literature, EM problem mainly considers fuel consumption saving aspects [11, 17], and the objective function of EM is typically decomposed as

$$f(\mathbf{P}^D) = \sum_{n \in \mathcal{D}} f_n(P_n^D) \tag{4.13}$$

where $f_n(P_n^D)$ is a function describing the fuel efficiency curve characteristic of the dispatchable energy source at bus n. Recently, components' degradation has been received more concerns. There are work adding components' degradation costs into the EM's objective function [105, 24]. Specifically, in [105], a linear degradation cost is added to the EM's objective function. Additionally, in [24], the degradation rate of a component is estimated from empirical data, and it is input into an economic model considering degradation, investment, fuel consumption costs to construct an objective cost for a component. Before going further to propose a new solution in adding degradation costs, the other strategy is analyzed.

The other strategy to change the operating condition of a component through EM is adjusting the maximum capacity. The constraint $\mathbf{P}_n^D \in \mathcal{C}^{\mathbf{P}^D}$ in (4.1b) is typically a box constraint as

$$\underline{P_n^D} \leq P_n^D \leq \overline{P_n^D} \tag{4.14}$$

The expression (4.14) is understood as a dispatchable source that has a lower and an upper limit on power generation or transfer. Reducing $\overline{P_n^D}$ likely reduces the component's operating condition as EM will respect the limit in its optimization process. However, in doing so, it reduces the system's capability to meet load demand, especially when load demand is at a peak; hence it reduces system reliability. Therefore, this work follows the first strategy that additional costs considering degradation costs are added.

Now the additional cost added to $f_n(P_n^D)$ is discussed. The objective is to reduce the total components' degradation costs. In the previous section, the capacity degradation metric $\delta_n^D(t_K)$ for a dispatchable energy source is introduced in (4.12). Let C_n^D be the capital cost of dispatchable component at bus n. Suppose the capital cost is linearly proportional to its maximum capacity. The

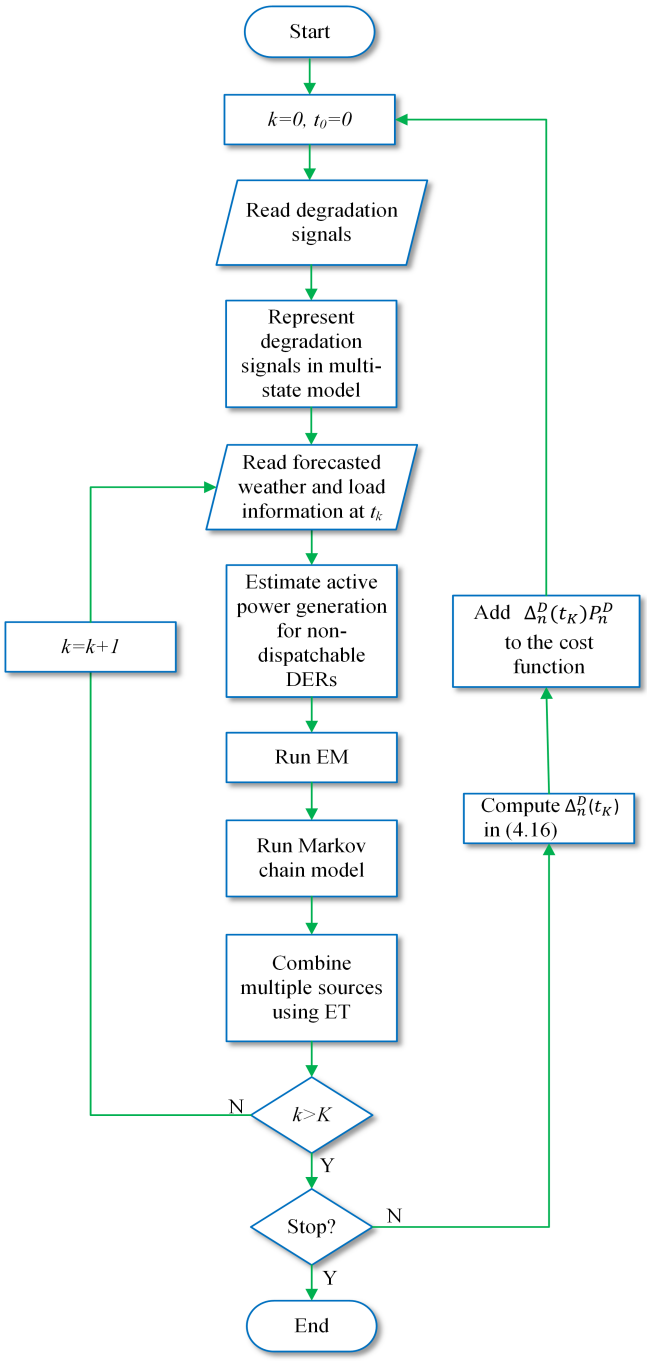

Figure 4.5: Degradation forecasting and abatement framework.

degradation cost c_n^D of component n from t_0 to t_K can be estimated as

$$c_n^D = \delta_n^D(t_K) * C_n^D * \frac{1}{1-\rho_3} \tag{4.15}$$

The term $\frac{1}{1-\rho_3}$ is included in the above equation (4.15) because a replacement is considered for a component entering state 4. Let $P_n^{*D}(t_k)$ be the optimized power generation of dispatchable component at bus n at t_k with the current cost function. The average degradation cost for each power unit is

$$\Delta_n^D(t_K) = \frac{c_n^D}{\sum_{k=0}^{K} P_n^{*D}(t_k)} \tag{4.16}$$

The EM's objective function is updated as

$$f(\mathbf{P}^D) = \sum_{n \in \mathcal{D}} \left(f_n(P_n^D) + \Delta_n^D(t_K) P_n^D \right) \tag{4.17}$$

The DFAF is illustrated in Figure 4.5.

Chapter 5

Degradation Forecasting and Abatement Framework: Numerical Simulation

Chapter 5's Nomenclature

DER	Distributed energy resource
MT	Microturbine
WT	Wind turbine
PV	Photo-voltaic
DG	Distributed generation
EM	Energy management
PM	Power management
DF	Degradation forecasting
DFAF	Degradation forecasting and abatement framework
ET	Evidence theory
CAPEX	Capital expenditure
MPPT	Maximum power point tracking
$\mathbf{\Pi}$	Markov transition matrix

λ_{ij} Degradation intensity from state i to state j

$\underline{\lambda_{ij}}$ Minimum degradation intensity from state i to state j

$\overline{\lambda_{ij}}$ Maximum degradation intensity from state i to state j

$\underline{\boldsymbol{\lambda}}$ Minimum degradation intensity matrix

$\overline{\boldsymbol{\lambda}}$ Maximum degradation intensity matrix

5.1 System Description

The degradation forecasting and abatement framework (DFAF) in Chapter 4 is validated by numerical simulations in this chapter. The IEEE 33 bus system in [71] with additions of DERs is used to validate the proposed scheme. This system consists of 33 buses and 32 lines, and it has a voltage of 12.66 kV. The system is geographically divided into 6 regions, with each corresponding to an EM agent. Microturbines (MTs) are deployed into the system as dispatchable energy sources, and a wind turbine (WT) and PV systems are added as non-dispatchable sources. Locations, rated power, and generation technologies of DERs are shown in Figure 5.1 and Table 5.1.

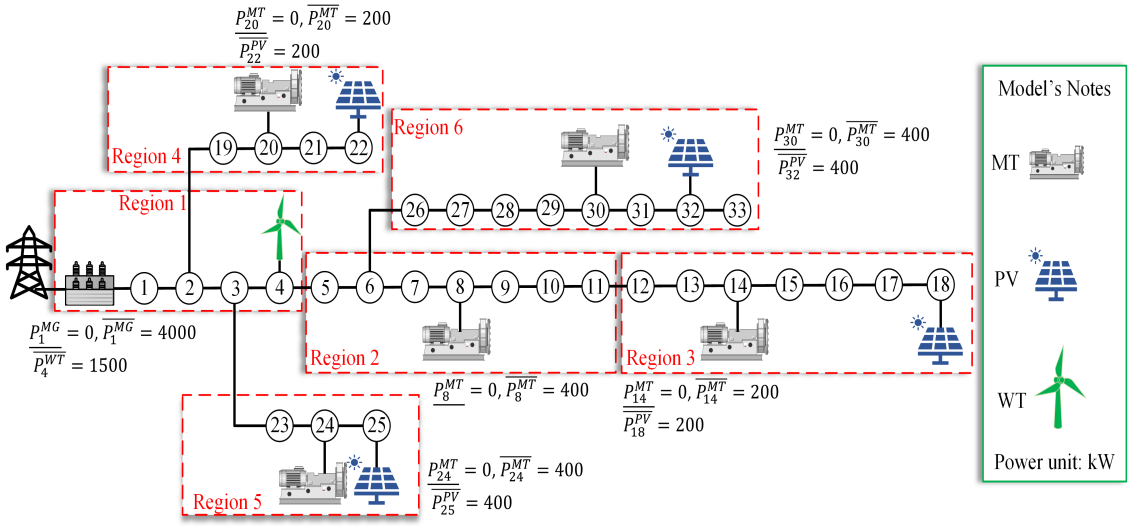

Figure 5.1: IEEE 33 system model.

MTs at buses 8, 24, and 30 has the following fuel efficiency curve

$$f(p) = 0.00052p^2 + 0.0152p + 0.65 \tag{5.1}$$

Table 5.1: Component list.

No.	Region	Bus	Technology	Capacity (kW)	CAPEX ($)	Note
1	1	1	Substation transformer	4000	30,800	
2	1	4	Wind turbine	1500	2,625,000	
3	2	8	Micro turbine	400	1,032,000	
4	2	6	Solar	200	552,000	Out of service
5	3	14	Micro turbine	200	516,000	
6	3	18	Solar	200	552,000	
7	4	20	Micro turbine	200	516,000	
8	4	22	Solar	200	552,000	
9	5	24	Micro turbine	400	1,032,000	
10	5	25	Solar	500	1,380,000	
11	6	30	Micro turbine	400	1,032,000	
12	6	32	Solar	200	552,000	

MTs at buses 14 and 24 has the following fuel efficiency curve

$$f(p) = 0.00042p^2 + 0.0185p + 0.4 \tag{5.2}$$

5.2 Data Preparation

5.2.1 Components' Initial Investment Costs

Components' initial investment cost is used to estimate their degradation costs in order to add them to EMs' objective functions. Initial investment costs include equipment costs and installation costs. Therefore, an investigation to obtain the prices of the considered components is carried out in this work. The wind turbine (WT) technology costs between $1,300,000 and $2,200,000 for each MW capacity [106], the cost of each kW capacity is $2580 for microturbine (MT) technology [107], and $2760 for PV technology [108]. In addition, a transformer in the range of 4 MVA generally costs $30,800 [109]. With those unit prices, initial investment costs of DERs are calculated to match with their capacities and are shown in Table 5.1.

5.2.2 Operational Data Generation

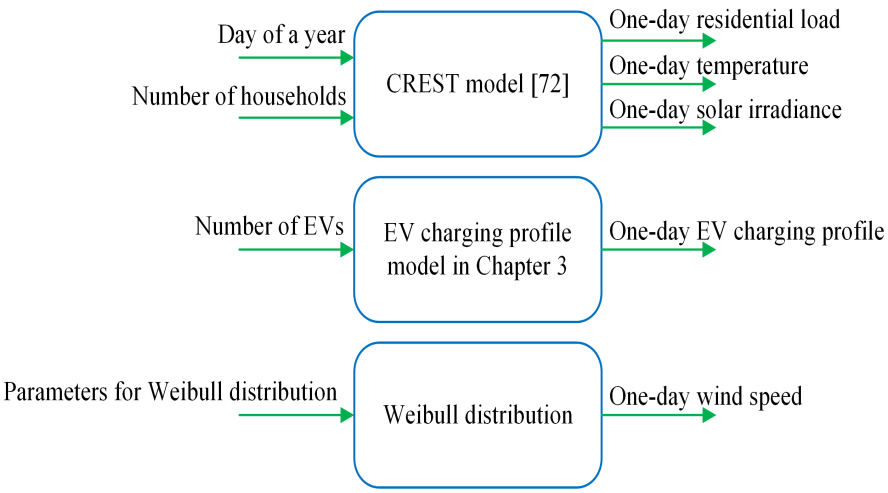

Figure 5.2: Data generation methodologies used in this work.

The proposed degradation model in (4.7) is load-dependent and the time step is 1 hour. Therefore, the information of hourly load and non-dispatchable power generation is needed to run the model. Residential load profiles, EV charging profiles, wind speed, solar irradiance, and temperature are stochastically generated by methodologies discussed in section 3.4 of Chapter 3. While residential load profiles, solar irradiance, and temperature are generated using the CREST model in [76], EV charging profiles are generated by the new methodology presented in Chapter 3. Because the CREST model does not consider wind, wind speed data is simply generated by the Weibull distribution. These data generation methodologies are depicted in Figure 5.2.

Non-dispatchable renewable power generation data such as wind power generation and solar power generation is estimated using maximum power point tracking (MPPT) models as illustrated in Figure 5.3.

Figure 5.4 shows load profile data generated for a day. Figure 5.5 shows weather data and Figure 5.6 shows non-dispatchable power generation data generated for a day. It is noted that the models can generate data for all days of a year.

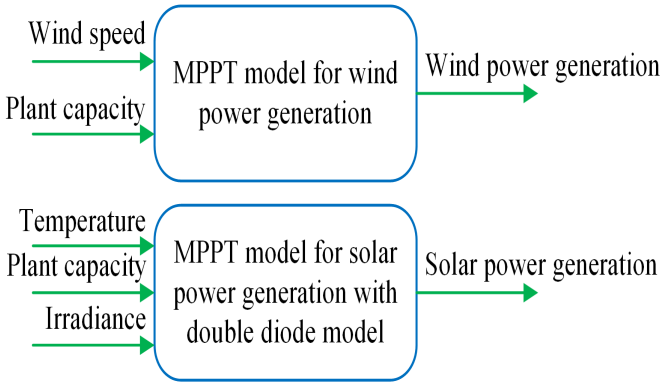

Figure 5.3: Non-dispatchable power generation estimation by MPPT models.

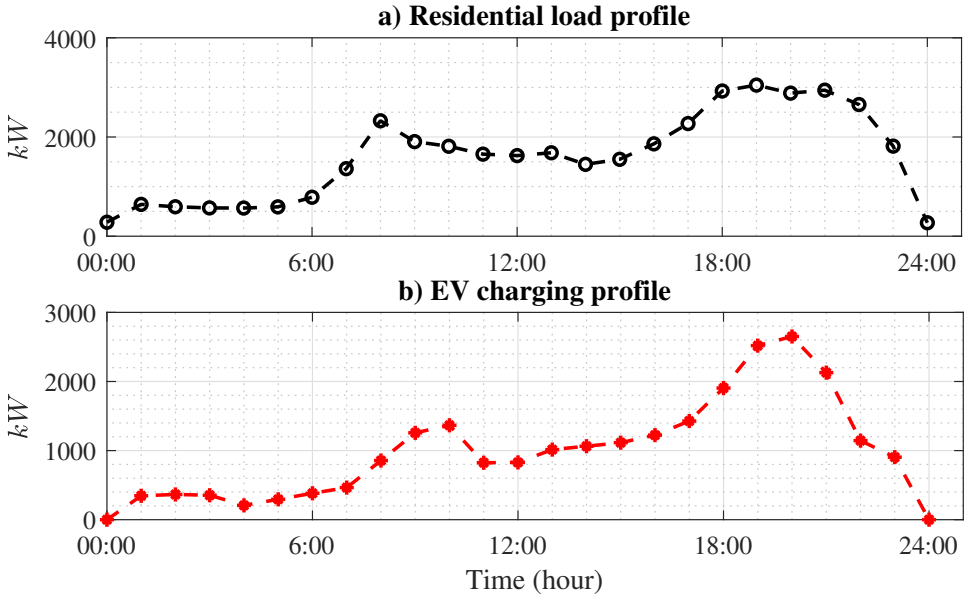

Figure 5.4: Load profile for a day: a) Residential load profile b) EV charging profile.

5.2.3 Degradation Data

5.2.3.1 Notional Degradation Data Generation

The estimation of $\overline{\lambda_{ij}}$ and $\underline{\lambda_{ij}}$ and data used for the estimation are discussed in section 4.3.2 of Chapter 4. Because degradation data is usually kept confidential by utilities, notional data is generated by the Wiener process which has been widely used to model degradation behaviors of an engineering system [110, 111]. Mathematically, the Wiener-process-based degradation model is expressed as

$$d(t) = \iota t + \nu B(t) \tag{5.3}$$

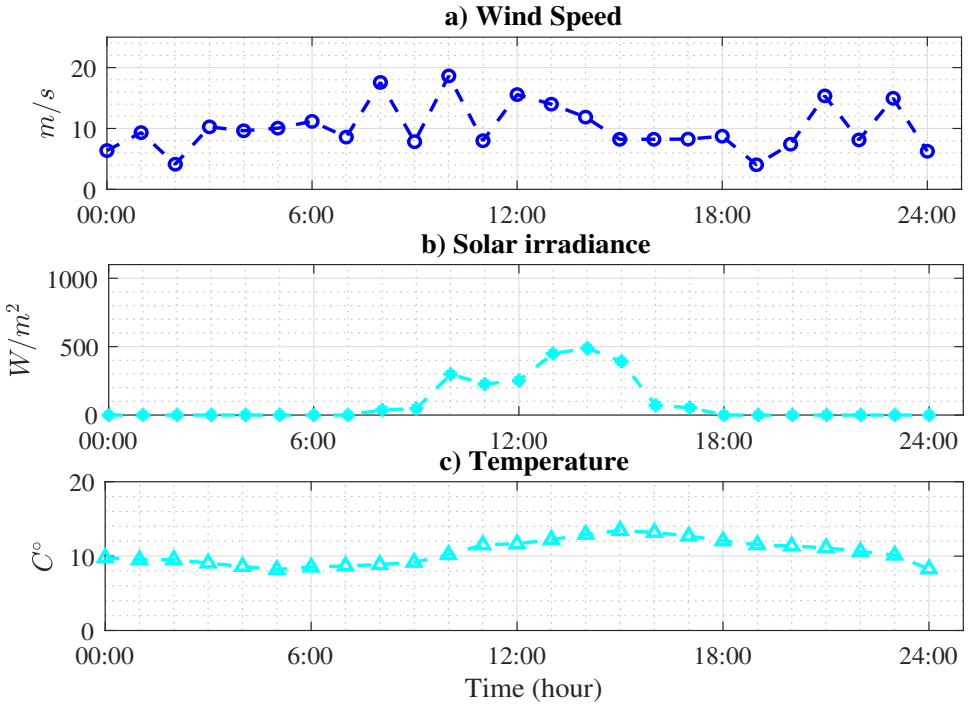

Figure 5.5: Weather data for a day: a) Wind speed b) Solar irradiance c) Environment temperature.

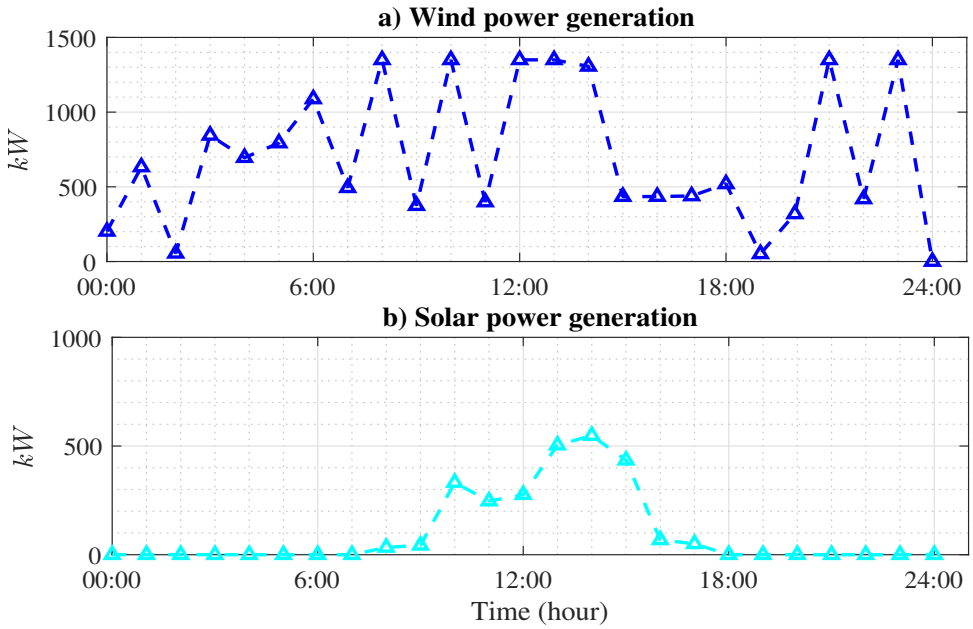

Figure 5.6: Non-dispatchable power generation for a day: a) Wind power generation b) Solar power generation.

where $d(t)$ is the degradation siganal at time t, ι is the drift coefficient, $\nu > 0$ is the diffusion coefficient, and $B(t)$ is the standard Brownian motion. The stochastic dynamics of the degradation process is presented by the Brownian motion. Degradation signal data can be generated by the above model if the parameters ι and ν are known. In this application context, ι relates to degradation rate and ν relates to noises. The notional data degradation generation is depicted in Figure 5.7.

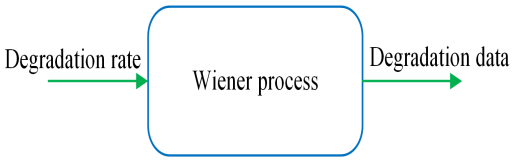

Figure 5.7: Generate notional degradation data using the Wiener process.

Table 5.2: Degradation rate.

No.	Technology	Min degradation rate ($\underline{\lambda_{ij}}$) (%/year)	Max degradation rate ($\overline{\lambda_{ij}}$) (%/year)
1	Transformer	1.5	3.0
2	MT	2.19	4.38
3	WT	1.4	1.6
4	PV	0.8	1.2

It is shown in [107] that an MT is expected to function between 40,000 hours and 80,0000 hours. Assume the minimum degradation rate is associated with 40,000 hours of operation and 80,000 hours of operations makes microturbines have the maximum degradation rate. Suppose a replacement is considered for an MT when its capacity's degradation reaches 80%, then the minimum degradation rate can be estimated around 2.19 %/year, and the maximum degradation rate is around 4.38 %/year. It is reported in [112] that wind turbine degradation rate has a range of $[1.4, 1.8]$ %/year. In [113], the degradation rate of a transformer with high-water content in the winding paper is reported to be in the range of [1.5,3.0] %/year. In [114], the degradation rate of a PV plant is reported in the range of [0.8,1.2] %/year. Table 5.2 shows degradation rates of power generation and delivery technologies used in this work. With data in the table, each minimum or maximum degradation rate is used to generate 30 degradation paths. The generated data is used to obtain the minimum degradation intensity matrix $\underline{\boldsymbol{\lambda}} = [\underline{\lambda_{ij}}]_{4\times 4}$ by Algorithm 5.1.

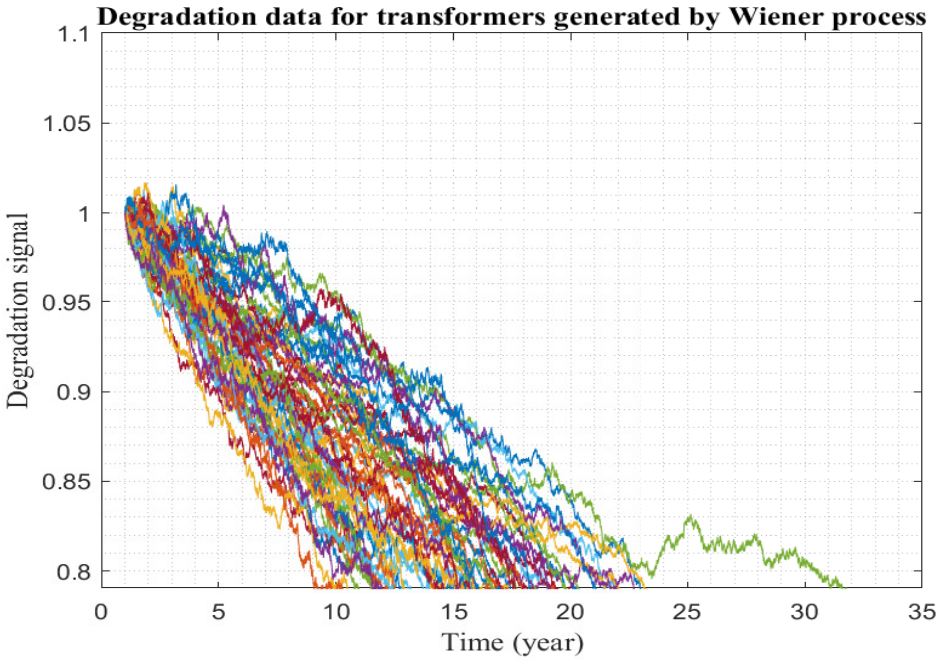

Figure 5.8: Degradation signals of transformers generated by the Wiener process.

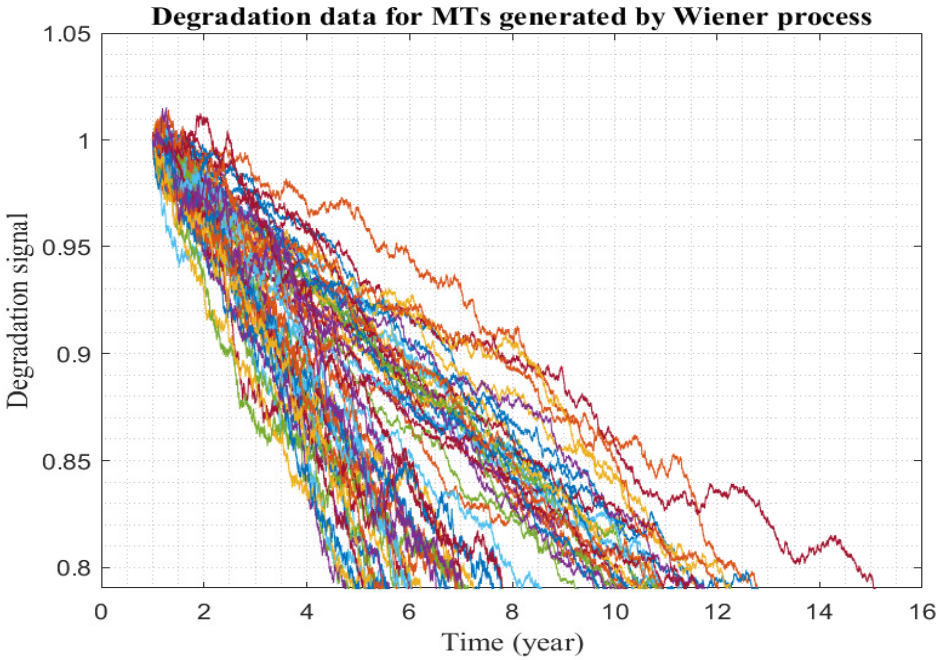

Figure 5.9: Degradation signals of MTs generated by the Wiener process.

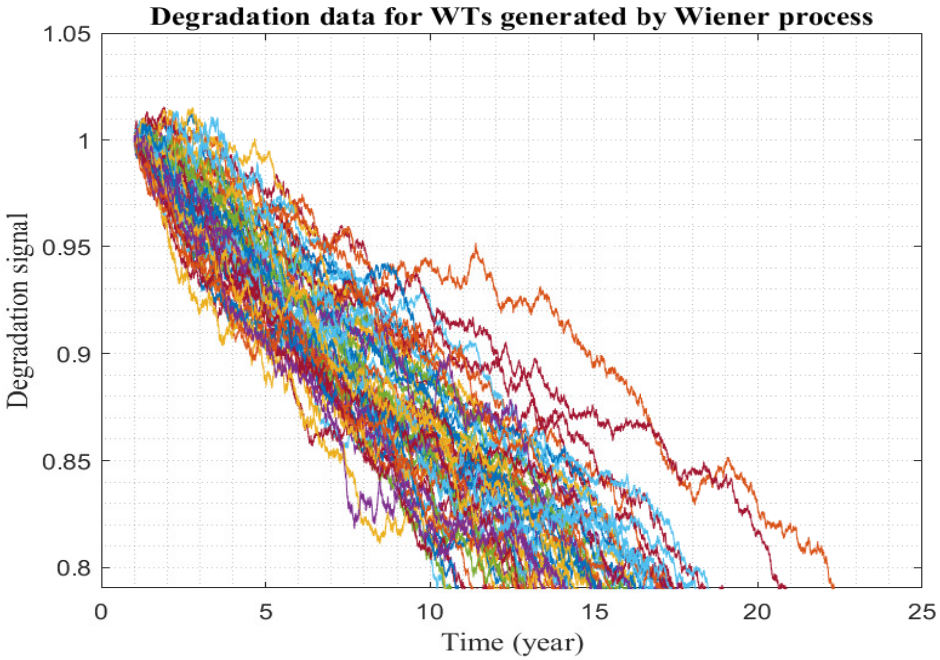

Figure 5.10: Degradation signals of WTs generated by the Wiener process.

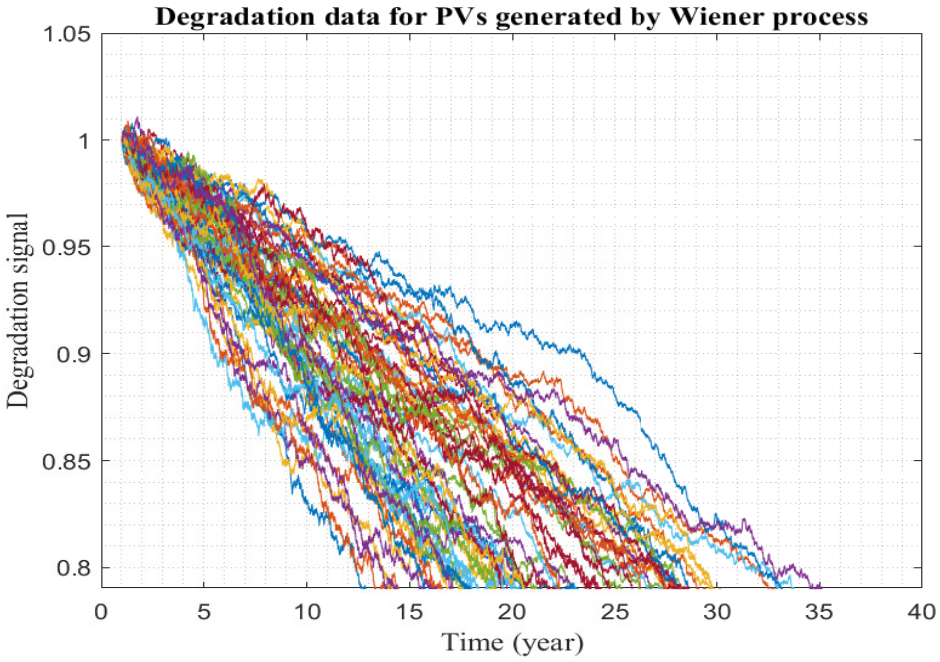

Figure 5.11: Degradation signals of PVs generated by the Wiener process.

5.2.3.2 Training Degradation Data

As can be seen in (4.3), the Markov-based degradation prediction model requires transition matrix $\mathbf{\Pi}$. Let $\underline{\boldsymbol{\lambda}} = [\underline{\lambda_{ij}}]_{4\times4}$ be the minimum degradation intensity matrix and $\overline{\boldsymbol{\lambda}} = [\overline{\lambda_{ij}}]_{4\times4}$ be the maximum degradation intensity matrix. $\mathbf{\Pi}$ can be obtained if load conditions, $\underline{\boldsymbol{\lambda}}$, and $\overline{\boldsymbol{\lambda}}$ are known. Algorithm 5.1 is proposed to train the degradation data to obtain $\underline{\boldsymbol{\lambda}}$. Moreover, Figure 5.12 illustrates the training degradation data process. Particularly, degradation signals of minimum load condition are input to the algorithm. The algorithm will compute the transition probability among the states to output $\underline{\boldsymbol{\lambda}}$. Similarly, $\overline{\boldsymbol{\lambda}}$ can be obtained with the process.

Algorithm 5.1 Training minimum degradation intensity matrix

1. Input: Degradation paths $d_y, y \in \{1, ..., Y\}$
2. Initialize: $\underline{\boldsymbol{\lambda}} = [0]_{4\times4}$
3. **for** $y := 1$ *to* Y **do**
   - Assign state for $d_y(1)$: $S_y(1) = i$, i=1 or i=2 or i=3 or i=4
   - **for** $l := 2$ *to* $length(d_y) - 1$ **do**
     - Assign state for $d_y(l)$: $S_y(l) = i$, i=1 or i=2 or i=3 or i=4
     - $\underline{\boldsymbol{\lambda}}(S_y(l-1), S_y(l)) = \underline{\boldsymbol{\lambda}}(S_y(l-1), S_y(l)) + 1$
4. Normalize $\underline{\boldsymbol{\lambda}}$
5. **return** $\underline{\boldsymbol{\lambda}}$

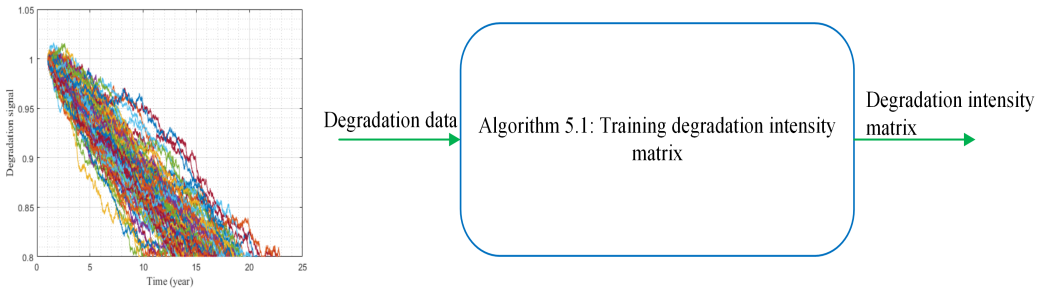

Figure 5.12: Illustration of training degradation intensity matrix.

5.3 Simulation Results and Discussion

5.3.1 Case 1:

In this case, the degradation model discussed in (4.3) and (4.7) is simulated with data in Figures 5.8, 5.9, 5.10, and 5.11. The EM's objective functions do not consider degradation costs.

The main purpose of this testing case is to see the degradation costs in 30 days of operation of the system. The degradation costs in 30 days of the components listed in Table 5.1 are estimated with three scenarios: 1) all the components start at state 1, 2) all the components start at state 2, and 3) all the components start at state 3. Figure 5.13 shows the simulation results. As can be seen in the figure, the total degradation cost for the dispatchable-source components is around $47.000, and that of non-dispatchable-source components is around $27.000. The objective of the proposed DFAF is to reduce the the total degradation cost for the dispatchable-source components which is shown next testing cases.

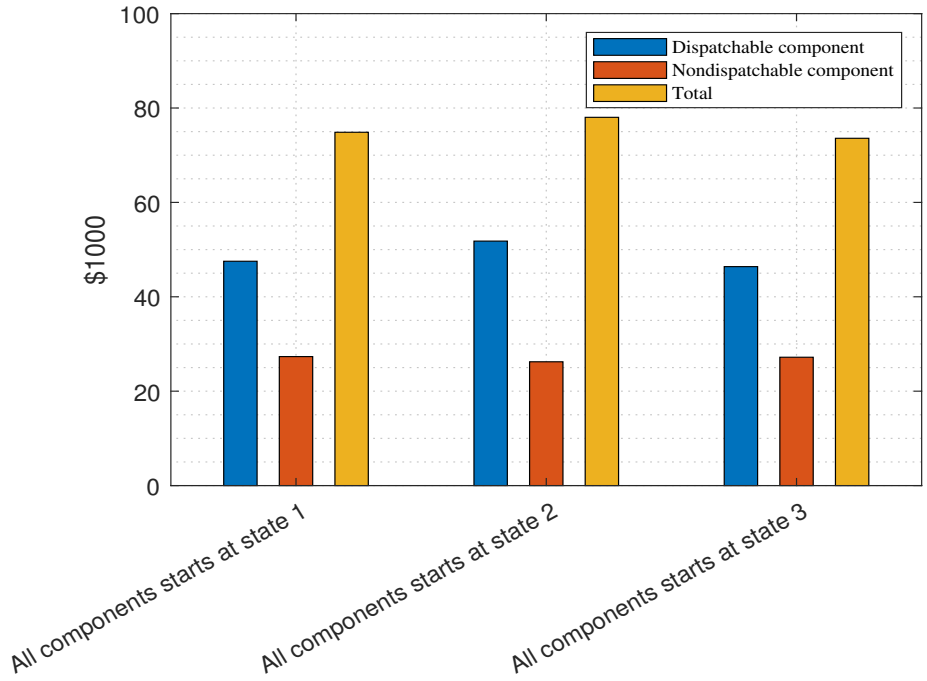

Figure 5.13: Case 1: Degradation cost in a 30 days.

5.3.2 Case 2:

Data used to train the Markov model is generated using degradation rates on Table 5.2. Figures 5.14 and 5.15 show simulation results. As can be seen in Figure 5.14, the degradation of components 3, 5, 7, 9, and 11 are abated at the expense of component 1. This is because the CAPEX of the MTs is more expensive than the transformer, while the degradation rates of the MTs are lower. Figure 5.15 shows cost savings of deploying DFAF compared to the case without DFAF.

The proposed strategy saves $1634 for the total degradation cost, but the system spends $802 more on fuel consumption. However, the total saving is $832.

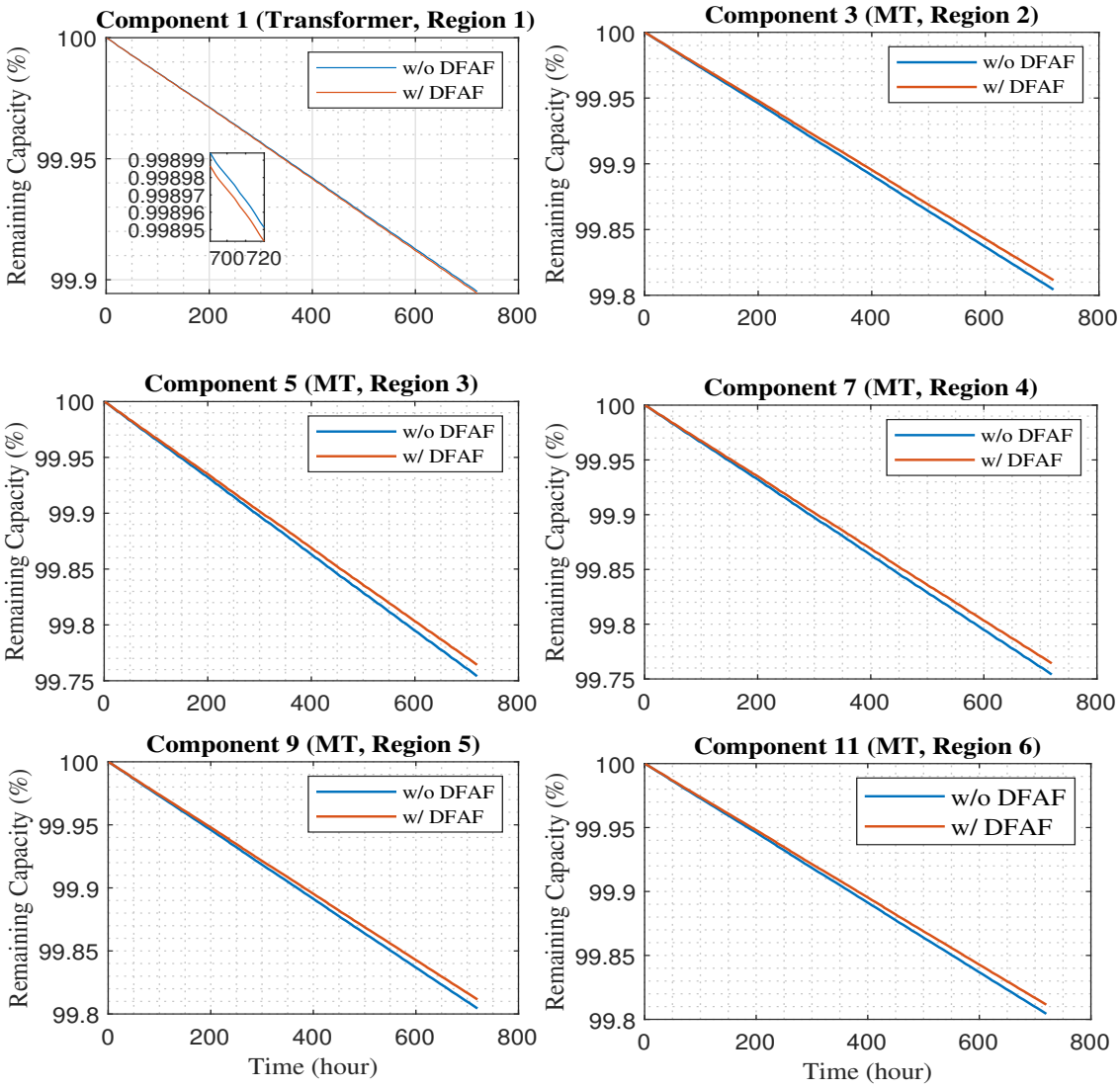

Figure 5.14: Case 2: The degradation of the components with and without DFAF.

5.3.3 Case 3:

In this case, the effectiveness of ET is shown. In the previous cases, data used to train the Markov model is generated using degradation rates on Table 5.2. In this case, for component 3, two data sets are generated using the degradation rates on Table 5.2, which are called source 2 and source 3, another data set is generated by using degradation range [2.9200,5.8400] %/year, which

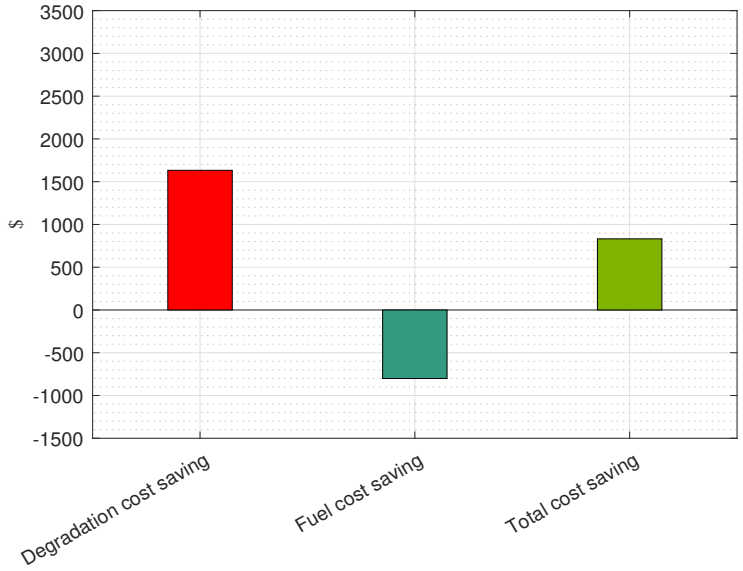

Figure 5.15: Case 2: Cost savings with DFAF.

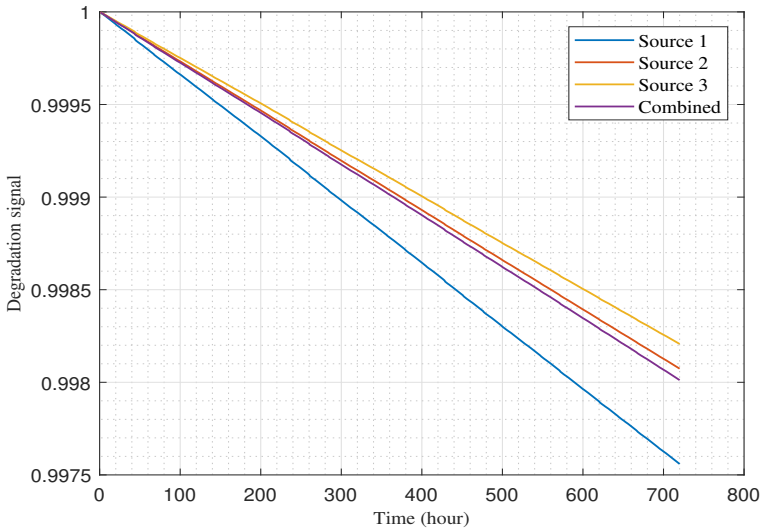

Figure 5.16: Case 3: Predicted degradation of component 3.

is called source 1. Suppose source 1 is an unreliable source. As can be seen in Figure 5.16, ET can discern the unreliability of source 1 as the combined result is closer to source 2 and source 3 compared to source 1.

Chapter 6

Degradation Forecasting and Abatement Framework: CHIL Experimentation

Chapter 6's Nomenclature

CHIL	Controller-hardware-in-the-loop
DER	Distributed energy resource
DRTS	Digital real-time simulator
MT	Microturbine
WT	Wind turbine
PV	Photo-voltaic
DG	Distributed generation
EM	Energy management
PM	Power management
DF	Degradation forecasting
DFAF	Degradation forecasting and abatement framework

6.1 System Description

The strategy proposed in Chapter 4 is realized by a controller-hardware-in-the-loop (CHIL) experimentation. The IEEE 33 bus system [71], which is used to verify the proposed EM strategy in Chapter 3, is used to validate the proposed degradation forecasting and abatement framework (DFAF) discussed in Chapter 4 and simulated in Chapter 5. For the sake of completeness of this chapter, the the IEEE 33 bus system is briefly described here. The IEEE 33 bus system has 33 buses operating in a voltage of 12.66 kV. It connects to a main grid at bus 1 via a substation. Distributed energy resources (DERs) are deployed into the system. In particular, microturbines, PV systems, and a wind turbine are deployed into the distribution grid. The system is geographically divided into 6 regions. The location and installation costs of the DERs are shown in Table 5.1 in Chapter 5.

6.2 CHIL Experimentation Setup

6.2.1 System's MATLAB/Simulink Model

The IEEE 33 bus system is simulated by the MATLAB/Simulink software. The model is later compiled into the C programming language by OPAL-RT Technologies's RT-LAB software, and the compiled program is deployed into a digital real-time simulator (DRTS) OPAL-RT OP4510. Average models are used to model DERs instead of detailed models because the DRTS has a limited computational power to run detailed models of all the DERs in real-time. However, average models are sufficient enough to demonstrate the DFAF strategy. The sampling time used in this work is 80 μs. The MATLAB/Simulink program is shown in Figure 6.1.

For the sake of simplicity, the degradation processes of the system's components are model by the Wiener process included in the MATLAB/Simulink model to generate degradation signals. Those degradation signals are sent to the controller, which implements the DF function.

6.2.2 Energy Management

It is noted that EM strategy is discussed detailedly in Chapter 3. For the sake of completeness, the CHIL implementation of EMs is briefly presented here. Each region has an EM to manage the region in collaboration with other EMs in a distributed manner. The EM strategy is realized by the LabVIEW software, and then it is deployed into 6 real-time controllers NI sbRIO 9627. In this

Figure 6.1: MATLAB/Simulink model of the IEEE 33 bus system.

work, EMs only concern about economic gains in their optimization problems.

6.2.3 Degradation Forecasting

A DF layer is integrated into the system. It forecasts the degradation paths of the system's components. Then, the forecasted results are used to add additional costs to EMs' objective functions. This proposed strategy is called the degradation forecasting and abatement framework (DFAF). The details of the strategy is discussed in Chapter 4 and numerically simulated in Chapter 5. The proposed DF strategy is realized in the LabVIEW environment and deployed into a real-time NI sbRIO 9627 controller. The time step for DF is 1 hour.

6.2.4 Controller-hardware-in-the-loop Experimentation System

The proposed DFAF is realized by a controller-hardware-in-the-loop (CHIL) experimentation. Figure 6.2 describes the CHIL experimentation setup. In addition to those components described in Sections 6.2.1, 6.2.2, and 6.2.3, there is a computer playing as a server is added. The MATLAB script module in LabVIEW is used to implement the server functionalities. The server stores data and trains the data to obtain the Markov-based degradation models. The server will send trained models whenever the real-time controller implementing the degradation forecasting queries

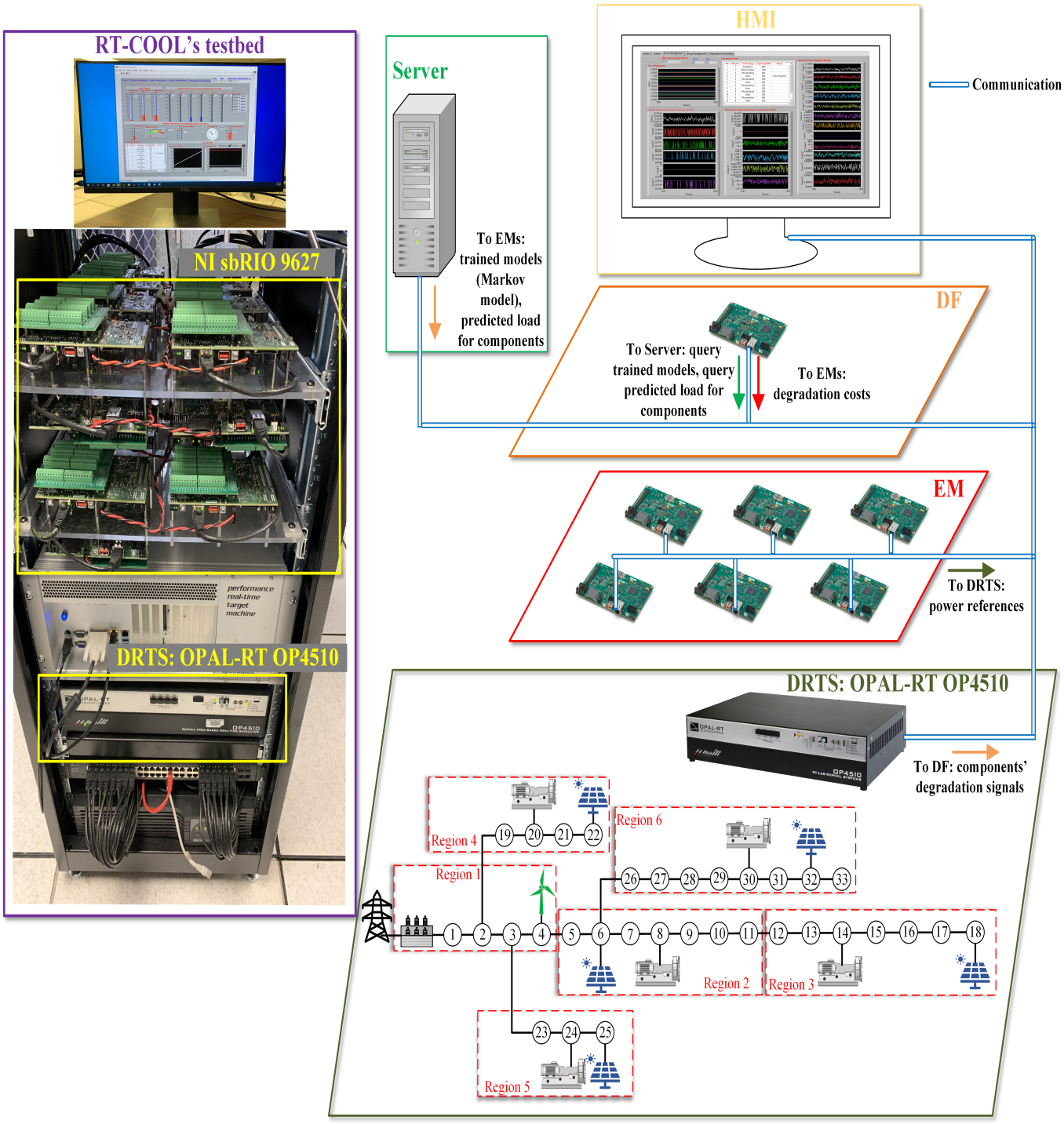

Figure 6.2: Illustration of the CHIL implementation of integrating DFAF.

for the models. Furthermore, the server will respond to the real-time controller's query for predicted power generation or delivery. In particular, the server will implement power generation optimization

a) System Monitoring

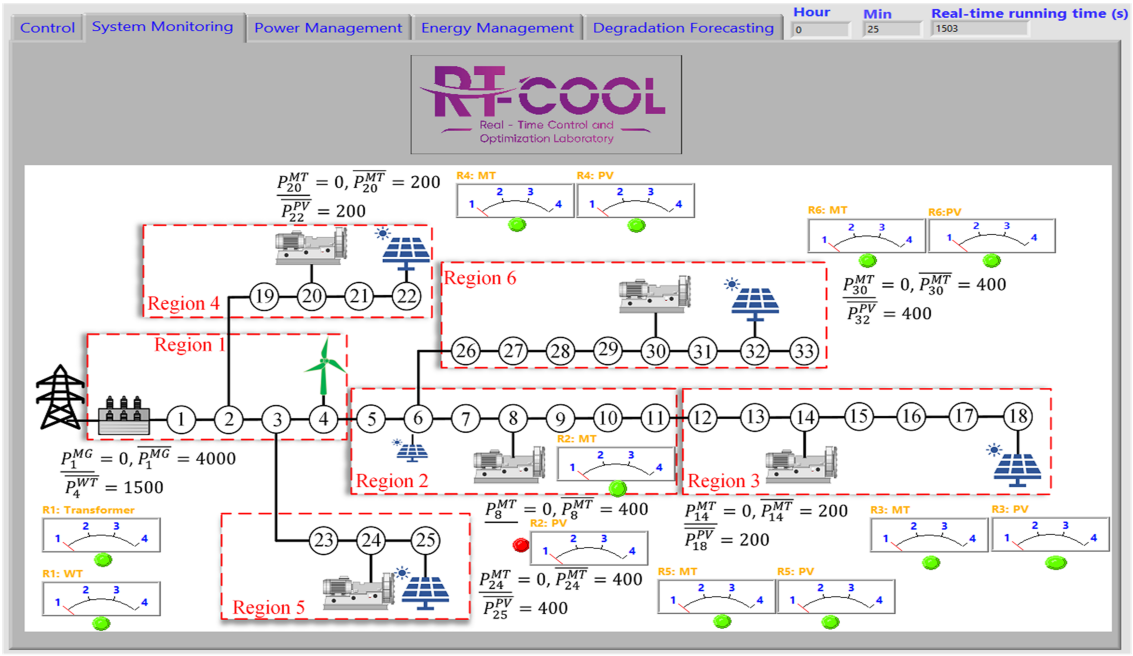

b) Power Management

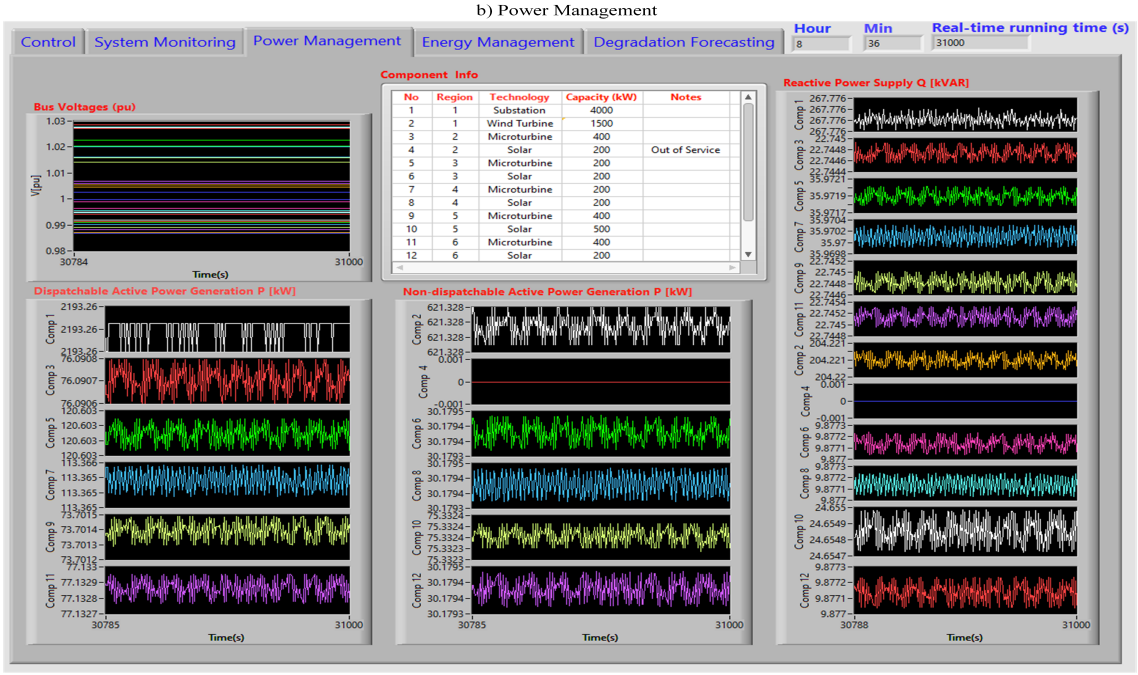

Figure 6.3: HMI display: a) System Monitoring screen b) Power Management screen.

with current EM's objective function and with renewable generation and load data. Moreover, the server will estimate the power generation for non-dispatchable components from weather data. The power generation is then sent to the DF controller.

a) Energy Management

b) Degradation Forecasting

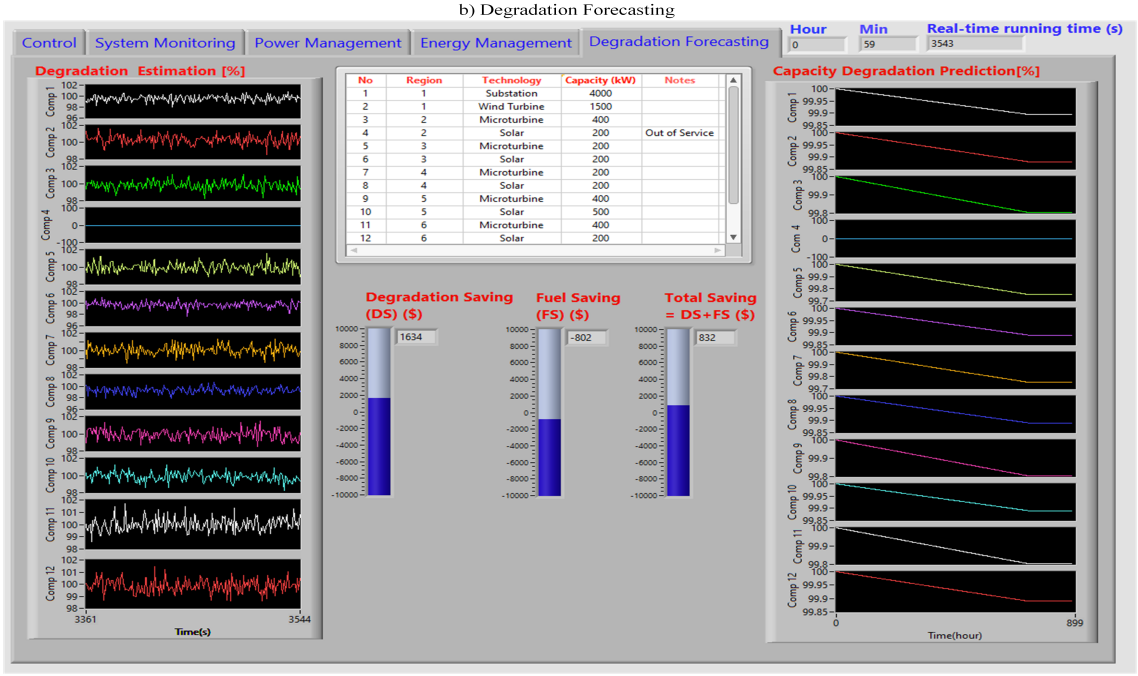

Figure 6.4: HMI display: a) Energy Management screen b) Degradation Forecasting screen.

There is also a human-machine interface (HMI) added to monitor the system, and an NI sbRIO 9627 real-time controller board is set up for this function. The HMI collects operating data from the DRTS, the EM controllers, and the DF controller, and then it displays them on a monitor.

There are five main displaying screens. First, the Control screen has start/stop buttons to control the experimentation, and it also has inputs for the CHIL system's information, such as controllers' IP addresses. Second, the System Monitoring screen displays components' statuses with the grid diagram. Third, the Power Management screen shows bus voltages, measured active and reactive power from DERs and the substation transformer. Fourth, the Energy Management screen is to show weather information, non-dispatchable power generation, load demand, optimal power generation and delivery of dispatchable sources. Finally, the Degradation Forecasting displays the degradation signals received from the model running in the DRTS and the degradation predictions of the grid's components. Figure 6.3 shows the System Monitoring and Power Management screens. Figure 6.4 shows the Energy Management and Degradation Forecasting screens.

6.3 Experimental Results

The proposed strategy is now run on the CHIL setup. It predicts the degradation of the components in 30 days, i.e., 720 hours. The time step to predict for each hour is 4 seconds and predicted results are sent to the HMI to show on its monitoring screen. The data is also sent to the server for data storage. To show the benefits of the proposed strategy, the server is also requested to run the degradation model without adjusting the EM's objective function.

The constructed CHIL system described in Figure 6.2 is run, and the three layers PM, EM, and DF work synergically. As can be seen in Figure 6.4b), degradation signals are sent from the model to HMI running in the DRTS for displaying. It is noted that component 4 is out of service; therefore, the degradation signal is zero. On the left side of the figure, it shows the predicted degradation paths of the components. To show the effectiveness of the proposed strategy, the server is requested to compute costs saved by the strategy. As can be in the middle of the figure, DFAF saves $\approx$ \$1634 in degradation costs in 30 days. However, the fuel cost increases by $\approx$ \$802 because the EM's objective function is adjusted. But overall, the proposed strategy saves $\approx$ \$832 for the system. The experimental results match with the numerical simulations. Figure 6.5 shows recorded real-time predictions and predictions from running offline in a computer. As can be seen, they are considered identical.

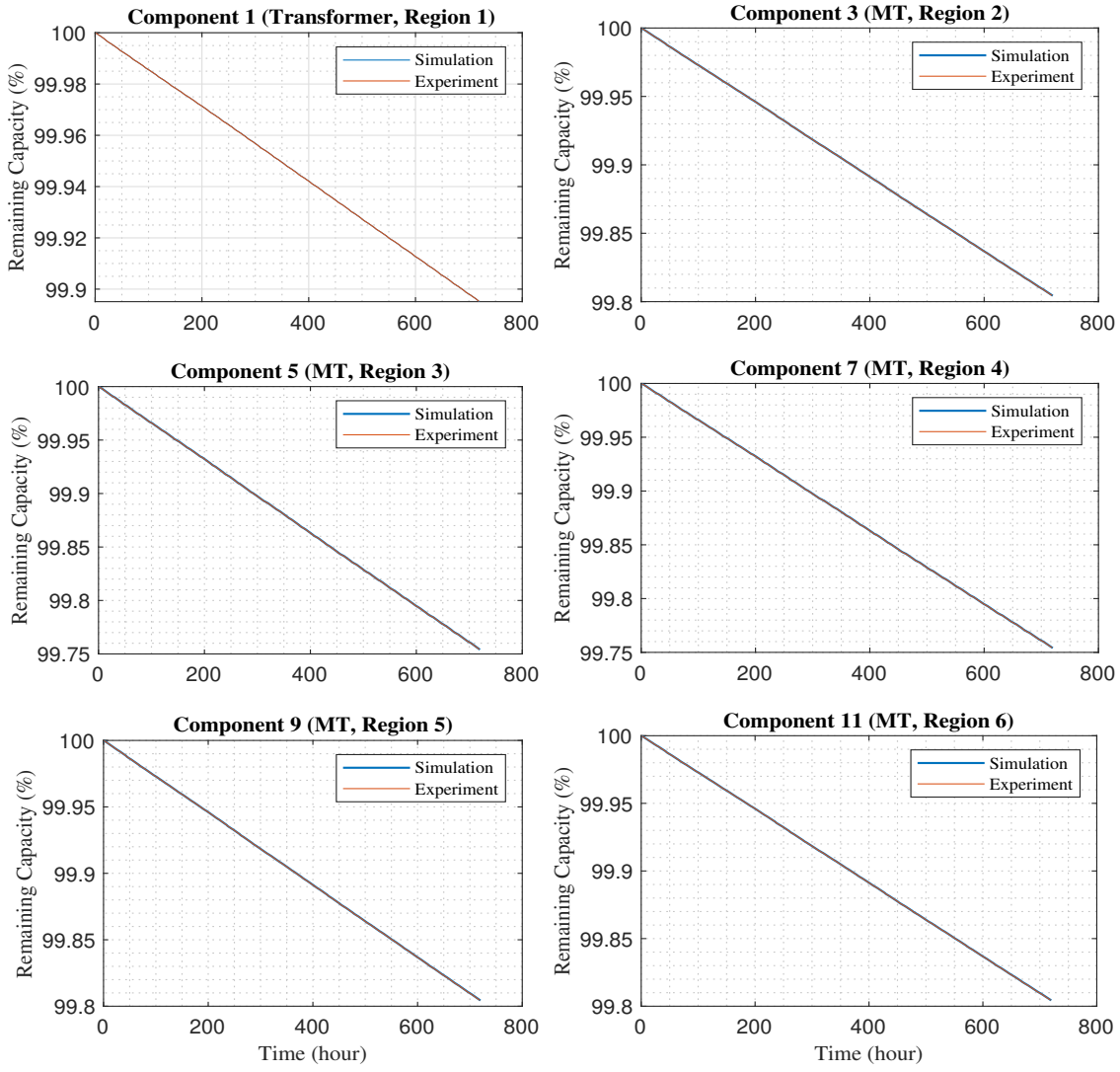

Figure 6.5: Numerical simulation result and real-time experimental result.

Chapter 7

Conclusion

The aim of this dissertation is to develop a degradation forecasting (DF) layer to integrate into the advanced distribution management system (ADMS) of distribution grids, forming a degradation forecasting and abatement framework (DFAF) to enhance system reliability, aid system operation and planning, and reduce system operation cost. In realizing this goal, there are existing issues needed to be solved 1) the global optimality of distributed energy management (EM), 2) the uncertainty quantification of degradation forecasting, and 3) the lack of a degradation forecasting framework to integrate into ADMSs. The contributions of this dissertation are discussed in Chapters 2, 3, and 4. It is summarized as follows.

- In Chapter 2, a new combination rule for ET is introduced. The new rule considers the possibility of a non-exhaustive frame of discernment (FoD) and the unreliability of sources. A sequence of combinations for multiple basic probability assignments (BPAs) has also been proposed. The underlying idea of the proposed sequence is that it allows interactions among the BPAs before performing combinations to rank the degree of reliability based on sums of conflict, and then the more a source is reliable, the later it is involved in the combinations. The newly developed combination rule is used in Chapter 4 for uncertain quantification.

- In Chapter 3, a distributed EM to efficiently manage distribution grids with the penetration of heterogeneous distributed energy sources (DERs) and electric vehicles (EVs) is introduced. The strategy includes two steps that the first step enhances the global optimality searching for the second step. In addition, information after running step 1 is used to reconfigure constraints to

ensure that the power factor limits of generators and the substation transformer are respected. The effectiveness of the proposed strategy is validated by a controller-hardware-in-the-loop (CHIL) experimentation on the IEEE 33 bus system.

- In Chapter 4, a DFAF is proposed. A Markov chain-based DF model is constructed to predict degradation behaviors of a grid's components in which components' states are modeled by a multi-state model. It is integrated into the existing hierarchical ADMS as an upper layer to EM. As a feedback mechanism, the DFAF collaborates with EM to reach a solution that compromises fuel consumption cost and degradation cost by abating components' degradation. In particular, the DFAF adjusts the objective function of EM-based on degradation forecasting. Because degradation data is typically scarce, multiple sources of information are used to quantify uncertainty, and Evidence Theory (ET) is used to fuse multiple sources. However, the unreliability of information sources becomes an issue in existing ET's combination rules. Therefore, a new combination rule introduced in Chapter 2 is used. The effectiveness of the proposed framework is demonstrated by numerical simulations in Chapter 5 and realized by a CHIL experimentation in Chapter 6 with the IEEE 33 bus system as the testing system.

There are some research directions that can expand this work.

- First, predicted degradation results could be used to design optimal maintenance planning. With this consideration, decision makings should consider factors that impact maintenance planning.

- Second, as mentioned, EM is expected to be deployed into electrical systems ranging from MW-scale systems like terrestrial power systems and ship power systems to kW-scale systems like electrified vehicles' powertrain systems. A DF layer can be added to these electrical systems' control and management to adjust EM to reduce operational costs.

- Third, multiple-objective optimization can be developed to determine optimal operating values for both EM and DF layers.

Bibliography

[1] J. M. Guerrero et al. “Hierarchical control of droop-controlled AC and DC microgrids—A general approach toward standardization”. In: *IEEE Transactions on Industrial Electronics* 58.1 (2011), pp. 158–172. DOI: 10.1109/TIE.2010.2066534.

[2] T. V. Vu et al. “Predictive control for energy management in ship power systems under high-power ramp rate loads”. In: *IEEE Transactions on Energy Conversion* 32.2 (2017), pp. 788–797. DOI: 10.1109/TEC.2017.2692058.

[3] M. A. Hannan et al. “State-of-the-art and energy management system of lithium-ion batteries in electric vehicle applications: Issues and recommendations”. In: *IEEE Access* 6 (2018), pp. 19362–19378. DOI: 10.1109/ACCESS.2018.2817655.

[4] M. Henderson, D. Novosel, and M. L. Crow. “Electric power grid modernization trends, challenges, and opportunities”. In: *IEEE Power & Energy Society* (2017).

[5] Department of Energy. “Vision of the future grid”. In: *Energy.gov* (2020).

[6] U.S. Energy Information Administration. “Global EV outlook 2020, technical report”. In: *EIA Global Annual EV Outlook* (2020).

[7] U.S. Energy Information Administration. “Annual energy outlook 2016 early release: Annotated summary of two cases”. In: *EIA Annual Energy Outlook* (2016).

[8] Office of Electricity Delivery and Department of Energy Energy Reliability. “Voices of experience | Insights into advanced distribution management systems”. In: *IEEE Transactions on Smart Grid* (2015).

[9] T. V. Vu et al. “Predictive control for energy management in ship power systems under high-power ramp rate loads”. In: *IEEE Transactions on Energy Conversion* 32 (2017), pp. 788–797.

[10] B. P. Hayes and M. Prodanovic. “State forecasting and operational planning for distribution network energy management systems”. In: *IEEE Transactions on Smart Grid* 7.2 (2016), pp. 1002–1011.

[11] O. Ciftci, M. Mehrtash, and A. Kargarian. “Data-driven nonparametric chance-constrained optimization for microgrid energy management”. In: *IEEE Transactions on Industrial Informatics* 16.4 (2020), pp. 2447–2457.

[12] H. Kanchev et al. “Energy management and operational planning of a microgrid with a PV-based active generator for smart grid applications”. In: *IEEE Transactions on Industrial Electronics* 58.10 (2011), pp. 4583–4592.

[13] J. Lagorse, D. Paire, and A. Miraoui. “A multi-agent system for energy management of distributed power sources”. In: *Renewable Energy* 35.1 (2010), pp. 174–182.

[14] B. Papari et al. “Effective energy management of hybrid AC–DC microgrids with storage devices”. In: *IEEE Transactions on Smart Grid* 10.1 (2019), pp. 193–203.

[15] B. Papari, C. S. Edrington, and D. Gonsoulin. “Optimal energy-emission management in hybrid AC-DC microgrids with vehicle-2-grid technology”. In: *Journal of Renewable and Sustainable Energy* 11.1 (2019).

[16] B. Papari et al. “A heuristic method for optimal energy management of DC microgrid”. In: *2017 IEEE Second International Conference on DC Microgrids (ICDCM)*, pp. 337–343.

[17] S. Xia et al. “A fully distributed hierarchical control framework for coordinated operation of DERs in active distribution power networks”. In: *IEEE Transactions on Power Systems* 34.6 (2019), pp. 5184–5197. DOI: 10.1109/TPWRS.2018.2870153.

[18] S. Boyd, N. Parikh, and E. Chu. “Distributed optimization and statistical learning via the alternating direction method of multipliers”. In: *Now Publishers Inc* (2011).

[19] T. Erseghe. “Distributed optimal power flow using ADMM”. In: *IEEE Transactions on Power Systems* 29.5 (2014), pp. 2370–2380.

[20] S. Mhanna, G. Verbič, and A. C. Chapman. “Adaptive ADMM for distributed AC optimal power flow”. In: *IEEE Transactions on Power Systems* 34.3 (2019), pp. 2025–2035.

[21] Y. Zhang et al. “Distributed controllers seeking AC optimal power flow solutions using ADMM”. In: *IEEE Transactions on Smart Grid* 9.5 (2018), pp. 4525–4537.

[22] H. Liu. “Operational reliability assessment of power systems considering condition-dependent failure rate”. In: *IET Generation, Transmission Distribution* 4 (1 Jan. 2010), 60–72(12). ISSN: 1751-8687. URL: https://digital-library.theiet.org/content/journals/10.1049/iet-gtd.2009.0006.

[23] A. M. Emsley and G. C. Stevens. “Review of chemical indicators of degradation of cellulosic electrical paper insulation in oil-filled transformers”. In: *IEE Proceedings: Science, Measurement and Technology* 141.5 (1994), pp. 324–334. ISSN: 13502344. DOI: 10.1049/ip-smt:19949957.

[24] A. Cuneo et al. “Probabilistic analysis of a fuel cell degradation model for solid oxide fuel cell and gas turbine hybrid systems”. In: *Energy* 141 (2017). ISSN: 03605442. DOI: 10.1016/j.energy.2017.12.002. URL: https://doi.org/10.1016/j.energy.2017.12.002.

[25] G. Shafer. “A mathematical theory of evidence”. In: *Princeton University Press, NJ* (1976).

[26] A. P. Dempster. “Upper and lower probabilities induced by a multivalued mapping”. In: *The Annals of Mathematical Statistics* 38.2 (1967), pp. 325–339.

[27] L. A. Zadeh. “On the validity of Dempster’s rule of combination of evidence”. In: *ERL Memorandum M79/24, University of Berkeley, Berkeley, CA, USA* (1979).

[28] L. A. Zadeh. “Book review: A mathematical theory of evidence”. In: *AI Magazine* 5.3 (1984), pp. 81–83.

[29] J. Pearl. “Reasoning with belief functions: An analysis of compatibility”. In: *International Journal of Approximate Reasoning* 4.5 (1990), pp. 363–389.

[30] R. R. Yager. “On the Dempster-Shafer framework and new combination rules”. In: *Information Sciences* 41 (1987), pp. 93–137.

[31] P. Smets and R. Kennes. “The transferable belief model”. In: *Artificial Intelligence* 64.2 (1994), pp. 191–234.

[32] P. Smets. “Decision making in the TBM: the necessity of the pignistic transformation”. In: *Int. J. Approx. Reasoning* 38 (2005), pp. 133–147.

[33] H. T. Nguyen. “On random sets and belief functions”. In: *Journal of Mathematical Analysis and Applications* 65.3 (1978), pp. 531–542.

[34] D. Dubois and H. Prade. “On several representations of an uncertain body of evidence”. In: *Edited by M. M. Gupta and E. Sanchez, Fuzzy Information and Decision Processes, North-Holland Publishing Company, Amsterdam, The Netherlands* (1982), pp. 167–181.

[35] D. Dubois and H. Prade. “Representation and combination of uncertainty with belief functions and possibility measures”. In: *Computational Intelligence* 4 (1988), pp. 244–264.

[36] T. Denœux. “Conjunctive and disjunctive combination of belief functions induced by nondistinct bodies of evidence”. In: *Artif. Intell.* 172 (2008), pp. 234–264.

[37] T. Denœux. “Decision-making with belief functions: a review”. In: (2018). URL: `https://arxiv.org/pdf/1808.05322.pdf`.

[38] M. C. Florea et al. “Robust combination rules for evidence theory”. In: *Information Fusion* 10 (2009), pp. 183–197.

[39] Y. Deng. “Generalized evidence theory”. In: *Applied Intelligence* 43 (2015), pp. 530–543.

[40] J. Dezert, P. Wang, and A. Tchamova. “On the validity of Dempster-Shafer theory”. In: *2012 15th International Conference on Information Fusion* (2012), pp. 655–660.

[41] M. Beynon, D. Cosker, and D. Marshall. “An expert system for multi-criteria decision making using Dempster Shafer theory”. In: *Expert Systems with Applications* 20.4 (2001), pp. 357–367.

[42] P. P. Shenoy. “Using Dempster-Shafer’s belief-function theory in expert systems”. In: *Appeared in: Yager, R. R., M. Federizzi, and J. Kacprzyk, eds., Advances in the Dempster-Shafer theory of evidence, John Wiley & Sons, New York, NY* (1994), pp. 395–414.

[43] H.-R. Bae, R. V. Grandhi, and R. A. Canfield. “An approximation approach for uncertainty quantification using evidence theory”. In: *Rel. Eng. & Sys. Safety* 86 (2004), pp. 215–225.

[44] P. Soundappan et al. “Comparison of evidence theory and Bayesian theory for uncertainty modeling”. In: *Rel. Eng. & Sys. Safety* 85 (2004), pp. 295–311.

[45] J. Yang et al. “Risk evaluation in failure mode and effects analysis of aircraft turbine rotor blades using Dempster–Shafer evidence theory under uncertainty”. In: *Engineering Failure Analysis* 18.8 (2011), pp. 2084–2092.

[46] T. Denœux. “A k-nearest neighbor classification rule based on Dempster-Shafer theory”. In: *IEEE Transactions on Systems, Man, and Cybernetics* 25.5 (May 1995), pp. 804–813.

[47] S. Le Hegarat-Mascle, I. Bloch, and D. Vidal-Madjar. “Application of Dempster-Shafer evidence theory to unsupervised classification in multisource remote sensing”. In: *IEEE Transactions on Geoscience and Remote Sensing* 35.4 (July 1997), pp. 1018–1031.

[48] L. Jiao, T. Denœux, and Q. Pan. “A hybrid belief rule-based classification system based on uncertain training data and expert knowledge”. In: *IEEE Transactions on Systems, Man, and Cybernetics: Systems* 46.12 (Dec. 2016), pp. 1711–1723.

[49] T. Denœux. “Maximum likelihood estimation from uncertain data in the belief function framework”. In: *IEEE Transactions on Knowledge and Data Engineering* 25.1 (Jan. 2013), pp. 119–130.

[50] T. Denœux, S. Sriboonchitta, and O. Kanjanatarakul. “Evidential clustering of large dissimilarity data”. In: *Knowledge-Based Systems* 106 (2016), pp. 179–195.

[51] F. Li, S. Li, and T. Denœux. “k-CEVCLUS: Constrained evidential clustering of large dissimilarity data”. In: *Knowledge-Based Systems* 142 (2018), pp. 29–44.

[52] W. L. Oberkampf et al. “Challenge problems: uncertainty in system response given uncertain parameters”. In: *Reliability Engineering System Safety* 85.1 (2004), pp. 11–19.

[53] G. Shafer. “Dempster’s rule of combination”. In: *International Journal of Approximate Reasoning* 79 (2016). 40 years of Research on Dempster-Shafer Theory, pp. 26–40.

[54] F. Voorbraak. “On the justification of Dempster’s rule of combination”. In: *Artificial Intelligence* 48.2 (1991), pp. 171–197.

[55] W. Jiang and J. Zhan. “A modified combination rule in generalized evidence theory”. In: *Applied Intelligence* 46 (2016), pp. 630–640.

[56] T. Inagaki. “Interdependence between safety-control policy and multiple-sensor schemes via Dempster-Shafer theory”. In: *IEEE Transactions on Reliability* 40.2 (1991), pp. 182–188.

[57] E. M. Oblow. “Hybrid uncertainty theory”. In: *5th International workshop on expert systems and their applications, Avignon, France* (May 1985), pp. 1193–1201.

[58] G. A. Putrus et al. “Impact of electric vehicles on power distribution networks”. In: *2009 IEEE Vehicle Power and Propulsion Conference*, pp. 827–831.

[59] A. Supponen et al. “Power quality in distribution networks with electric vehicle charging - a research methodology based on field tests and real data”. In: *2016 Eleventh International Conference on Ecological Vehicles and Renewable Energies (EVER)*. 2016, pp. 1–11.

[60] R. Li, Q. Wu, and S. S. Oren. “Distribution locational marginal pricing for optimal electric vehicle charging management”. In: *IEEE Transactions on Power Systems* 29.1 (2014), pp. 203–211.

[61] J. Quiros-Tortos, L. F. Ochoa, and T. Butler. “How electric vehicles and the grid work together: Lessons learned from one of the largest electric vehicle trials in the world”. In: *IEEE Power and Energy Magazine* 16.6 (2018), pp. 64–76.

[62] Electric Vehicle Database. *All electric vehicles*. URL: `https://ev-database.org/`. (accessed: 22.08.2020).

[63] Argonne National Laboratory Energy Systems Division. *Light duty electric drive vehicles monthly sales updates*. URL: `https://www.anl.gov/es/light-duty-electric-drive-vehicles-monthly-sales-updates`. (accessed: 22.08.2020).

[64] M. G. Flammini et al. “Statistical characterisation of the real transaction data gathered from electric vehicle charging stations”. In: *Electric Power Systems Research* 166 (2019), pp. 136–150.

[65] F. Pallonetto et al. “A framework for analysis and expansion of public charging infrastructure under fast penetration of electric vehicles”. In: *World Electric Vehicle Journal* 11.1 (2020). ISSN: 2032-6653. URL: `https://www.mdpi.com/2032-6653/11/1/18`.

[66] P. Weldon et al. “An investigation into usage patterns of electric vehicles in Ireland”. In: *Transportation Research Part D: Transport and Environment* 43 (2016), pp. 207–225.

[67] J. Lavaei and S. H. Low. “Zero duality gap in optimal power flow problem”. In: *IEEE Transactions on Power Systems* 27.1 (2012), pp. 92–107.

[68] S. H. Low. “Convex relaxation of optimal power flow—part I: formulations and equivalence”. In: *IEEE Transactions on Control of Network Systems* 1.1 (2014), pp. 15–27.

[69] P. H. Hoang et al. “Distributed constrained optimization over networked systems via a singular perturbation method and application to economic dispatch”. In: *2020 Clemson University Power Systems Conference (PSC)*, pp. 1–6.

[70] P. H. Hoang et al. “Distributed constrained optimization by singular perturbation method and its application to energy networks by real-time implementation”. In: *Sustainable Energy, Grids and Networks* 27 (2021).

[71] M. E. Baran and F. F. Wu. “Network reconfiguration in distribution systems for loss reduction and load balancing”. In: *IEEE Transactions on Power Delivery* 4.2 (1989), pp. 1401–1407.

[72] W. I. Rowen. “Simplified mathematical representations of heavy-duty gas turbines”. In: *Journal of Engineering for Power* 105.4 (Oct. 1983), pp. 865–869.

[73] S. Grillo et al. “Microturbine control modeling to investigate the effects of distributed generation in electric energy networks”. In: *IEEE Systems Journal* 4.3 (2010), pp. 303–312.

[74] A. D. Hansen and I. D. Margaris. “Type IV wind turbine model”. In: *DTU Wind Energy* (2014).

[75] N. Femia et al. “A technique for improving P&O MPPT performances of double-stage grid-connected photovoltaic systems”. In: *IEEE Transactions on Industrial Electronics* 56.11 (2009), pp. 4473–4482.

[76] I. Richardson et al. “Domestic electricity use: A high-resolution energy demand model”. In: *Energy and Buildings* 42.10 (2010), pp. 1878–1887.

[77] J. Ponoćko and J. V. Milanović. “Forecasting demand flexibility of aggregated residential load using smart meter data”. In: *IEEE Transactions on Power Systems* 33.5 (2018), pp. 5446–5455.

[78] B. Johnson. “Power factor correction design for on-board chargers in electric vehicles”. In: *Texas Instruments’ Application Report* (2018).

[79] J. Wang et al. “Coordinated electric vehicle charging with reactive power support to distribution grids”. In: *IEEE Transactions on Industrial Informatics* 15.1 (2019), pp. 54–63.

[80] Global petrol prices. *United Kingdom gasoline price*. URL: https://www.globalpetrolprices.com/United-Kingdom/gasoline_prices/. (accessed: 24.08.2020).

[81] Julio Romero Aguero et al. “Modernizing the grid: challenges and opportunities for a sustainable future”. In: *IEEE Power and Energy Magazine* 15.3 (2017), pp. 74–83. ISSN: 15407977.

[82] National Renewable Energy Laboratory. “Insights into advanced distribution management systems”. In: *Voices of Experience-U.S. Department of Energy-Office of Electricity Delivery & Energy Reliability* (2015).

[83] X. Sun, R. V. K. Chavali, and M. A. Alam. “Real-time monitoring and diagnosis of photovoltaic system degradation only using maximum power point—the Suns-Vmp method”. In: *Progress in photovoltaics: Research and applications* 27.1 (2019), pp. 55–66. ISSN: 1099159X. DOI: 10.1002/pip.3043.

[84] X. Jia et al. “Wind turbine performance degradation assessment based on a novel similarity metric for machine performance curves”. In: *Renewable Energy* 99 (2016), pp. 1191–1201. ISSN: 18790682. DOI: 10.1016/j.renene.2016.08.018. URL: http://dx.doi.org/10.1016/j.renene.2016.08.018.

[85] P. H. Hoang et al. “An online degradation forecasting and abatement framework for hybrid electric vehicles”. In: *SAE Technical Papers* 2021 (2021), pp. 1–6. ISSN: 01487191. DOI: 10.4271/2021-01-0161.

[86] P. H. Hoang et al. “An Evidence Theory based advisory layer for all-electric ship power systems”. In: *2019 IEEE Electric Ship Technologies Symposium (ESTS)*. 2019, pp. 599–604. DOI: 10.1109/ESTS.2019.8847884.

[87] T. Olsson et al. “A data-driven approach for predicting long-term degradation of a fleet of micro gas turbines”. In: *Energy and AI* 4 (2021), p. 100064. ISSN: 26665468. DOI: 10.1016/j.egyai.2021.100064. URL: https://doi.org/10.1016/j.egyai.2021.100064.

[88] R. R. Richardson, M. A. Osborne, and D. A. Howey. “Gaussian process regression for forecasting battery state of health”. In: *Journal of Power Sources* 357 (2017), pp. 209–219. ISSN: 03787753. DOI: 10.1016/j.jpowsour.2017.05.004. eprint: 1703.05687. URL: http://dx.doi.org/10.1016/j.jpowsour.2017.05.004.

[89] D. Djurdjanovic, J. Lee, and J. Ni. "Watchdog agent - An infotronics-based prognostics approach for product performance degradation assessment and prediction". In: *Advanced Engineering Informatics* 17.3-4 (2003), pp. 109–125. ISSN: 14740346. DOI: 10.1016/j.aei.2004.07.005.

[90] R. Billinton and R. N. Allan. "Reliability evaluation of engineering systems: Concepts and techniques". In: *Longman Scientific & Technical* (1983).

[91] R. Billinton and R. N. Allan. "Reliability evaluation of power systems (second edition)". In: *Plenum Press, New York and London* (1996).

[92] Y.-F. Li and E. Zio. "A multi-state model for the reliability assessment of a distributed generation system via universal generating function". In: *Reliability Engineering System Safety* 106 (2012), pp. 28–36. ISSN: 0951-8320. DOI: https://doi.org/10.1016/j.ress.2012.04.008. URL: https://www.sciencedirect.com/science/article/pii/S0951832012000749.

[93] R. Moghaddass and M. J. Zuo. "Multistate degradation and supervised estimation methods for a condition-monitored device". In: *IIE Transactions* 46.2 (2014), pp. 131–148. DOI: 10.1080/0740817X.2013.770188. URL: https://doi.org/10.1080/0740817X.2013.770188.

[94] Z. Li et al. "Reliability modelling and analysis of a multi-state element based on a dynamic bayesian network". In: *Royal Society Open Science* 5.4 (2018). ISSN: 20545703. DOI: 10.1098/rsos.171438.

[95] A. Lisnianski et al. "A multi-state Markov model for a short-term reliability analysis of a power generating unit". In: *Reliability Engineering and System Safety* 98.1 (2012), pp. 1–6. ISSN: 09518320. DOI: 10.1016/j.ress.2011.10.008. URL: http://dx.doi.org/10.1016/j.ress.2011.10.008.

[96] B. Akay et al. "Investigation of the root flow in a Horizontal Axis". In: *Wind Energy* May 2015 (2013), pp. 1–20. DOI: 10.1002/we.

[97] Q. T. Tu Tran et al. "Online distribution service transformer health assessment using real-time grid energy monitor". In: *2020 IEEE Kansas Power and Energy Conference, KPEC 2020* (2020), pp. 2–7. DOI: 10.1109/KPEC47870.2020.9167580.

[98] U. Igie et al. "Evaluating gas turbine performance using machine-generated data: Quantifying degradation and impacts of compressor washing". In: *Journal of Engineering for Gas Turbines and Power* 138.12 (2016), pp. 1–18. DOI: 10.1115/1.4033748.

[99] M. L. Wymore et al. "A survey of health monitoring systems for wind turbines". In: *Renewable and Sustainable Energy Reviews* 52.1069283 (2015), pp. 976–990. ISSN: 18790690. DOI: 10.1016/j.rser.2015.07.110.

[100] H. Hanachi et al. "A framework with nonlinear system model and nonparametric noise for gas turbine degradation state estimation". In: *Measurement Science and Technology* 26.6 (2015). ISSN: 13616501. DOI: 10.1088/0957-0233/26/6/065604.

[101] D. C. Jordan et al. "Robust PV degradation methodology and application". In: *IEEE Journal of Photovoltaics* 8.2 (2018), pp. 525–531. ISSN: 21563381. DOI: 10.1109/JPHOTOV.2017.2779779.

[102] J. Y. Ye et al. "Effect of solar spectrum on the performance of various thin-film PV module technologies in tropical Singapore". In: *IEEE Journal of Photovoltaics* 4.5 (2014), pp. 1268–1274. ISSN: 21563381. DOI: 10.1109/JPHOTOV.2014.2328585.

[103] Y. S.H. Najjar, O. F.A. Alalul, and A. Abu-Shamleh. "Degradation analysis of a heavy-duty gas turbine engine under full and part load conditions". In: *International Journal of Energy Research* 44.6 (2020), pp. 4529–4542. ISSN: 1099114X. DOI: 10.1002/er.5229.

[104] T. Thampan, Y. Ding, and L. Toomey. "Accelerated degradation of Li-Ion batteries for high rate discharge applications". In: *SAE Technical Papers* 2020-April.April (2020), pp. 2–5. ISSN: 01487191. DOI: 10.4271/2020-01-0452.

[105] Z. Shi et al. "Distributionally robust chance-constrained energy management for islanded microgrids". In: *IEEE Transactions on Smart Grid* 10.2 (2019), pp. 2234–2244. ISSN: 19493053. DOI: 10.1109/TSG.2018.2792322.

[106] Windustry. "How much do wind turbines cost?" In: *https://www.windustry.org/* (2021). URL: https://www.windustry.org/how_much_do_wind_turbines_cost.

[107] Ezekiel Enterprises LLC. "Microturbine generators". In: *Ezekiel Enterprises Continuing Education for Licensed Professional Engineers* (2021). URL: https://cdn.ez-pdh.com/course-material/EE1285-Microturbine-Generators.pdf.

[108] Energy Sage. "How much does a solar panel installation cost?" In: *https://www.energysage.com/* (2021). URL: https://news.energysage.com/how-much-does-the-average-solar-panel-installation-cost-in-the-u-s/.

[109] Alibaba.com. In: *Alibaba.com* (2021). URL: https://www.alibaba.com/product-detail/Price-for-35kv-5000-kva-4_1600289293351.html?spm=a2700.pc_countrysearch.main07.8.16087df8lGkPFX.

[110] X. S. Si et al. "A Wiener-process-based degradation model with a recursive filter algorithm for remaining useful life estimation". In: *Mechanical Systems and Signal Processing* 35.1-2 (2013), pp. 219–237. ISSN: 08883270. DOI: 10.1016/j.ymssp.2012.08.016. URL: http://dx.doi.org/10.1016/j.ymssp.2012.08.016.

[111] X. Wang. "Wiener processes with random effects for degradation data". In: *Journal of Multivariate Analysis* 101.2 (2010), pp. 340–351. ISSN: 0047259X. DOI: 10.1016/j.jmva.2008.12.007. URL: http://dx.doi.org/10.1016/j.jmva.2008.12.007.

[112] I. Staffell and R. Green. "How does wind farm performance decline with age?" In: *Renewable Energy* 66 (2014), pp. 775–786. ISSN: 0960-1481. DOI: https://doi.org/10.1016/j.renene.2013.10.041. URL: https://www.sciencedirect.com/science/article/pii/S0960148113005727.

[113] T&D World. "How Transformers Age". In: *https://www.tdworld.com/* (2019). URL: https://www.tdworld.com/substations/article/20972255/how-transformers-age.

[114] M. Bolinger, W. Gorman, D. Millstein, and D. Jordan. "System-level performance and degradation of 21 GWDC of utility-scale PV plants in the United States". In: *Journal of Renewable and Sustainable Energy* 12 (2020).